TSALLIS ENTROPY BASED VELOCITY DISTRIBUTIONS IN OPEN CHANNEL FLOWS

A Thesis

by

HAO LUO

Submitted to the Office of Graduate Studies of
Texas A&M University
in partial fulfillment of the requirements for the degree of

MASTER OF SCIENCE

December 2009

Major Subject: Biological and Agricultural Engineering

TSALLIS ENTROPY BASED VELOCITY DISTRIBUTIONS IN OPEN CHANNEL FLOWS

A Thesis

by

HAO LUO

Submitted to the Office of Graduate Studies of
Texas A&M University
in partial fulfillment of the requirements for the degree of

MASTER OF SCIENCE

Approved by:

Chair of Committee,	Vijay Singh
Committee Members,	Goong Chen
	Ralph Wurbs
Head of Department,	Gerald Riskowski

December 2009

Major Subject: Biological and Agricultural Engineering

ABSTRACT

Tsallis Entropy Based Velocity Distributions in Open Channel Flows.

(December 2009)

Hao Luo, B.E.; B.A., Beijing University of Aeronautics and Astronautics

Chair of Advisory Committee: Dr. Vijay P. Singh

The Tsallis entropy is applied to derive both 1-D and 2-D velocity distributions in an open channel cross section. These distributions contain a parameter *m* through which the Tsallis entropy becomes a generalization of the Shannon entropy. Different *m* parameter values are examined to determine the best value for describing the velocity distribution. Two Lagrangian parameters that are involved in the final form of 1-D velocity distribution equation are determined from observations of mean velocity and the maximum velocity at the water surface. For channels which are not wide and where the maximum velocity does not occur at the water surface, a 2-D velocity distribution is more appropriate. The Tsallis entropy is applied to derive 2-D velocity distributions. A new parameter *M* is introduced which represents the hydraulic characteristics of the channel. The derived velocity distributions are verified using both field data and experimental data. The advantages are found by comparing with Parandtl-von Karman, power law and Chiu's velocity distributions.

DEDICATION

I would like to dedicate this work to my grandparents, Mr. Wu and Mrs. Wu, who encouraged me to go for my academic goal from the time I was little.

ACKNOWLEDGEMENTS

I would like to thank my committee chair, Dr. Singh, who introduced me to the Water Resources field and gave me the chance to work on this topic and my committee members, Dr. Chen and Dr. Wurbs, for their guidance and support throughout my study in Texas A&M University.

Thanks also go to my friends and colleagues in Dr. Singh's Water Resource Group and the department faculty and staff for making my time at Texas A&M University a great experience. I also want to extend my gratitude to all the instructors of the courses I took in Texas A&M for their helpful instructions and assistance..

Finally, thanks to my parents, Mr. Luo and Mrs. Luo, for their encouragement and support all the time.

TABLE OF CONTENTS

TABLE OF CONTENTS (*continued*)

LIST OF FIGURES

LIST OF FIGURES (*continued*)

LIST OF FIGURES (*continued*)

LIST OF FIGURES (*continued*)

LIST OF TABLES

LIST OF TABLES (*continued*)

1. INTRODUCTION

1.1. Rationale and significance

There appears to be a remarkable shortage of reliable data of discharge in rivers and streams during unsteady high flows such as floods, in which the discharge changes rapidly. This shortage seems to be due to technical difficulties, and the fact that conventional methods of discharge measurements require too much time to be applicable. These data, however, are essential to understand the stage-discharge relationship needed in flow forecasting and in the design of flood control structures. Therefore, efficient methods of discharge measurement that will require only a simple sampling of velocity and that can be quickly accomplished or automated are highly desirable.

Discharge measurements involve velocity sampling in order to determine the cross-sectional mean velocity. Therefore, for discharge measurements to be simple and efficient, the number of velocity samples to be taken must be sufficiently small so that the sampling may be accomplished quickly and within the time frame of the particular flow and velocity regime being investigated. Translating a small number of velocity samples into the cross-sectional mean velocity requires a novel velocity distribution equation. Such a velocity distribution equation can be derived using entropy.

Fundamental to hydraulic modeling of flow propagation, sediment transport, pollutant transport, and river behavior is the velocity distribution at river cross-sections.

This thesis follows the style of *Journal of Hydrologic Engineering.*

The velocity distribution has been investigated using deterministic approaches as well as probabilistic approaches. The probability law describing the velocity distribution at a channel section in rivers and streams is resilient and invariant with time and discharge. This is based on the observation that its parameter, the average ratio of the mean and maximum velocities, is invariant with discharge and water level. This in turn can serve as a basis for an efficient method of discharge measurements in rivers and streams. The method is applicable in both steady and unsteady flows in rivers and can be used with any velocity-measuring equipment to drastically reduce the time and cost of discharge measurements. Its most important utility, however, is its applicability in unsteady, high flows to collect data that are essential in critical situations such as flow forecasting but cannot be measured by conventional methods.

Regularities, such as the ratio between mean velocity and maximum velocity (Chiu and Said 1995; Moramarco and Singh 2004) holds constant, exist in fluid flows, especially in the velocity distribution, and can be represented by a set of constants such as the conservation of mass, momentum and energy. These constants are functions of the parameter of a probability distribution that exhibits resilience and stability under various flow conditions. The regularities explain the various fluid-flow phenomena and can be used in the analysis of rivers and streams. For example, they can be used as a basis to develop simple and efficient methods for discharge measurements which only require velocity sampling at a single point on a water surface or a few points on a single vertical. Because of their simplicity and the short time requirement, these methods can be easily automated for collecting velocity and discharge data in unsteady, high flows that are

badly needed for real-time flow forecasting and design of flood control structures, and for advancing the fundamental, scientific knowledge in hydrology.

The flow in an open channel at a given time and location can be laminar, turbulent or mixed (transitional). The flow in open channels on alluvial sand beds is generally hydraulically rough and therefore turbulent flow prevails for most natural conditions. If the flow is laminar, then velocity can be defined accurately. However, in turbulent flow the velocity vector is not constant and the velocity fluctuates both spatially and temporally. The discussion in this thesis is restricted to time averaged velocity at a given location.

Much research has been done in predicting velocity profiles using classic deterministic methods. Today, hydraulic analysis and modeling are, for the most part, based on rational hydrodynamics founded on the deterministic laws of physics that treats fluid flows as boundary-value problems and attempts to make predictions with certainty by deductive reasoning. In the process, however, the physical laws are supplemented by plausible or intuitive hypotheses and assumptions that compounded with often incomplete information about input and boundary conditions create paradoxes or the inconsistencies between observed facts and mathematical predictions.

In hydraulics the very popular velocity distributions are Prandtl-von Karman universal velocity distribution and power law velocity distribution. Limitations of these velocity distributions have been discussed by Chiu (1987), Singh (1996), amongst others. Chiu (1987) proposed a probabilistic approach, using the principle of maximum entropy (POME) (Jaynes 1957), to derive velocity distributions, subject to specified constraints.

The distributions thus derived are considered to be the most probable or objective on the basis of the available information. Tsallis entropy, a generalization of the Shannon entropy, has not been applied to derive velocity distributions. This thesis therefore employs the Tsallis entropy. The comparison between different velocity distributions will be presented as well to show the characteristics Tsallis entropy based velocity equation have over the other velocity equations.

1.2. Objectives

The objective of this study is to develop an entropy theory using the Tsallis entropy, which is a generalization of the Shannon entropy, for deriving velocity distributions for flow in open channels, and test the derived distributions using experimental (laboratory) and field measurements. The thesis is directed at demonstrating the accuracy appropriateness and feasibility of the derived distributions from a scientific point of view. A simple method for estimation of 1-D and 2-D velocity distributions using the Tsallis entropy at a river section is thus developed. This has direct implications for measurement and estimation of transport of mass, momentum and energy in fluid flows. The method, based on the velocity distribution equation derived by Singh and Luo (2009) using the probabilistic formulation and entropy maximization, is capable of determining velocity profiles with reasonable accuracy, even near the side walls. Furthermore, there are regularities in open channel flows that, if detected, analyzed, and properly understood, can be used as a basis to simplify data collection and improve flow forecasting, design and control of engineering systems. The regularities are natural laws

governing flows, and their detection will be aided by theoretical analysis and illustrated in this thesis as well. The specific objectives of the thesis are:

1. Derivation of 1-D (time averaged) velocity distribution equations in a given cross-section, using the Tsallis entropy.
2. Derivation of 2-D (time averaged) velocity distribution equations in a channel cross section, using the Tsallis entropy.
3. Derivation of equations concerning the relationship between the mean and maximum velocities and their locations.
4. Derivation of equations for related regularities that can be used to provide additional attributes of velocity distribution.
5. Investigation of a new hydraulic parameter M of the 2-D velocity distribution equations.
6. Testing of the applicability of derived velocity distribution equations for different kinds of flows.

1.3. Experimental and field data

The 1-D velocity distributions based on Tsallis entropy were tested using a large set of experimental data collected by Einstein and Chien (1955) , Coleman (1986), Tu and Graf (1992) plus with field data collected by Afzalmehr (2008) for channels in Iran. There are 84 sets of velocity data that were used here.

The laboratory data collected by Einstein and Chien (1955) were used to evaluate the effect of suspended sediment and the coarseness of channel bed on the velocity profile near the channel bed. A total of 29 runs were made, 13 of them with clear water and the

rest with sediment-laden flow. The experiments were conducted in a painted steel flume 1.006 ft wide by 1.17 ft deep and 40 ft long. The slope was adjustable by means of an especially designed jack and varied from 0.0185 to 0.025, and the discharge was variable from 2.6 to 3.0 cfs by changing the speed of the pump. The water depth ranged from 0.36 to 0.49 ft and the average velocity of different runs changed from 6.1 fps to 8.7 fps.

Coleman's experiments investigated the response of complete boundary layer velocity profile to sediment concentration. The experiments were performed in a recirculating flume with a rectangular Plexiglas channel 356 mm wide and 15 m long, with slope adjustment capability for maintaining uniform flow. 40 velocity profiles were measured at a vertical located on the flume channel centerline 12 m downstream from the entrance. The experiment was to establish a uniform flow at constant discharge, depth, and energy gradient, to establish the clear-water velocity profile by local velocity measurement at standard elevations, and then to monitor changes in the velocity profile resulting from systematic increases in suspended sediment concentration while holding other flow conditions constant. The discharge was held at 0.064 m^3/s, while the flow depths varied between 168 mm and 174 mm with an average of 169 mm and a standard deviation of 1.69 mm, and the channel width was 35.6, giving an aspect ratio of around 2. The maximum velocity varied from 1.024 m/s to 1.118 m/s.

Ten sets of flume data collected by Tu and Graf (1992) were used to test the applicability of the model in unsteady flows. In their experiments natural hydrographs were passed through a gravel-bed flume which was 16.8 m long, 0.6 m wide and 0.8 m high, with glass side walls and a smooth steel floor being covered with gravels and with

bed slope as 0.002. The evolution of the vertical velocity profiles during the passage of hydrograph NS1(1) was presented for several different time instants. The water depth ranged between 9.0 cm and 21.2 cm, the average velocity varied between 40.8 cm/s and 94.9 cm/s and discharge varied from 60.6 l/s to 90.5 l/s.

Data from rivers in Iran (Afzalmehr 2008) was collected from wide rectangular channels with clear flow and the observations were for the whole water depth. 5 runs were used to test the overall performance of the Tsallis entropy based velocity distribution.

The goodness of the 2-D Tsallis velocity model, the accuracy of a linear relation between the mean and maximum velocities and a reasonable range of parameter M were investigated using 190 sets of vertical velocity data collected during a period of 20 years for four gauged sections in the upper Tiber basin and two flood events happened at Pontelagoscuro station in Po River in Central Italy. The discharge for different events varied between 1.5 m^3/s and 537 m^3/s with the mean velocity ranged between 0.12 m/s to 2.42 m/s and the maximum water depth between 0.8 m and 6.7m.

Field data obtained by Blaney (1937) from 10 canals in the Imperial Valley during 1918-1919 was also used in the investigations on M. The canals had widths between 4 ft and 50 ft, the width-to-depth ratio was variable between 2.3 ft and 9.3 ft and the average velocity ranged from 1.56 ft/s to 4.04 ft/s.

Furthermore, there were a total of 10 sets of experimental data for rectangular flume with both uniform and nonuniform flows collected by Guy (1966) and Guo (1990) that were also chosen to show the performance of the new model in both uniform and

nonuniform flows. The data obtained by Guy was from a channel which was 2 ft wide and 0.60 ft deep with a discharge as 3.54 cfs. The observations made by Guo (1990) were from a flume which was 10 cm wide and 2.31 deep with a discharge as 669 cm^3/s.

Sixteen sets of Tu's (Tu 1995) laboratory data were selected to verify the applicability of Tsallis entropy based 2-D velocity distribution model in unsteady flows. The flume used to simulate unsteady flows was 25 m long, 0.6 m high and 1m wide with discharge varying between 11 l/s and 25 l/s and the water depth from 7cm to 9 cm. The width of the main channel was 40 cm and the floodplain was 60 cm wide. Flow velocities were measured on 16 vertical profiles at every 5 mm along each profile. The first measuring point on each profile was 10 mm from the channel bed. The flood plain had vegetation 6.45 cm high. The diameter and height of the model plants were 2 mm. The space between plants was 2.5 cm. The slope of the tilting flume was 1/2000.

2. 1-D VELOCITY DISTRIBUTION

2.1. Derivation of velocity distributions and related probability functions

2.1.1. Hypothesis for cumulative probability distribution

The velocity of flow at any point or in any cross-section varies with time. It is therefore assumed that the time-averaged velocity at any point in a cross-section is a random variable. The entropy theory proposed here for deriving velocity distributions is comprised of four parts: (1) Tsallis entropy, (2) principle of maximum entropy, (3) specification of constraints, and (4) maximization of Tsallis entropy. Before developing the entropy theory, the cumulative probability distribution of velocity distribution is needed.

It is hypothesized that the cumulative probability distribution of velocity can be expressed as a ratio of the flow depth to the point where velocity is to be considered and the depth up to the water surface. Put algebraically,

$$F(u) = \frac{y}{D} \tag{1}$$

$F(u)$ denotes the cumulative distribution function, u= velocity, y= distance from the bed, D= water depth, and the probability density function f(u) is:

$$f(u) = \frac{dF(u)}{du} = \frac{1}{D}\frac{dy}{du} \tag{2}$$

To test whether this hypothesis hold true for natural rivers and laboratory measurement, we took one set field data that was collected from Iran (Afzalmehr 2008) and Coleman's experimental data (Coleman 1986) to show the relationship between the cumulative probability $F(u)$ against the ratio y/D.

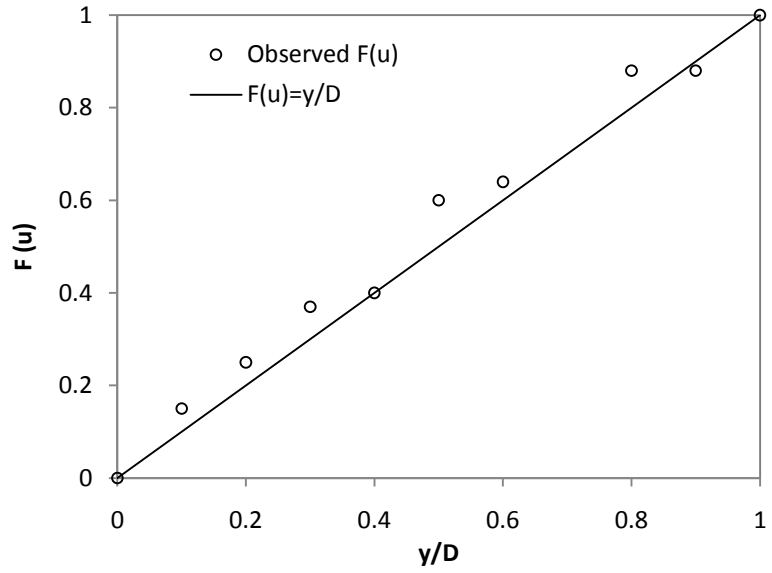

(a)

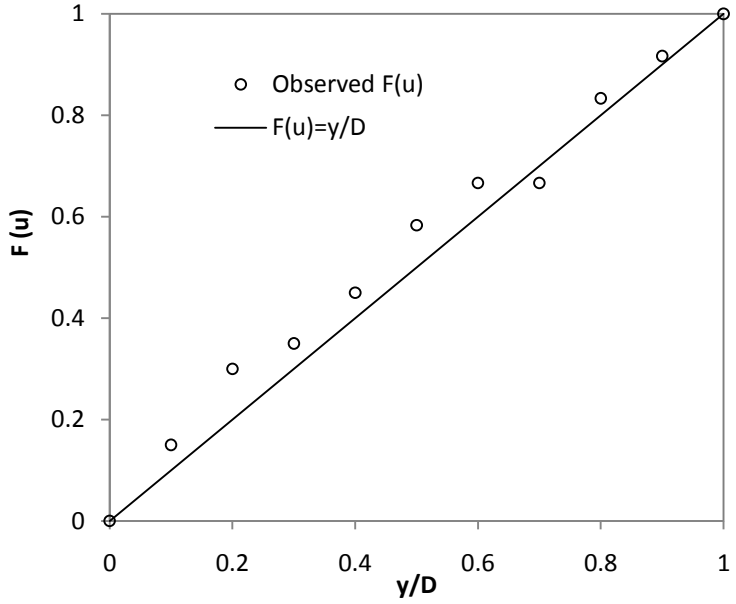

(b)

Fig. 1. Cumulative probability *F(u)*. (a) Field data from Iran (Afzalmehr 2008); (b) Experimental data collected by Coleman (1986).

These two data sets were chosen because the measurements were made along the whole water depth as shown in Fig. 1(a). And it is also good to show the frequency of the velocity for either the lower region near bottom or the higher region up to water surface as shown in Fig. 1(b).

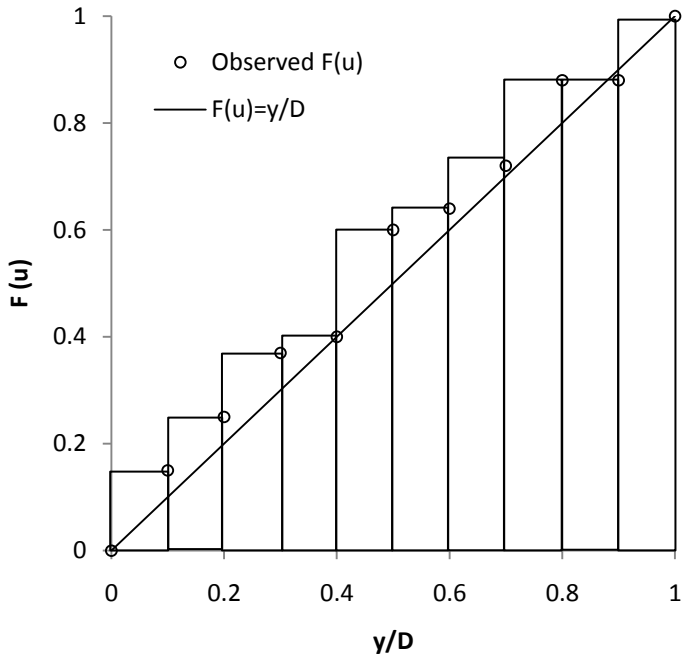

(a)

Fig. 2. Histogram of cumulative probability based on observations. (a) Field data from Iran (Afzalmehr 2008); (b) Experimental data collected by Coleman(1986).

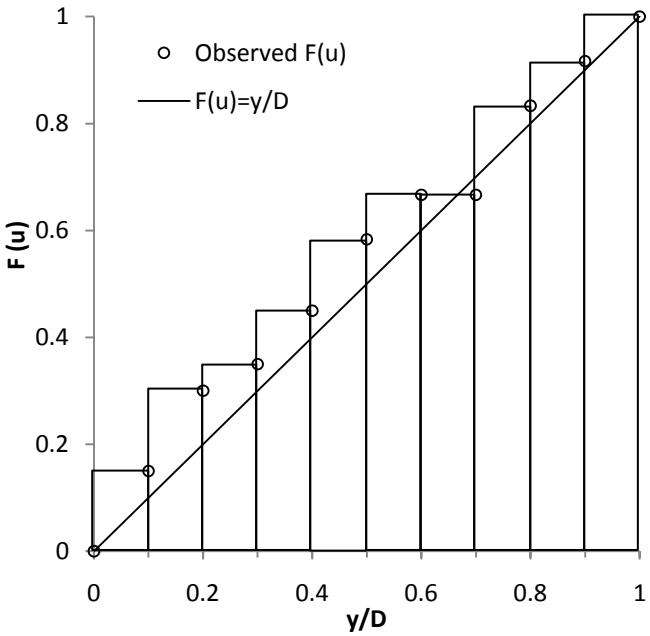

(b)

Fig. 2. continued

Fig. 1 and Fig.2 shows the cumulative probability of flow velocity almost obeys the relationship given by *y/D*; to that end 17 field velocity points and 12 experimental velocity points were examined to find this trend. The objective is to determine the probability density function of *u*, *f(u)*. This is accomplished by maximizing the Tsallis entropy of velocity, which is given below.

2.1.2. Tsallis entropy

Tsallis (Tsallis 1988; Gell-Mann and Tsallis 2004) proposed a generalized form of entropy *H*, now called Tsallis entropy, as:

$$H = \frac{1}{(m-1)}\left[1-\sum_{i=0}^{n} p_i^m\right] = \frac{1}{(m-1)}\sum_{i=0}^{n} p_i(1-(p_i)^{m-1}) \qquad (3)$$

where $p_i = p(u_i)$, $i = 1, 2, \cdots n$ or p_i, i=1, 2, …, n, are probabilities of u_i, i=1, 2, …, n; and m is a real number. Using Eq. (3), it can be known that as $m \to 1$, Eq. (3) reduces to the Shannon entropy. H is maximum for $p_i = \frac{1}{n}$ for m≥0, whereas, it is minimum for $m < 0$.

For continuous non-negative velocity (where $u = u_D, y = D$), the Tsallis entropy can be expressed as

$$H = \frac{1}{m-1}\left[1 - \int_0^{u_D} \left(f(u)\right)^m du\right] = \frac{1}{m-1}\int_0^{u_D} f(u)\left\{1 - \left[f(u)\right]^{m-1}\right\} du \tag{4}$$

2.1.3. Principle of maximum entropy

Jaynes (1957) developed the principle of maximum entropy (POME) which states that the most appropriate probability distribution is the one that has the maximum entropy or uncertainty, subject to given constraints. Accordingly, the probability distribution of the velocity should be derived, subject to given constraints, such that it maximizes the uncertainty given by entropy.

2.1.4. Specification of constraints

The flow in a channel satisfies the laws of conservation of mass, momentum and energy, and these laws can be employed to define constraints that the velocity distribution must obey. Therefore, the constraints are defined as follows. Since integration of the probability density function of velocity must always be unity, one can write:

$$C_1 = \int_0^{u_D} f(u) du = 1 \tag{5}$$

Eq. (5) can be considered to prescribe the first constraint C_1.

The second constraint C_2 can be obtained from the conservation of mass as:

$$C_2 = \int_0^{u_D} uf(u)du = u_m \tag{6}$$

where u_m is the cross-sectional mean velocity or *Q/A*, where *Q* is discharge passing through a cross-sectional area *A*.

The third constraint C_3 can be obtained from the momentum conservation as:

$$C_3 = \int_0^{u_D} u^2 f(u)du = \beta u_m^2 \tag{7}$$

where β is the momentum distribution coefficient.

The fourth constraint C_4 can be obtained from the energy conservation as:

$$C_4 = \int_0^{u_D} u^3 f(u)du = \alpha u_m^3 \tag{8}$$

where α is the energy distribution coefficient.

2.1.5. Least-biased probability distribution

In order to obtain the least biased probability distribution of *u*, *f*(*u*), the Tsallis entropy, given by Eq. (4), can be maximized, subject to Eq. (5) to Eq. (8). To that end, the method of Lagrange multipliers is employed. For $m > 0$, the Lagrange function becomes:

$$\begin{aligned} H = &\int_0^{u_D} \frac{f(u)}{m-1}\left\{1-\left[f(u)\right]^{m-1}\right\}du + \lambda_0\left(\int_0^{u_D} f(u)du - 1\right) + \lambda_1\left(\int_0^{u_D} uf(u)du - u_m\right) \\ &+ \lambda_2\left(\int_0^{u_D} u^2 f(u)du - \beta u_m^2\right) + \lambda_3\left(\int_0^{u_D} u^3 f(u)du - \alpha u_m^3\right) \end{aligned} \tag{9}$$

or

$$\begin{aligned} H = &\int_0^{u_D} f(u)\left\{\frac{1-\left[f(u)\right]^{m-1}}{m-1} + \lambda_0 + \lambda_1 u + \lambda_2 u^2 + \lambda_3 u^3\right\}du \\ &-(\lambda_0 + \lambda_1 u_m + \lambda_2 u_m{}^2 + \lambda_3 u_m{}^3) \end{aligned} \tag{10}$$

where λ_0, λ_1, λ_2 and λ_3 are Lagrange parameters. Differentiating Eq. (9) or Eq. (10) with respect to *f(u)* and equating the derivative to zero, one obtains:

$$f(u) = \left\{ \frac{m-1}{m} \left[\frac{1}{m-1} + (\lambda_0 + \lambda_1 u + \lambda_2 u^2 + \lambda_3 u^3) \right] \right\}^{m-1} \tag{11}$$

Define $\lambda_V = \lambda_0 + \frac{1}{m-1}$, Eq. (11) can be cast as:

$$f(u) = \left\{ \frac{(m-1)}{m} \left[\lambda_V + \lambda_1 u + \lambda_2 u^2 + \lambda_3 u^3 \right] \right\}^{\frac{1}{m-1}} \tag{12}$$

Eq. (12) defines the least biased probability distribution of velocity that satisfies Eq. (5) to Eq. (8) and is based on the Tsallis entropy. In this equation, parameters λ_V, λ_i, i=1, 2, 3, are determined using Eq. (5) to Eq. (8).

Substituting Eq. (12) in Eq. (4) yields the maximum Tsallis entropy as:

$$H = \int_0^{u_D} \left[\frac{m-1}{m} \left(\lambda_V + \lambda_1 u + \lambda_2 u^2 + \lambda_3 u^3 \right) \right] du \tag{13}$$

Eq. (12) is a general equation and can therefore be simplified for practical applications. Two simplifications are presented here.

2.1.6. Velocity distributions

Simplification I: It is assumed that no conservation laws are needed or specified. This means that $\lambda_1 = \lambda_2 = \lambda_3 = 0$. Eq. (12) then simplifies to:

$$f(u) = \left[\frac{(m-1)}{m} \lambda_V \right]^{\frac{1}{m-1}} \tag{14}$$

This is the simplest case and the probability obeys a uniform distribution.

Simplification II: It is assumed that the conservation of momentum and energy constraints are not needed or specified. This means that $\lambda_2 = \lambda_3 = 0$. Eq. (12) then simplifies to:

$$f(u) = \left[\frac{(m-1)}{m} \left(\lambda_V + \lambda_1 u \right) \right]^{\frac{1}{m-1}} \tag{15}$$

Eq. (14) is based on the mass conservation only.

Simplification III: It is assumed that the conservation of energy is not needed or specified. This means that $\lambda_3 = 0$. Eq. (12) then simplifies to:

$$f(u) = \left[\frac{(m-1)}{m} \left(\lambda_V + \lambda_1 u + \lambda_2 u^2 \right) \right]^{\frac{1}{m-1}} \tag{16}$$

Eq. (15) satisfies the conservation of mass and momentum.

This study considers only the second simplification, because mass conservation is most basic physical law to that must be taken into account. The second simplification is the simplest and realistic case, because Tsallis has never been applied to velocity distributions before, it is meaningful and easy to start with the simplest case. Eq. (2) has two parameters: λ_V, and λ_1 which can be determined from Eq. (5) and Eq. (6). Introducing Eq. (5) in Eq. (14), one can write:

$$\int_0^{u_D} \left[\frac{m-1}{m} (\lambda_V + \lambda_1 u) \right]^{\frac{1}{m-1}} du = 1 \tag{17}$$

After integration,

$$\left[\frac{(m-1)}{m} (\lambda_V + \lambda_1 u_D) \right]^{\frac{m}{m-1}} = \lambda_1 + \left[\left(\frac{m-1}{m} \right) \lambda_V \right]^{\frac{m}{m-1}} \tag{18}$$

Using Eq. (6), we have

$$\int_0^{u_D} u\left[\left(\frac{m-1}{m}\right)\left(\lambda_V+\lambda_1 u\right)\right]^{\frac{1}{m-1}} du = u_m \tag{19}$$

Integrating by parts, one obtains:

$$\begin{aligned}&\frac{u_D}{\lambda_1}\left[\left(\frac{m-1}{m}\right)\left(\lambda_V+\lambda_1 u_D\right)\right]^{\frac{m}{m-1}} - \frac{1}{\lambda^2}\left(\frac{m}{2m-1}\right)\left[\left(\frac{m-1}{m}\right)\left(\lambda_V+\lambda_1 u_D\right)\right.\\ &\left.+\frac{1}{\lambda^2}\left(\frac{m}{2m-1}\right)\left[\left(\frac{m-1}{m}\right)\lambda_V\right]^{\frac{2m-1}{m-1}} = u_m\right.\end{aligned} \tag{20}$$

Eq. (17) and Eq. (19) can be used to solve for λ_V and λ_1.

The objective is to derive the velocity distribution in terms of flow depth. Recalling Eq. (2) and Eq. (14), one obtains:

$$\left[\frac{(m-1)}{m}\left(\lambda_V+\lambda_1 u\right)\right]^{\frac{1}{m-1}} = \frac{1}{D}\frac{dy}{du} \tag{21}$$

Integrating of Eq. (20) leads to:

$$\left[\left(\frac{m-1}{m}\right)\left(\lambda_V+\lambda_1 u\right)\right]^{\frac{m}{m-1}} = \lambda_1\frac{y}{D}+\left[\left(\frac{m-1}{m}\right)\lambda_V\right]^{\frac{m}{m-1}} \tag{22}$$

From Eq. (22), the velocity distribution as a function of y can be obtained as:

$$u = \left(\frac{m}{m-1}\right)\frac{1}{\lambda_1}\left\{\left(\lambda_1\frac{y}{D}\right)+\left[\left(\frac{m-1}{m}\right)\lambda_V\right]^{\frac{m}{m-1}}\right\}^{\frac{m-1}{m}} - \frac{\lambda_V}{\lambda_1} \tag{23}$$

Denoting $\frac{m}{m-1}$ as k, Eq. (23) can be expressed as:

$$u = \frac{k}{\lambda_1}\left[\lambda_1 \frac{y}{D} + (\lambda_V / k)^k\right]^{\frac{1}{k}} - \frac{\lambda_V}{\lambda_1} \tag{24}$$

The velocity distribution given by Eq. (24) is based on the Tsallis entropy and is for flow in wide open channels where velocity varies with the vertical distance from the channel bed to the water surface.

2.1.7. Dimensionless velocity

The dimensionless velocity can be expressed by using shear velocity u_* as the normalizing quantity:

$$\frac{u}{u_*} = \frac{1}{u_*}\left\{\frac{k}{\lambda_1}\left[\lambda_1 \frac{y}{D} + (\lambda_V / k)^k\right]^{\frac{1}{k}} - \frac{\lambda_V}{\lambda_1}\right\} \tag{25}$$

in which u_* is the shear velocity equal to $\sqrt{gDS}$, where g is the gravitational acceleration, and S is the channel slope.

2.2. Sensitivity of parameters in Tsallis entropy based velocity distributions

The velocity distribution Eq. (24) contains four parameter which are the exponent parameter m (or k), λ_1, λ_V and D. Exponent parameter m is a real number and the feasible range of it is found to be within 0-2 and more details will be presented in the following section. Parameters λ_1 and λ_V are the Lagrange multipliers. There are several ways to estimate the parameters of the velocity distribution equation, such as the method of least squares, method of moments, maximum likelihood, and Principle of Maximum Entropy. In a steady equilibrium condition a system tends to maximize the entropy under the prevailing constraints which are described by Eq. (5) and Eq. (6). With the maximum and mean velocities known or assumed, for a fixed m, the remaining two parameters λ_1

and λ_V can be obtained by solving Eq. (17) and Eq. (19) numerically. *D* is nothing but water depth.

The water depth D, which is given or easy to measure, plays no role in the shape of the velocity curve. It will be interesting to explore variations in the characteristics of the derived velocity distribution with variations in the other three parameters. In order to evaluate the influence of a specific parameter on the velocity distribution, one parameter is examined at a time, and all the other parameters are held constant. Thus velocity was computed for different values of m, λ_1 and λ_V and is plotted in Fig. 3 to Fig. 5, respectively.

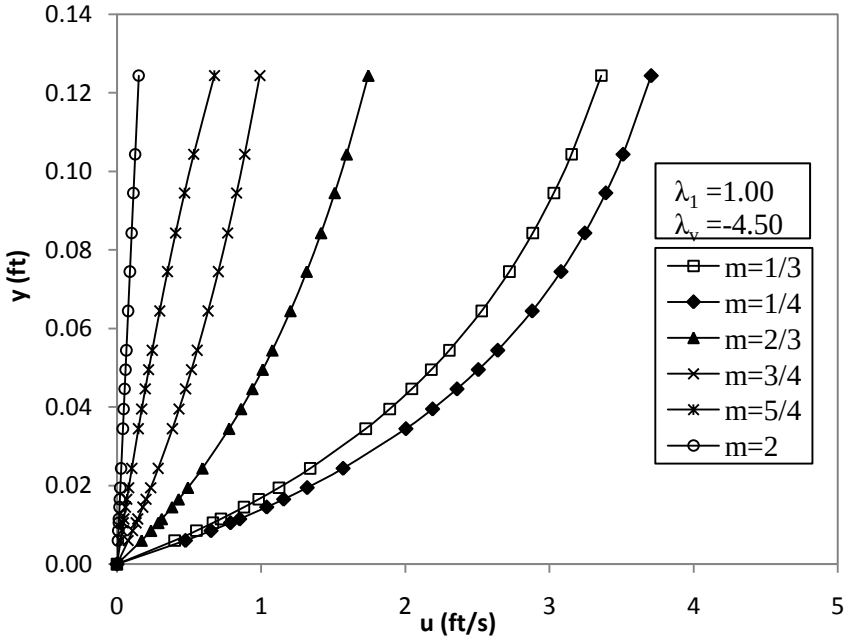

Fig. 3. Variation of *u* with *m*.

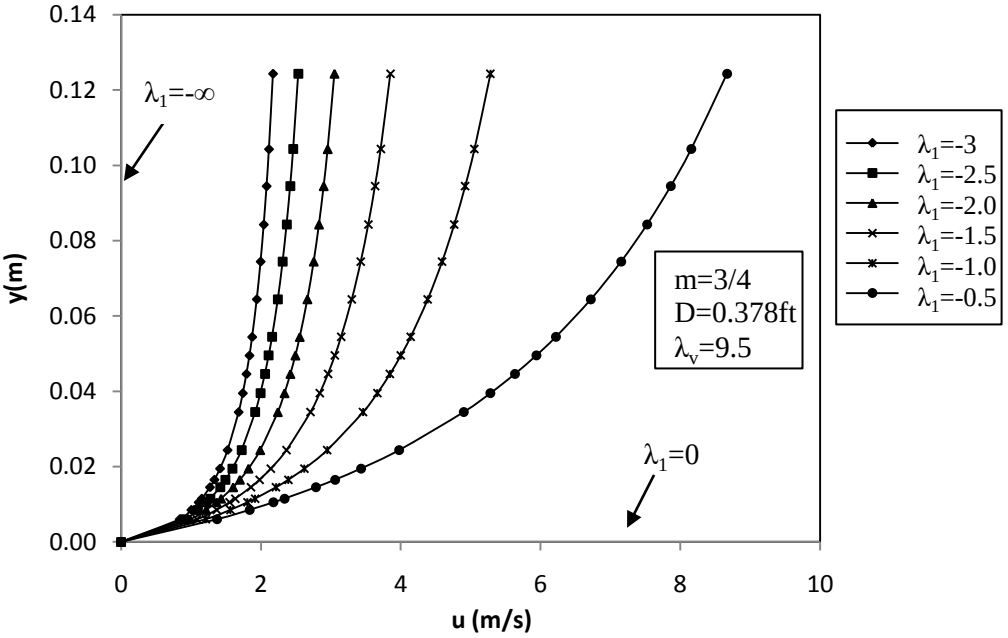

(a)

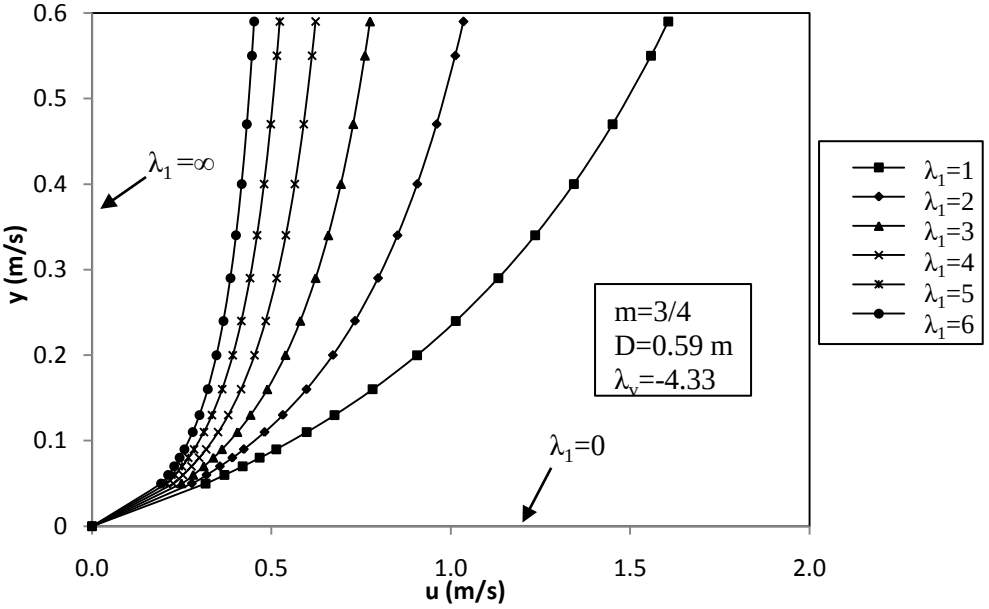

(b)

Fig. 4. Variation of u with λ_1. (a) $\lambda_1 < 0$; (b) $\lambda_1 > 0$.

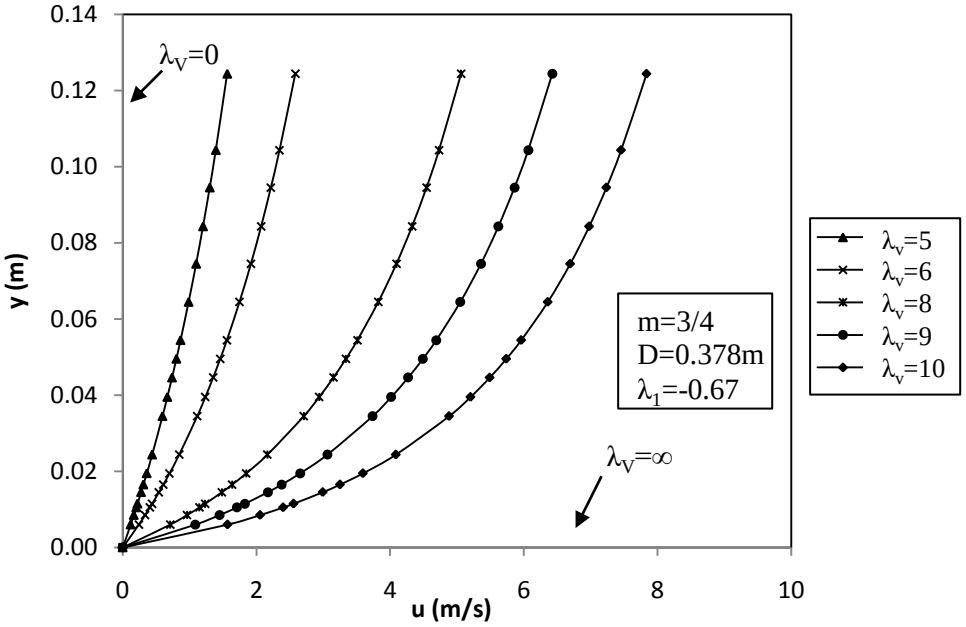

(a)

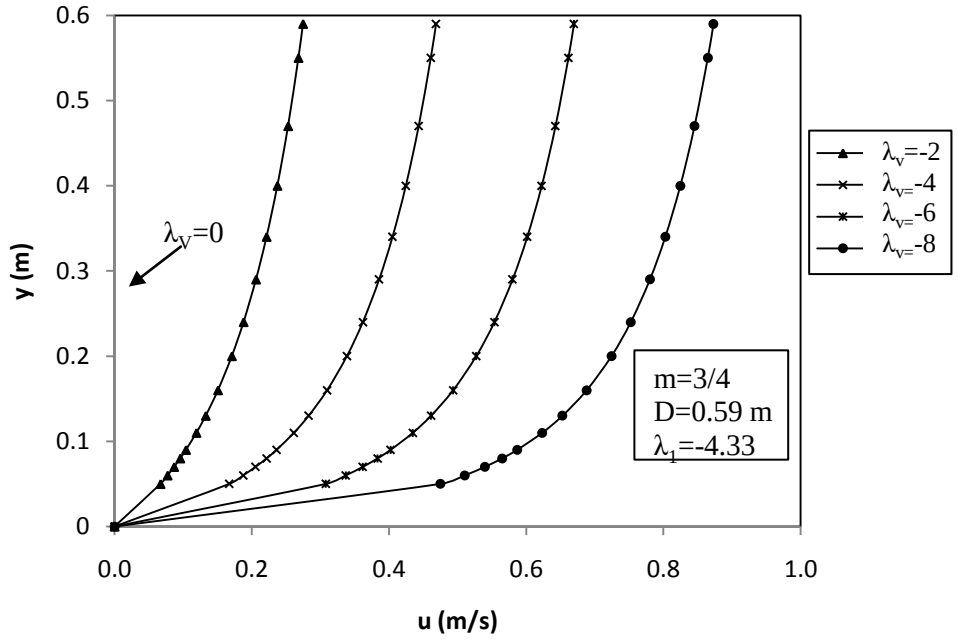

(b)

Fig. 5. Variation of u with λ_V. (a) $\lambda_V > 0$; (b) $\lambda_V < 0$.

Based on Fig. 3 to Fig. 5, we can see that the three parameters significantly influence the velocity distribution, i.e., any small change in any one of them can result in an appreciable change in the velocity distribution. In order to maximize the entropy, the exponent parameter $m > 0$ (Tsallis 1988). Further investigations showed that Eq. (17) and Eq. (19) with parameter $m > 2$ did not result in a real solution of λ_1 and λ_V, hence no good simulation can be performed. Therefore, we can narrow down the feasible range of exponent m between 0 and 2, and the velocity increases faster when m increases.

Parameters λ_1 and λ_V can be any real numbers, they are obtained from the solution of Eq. (17) and (19). To guarantee velocity as a positive quantity (i.e. $u > 0$), the two parameters λ_1 and λ_V always have opposite signs. When λ_1 is positive, the velocity goes up more slowly as λ_1 goes down; when λ_1 is negative, the velocity goes up more slowly as the absolute value of λ_1 goes down. On the other hand, if λ_V is positive the velocity increases more quickly with the increasing value of λ_V; if it is negative the velocity will increase more quickly as the absolute value of λ_V increases. Relatively, we can see by comparaing Fig. 4 and Fig. 5 that the velocity changes more dramatically with the variation of λ_1, and it seems parameter λ_1 plays a more important part in the shape of the velocity curve. It may be interesting to find out how this parameter will relate to the hydraulic characteristics of open channel flows in the following sections.

2.3. Probability distribution of dimensional and dimensionless velocity

Based on Eq. (5), take u/u_* as a new term w, the probability density function of dimensionless velocity can be derived as:

$$\int_0^{u_D} f(u)du = \int_0^{u_D/u_*} f(w)dw = \int_0^{u_D} f(u/u_*)du/u_*$$
$$f(w) = f(u/u_*) = u_* f(u) \tag{26}$$

The maximum and mean velocities sampled from the experimental data collected by Einstein and Chien (1955) and Coleman (1986), and field data collected by Afzalmehr (2008) were applied here to get the parameter values of Eq. (14). Parameters of Eq. (14) were computed and are given for different exponent parameter m values in Table 1.

Table 1 Parameters of velocity distribution and probability density function.

m	k	S4 series (Einstein and Chien 1955)		S5 series (Einstein and Chien 1955)		Iran Data 1 (Afzalmehr 2008)	
		λ_1	λ_v	λ_1	λ_v	λ_1	λ_v
		u_D=9.194 ft/s u_m=7.303 ft/s		u_D=11.42ft/s u_m=8.7ft/s		u_D=0.535 m/s u_m=0.412 m/s	
1/4	-0.33	0.672	-6.473	0.528	-6.489	1.190	-0.680
1/3	-0.50	0.746	-7.354	0.576	-7.289	1.675	-0.984
2/3	-2.00	0.712	-8.839	0.527	-8.644	4.109	-3.140
3/4	-3.00	-0.665	9.499	-0.483	9.255	4.861	-4.333
5/4	5.00	-0.864	3.218	0.672	-3.214	-10.804	-2.271
3/2	3.00	-0.273	0.505	-0.224	0.783	-15.026	0.638
2.00	2.00	0.084	-0.167	0.049	-0.106	22.585	-2.303

Table 1（*continued*）

m	k	Iran Data 2 (Afzalmehr 2008)		Run 09 (Coleman 1986)	
		λ_1	λ_v	λ_1	λ_v
		u_D=1.046 m/s u_m=0.890 m/s		u_D=1.050 m/s u_m=0.895 m/s	
1/4	-0.33	1.636	-1.742	1.651	-1.764
1/3	-0.50	2.173	-2.345	2.192	-2.373
2/3	-2.00	4.281	-5.429	4.313	-5.477
3/4	-3.00	4.799	-6.787	5.915	-7.865
5/4	5.00	12.125	-4.532	12.022	-4.482
3/2	3.00	-6.868	1.515	6.828	-1.512
2.00	2.00	7.696	-2.113	7.671	-2.122

Using Eq. (14), the probability density function of velocity was computed and is plotted in Fig. 6.

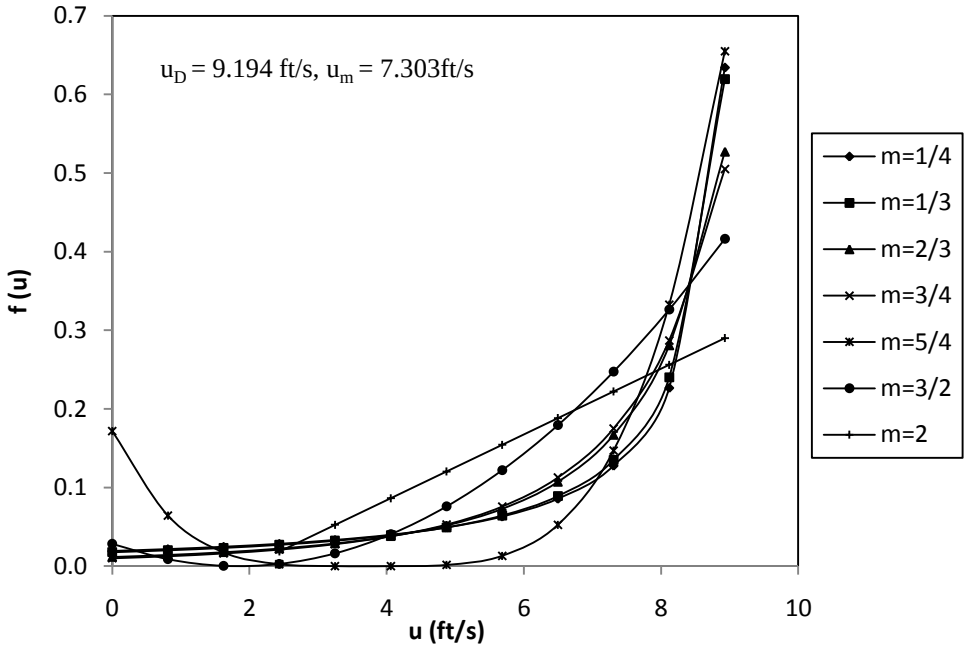

(a)

Fig. 6. Probability density functions for different datasets. (a) Data from S4 series (Einstein and Chien 1955); (b) Data from S5 series (Einstein and Chien 1955); (c) Iran data 1 (Afzalmehr 2008); (d) Iran data 2 (Afzalmehr 2008); (e) Data for Run 09 (Coleman 1986).

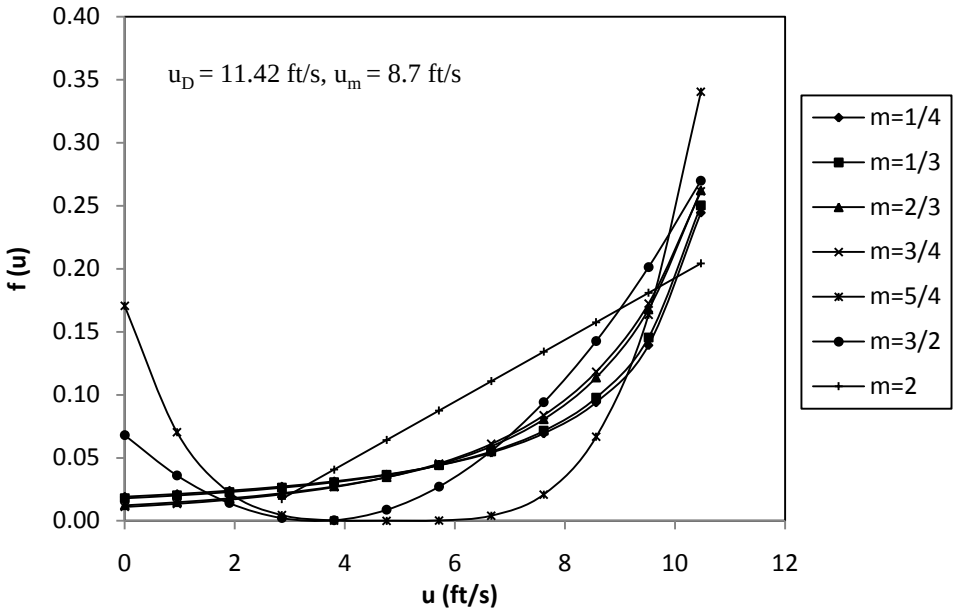

(b)

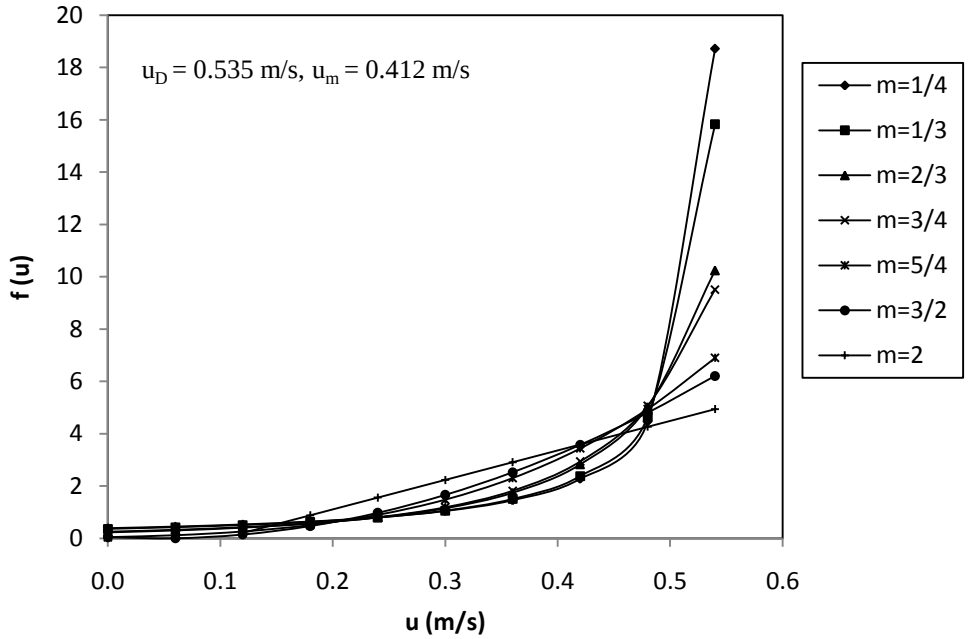

(c)

Fig. 6. continued

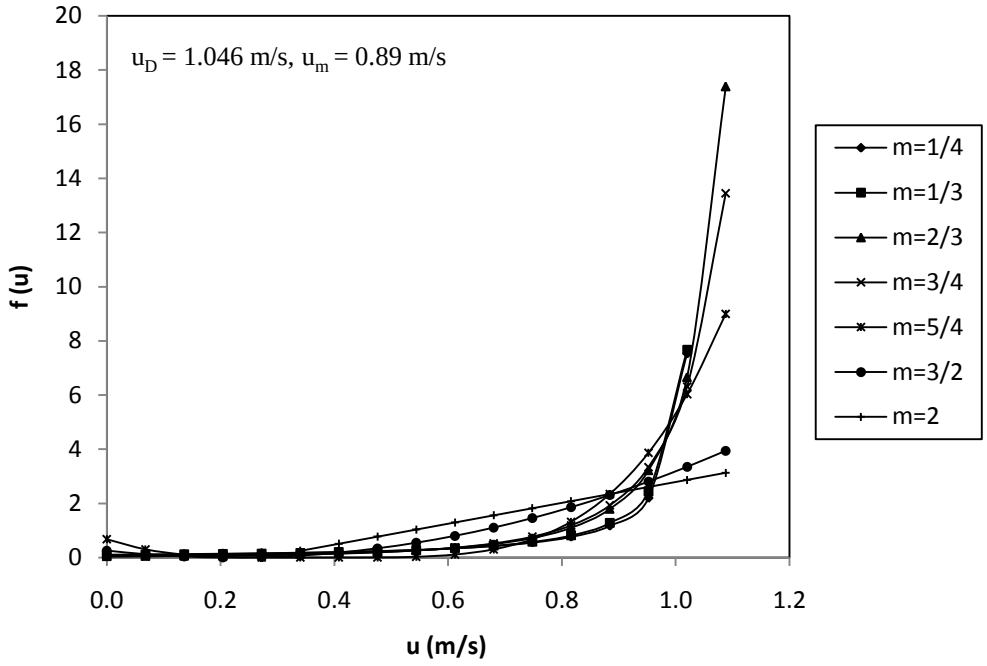

(d)

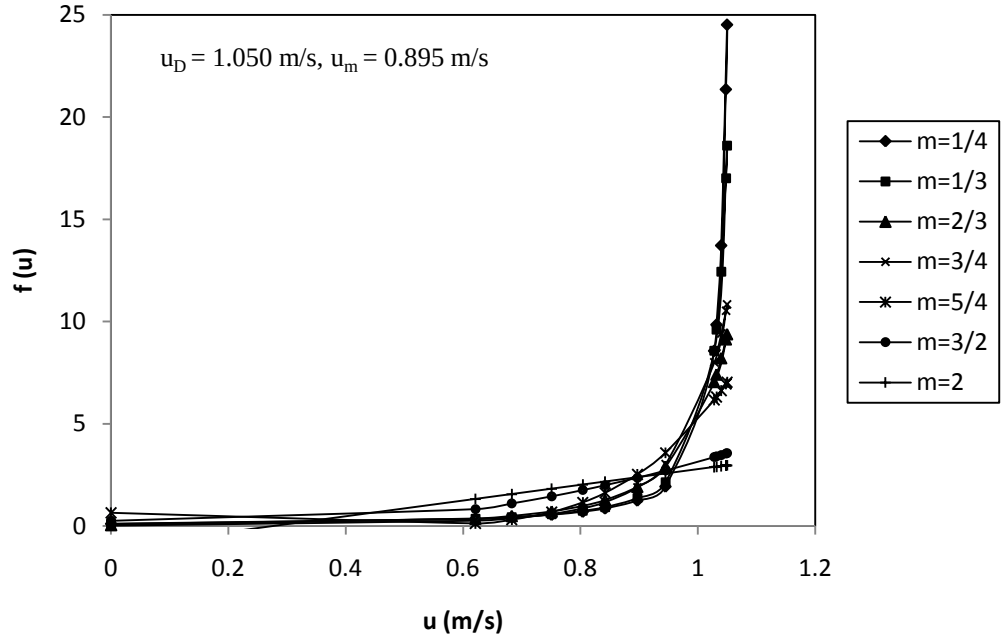

(e)

Fig. 6. continued

The corresponding probability density of dimensionless velocity is plotted in Fig. 7.

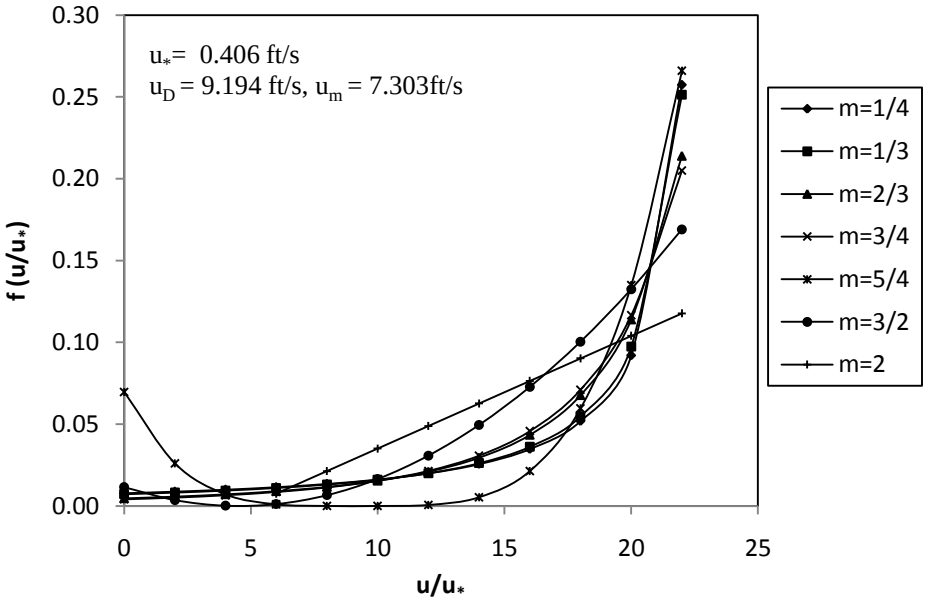

(a)

Fig. 7. Probability density functions of dimensionless velocity for different datasets. (a) Data from S4 series (Einstein and Chien 1955); (b) Data from S5 series (Einstein and Chien 1955); (c) Iran data 1 (Afzalmehr 2008); (d) Iran data 2 (Afzalmehr 2008); (e) Data for Run 09 (Coleman 1986).

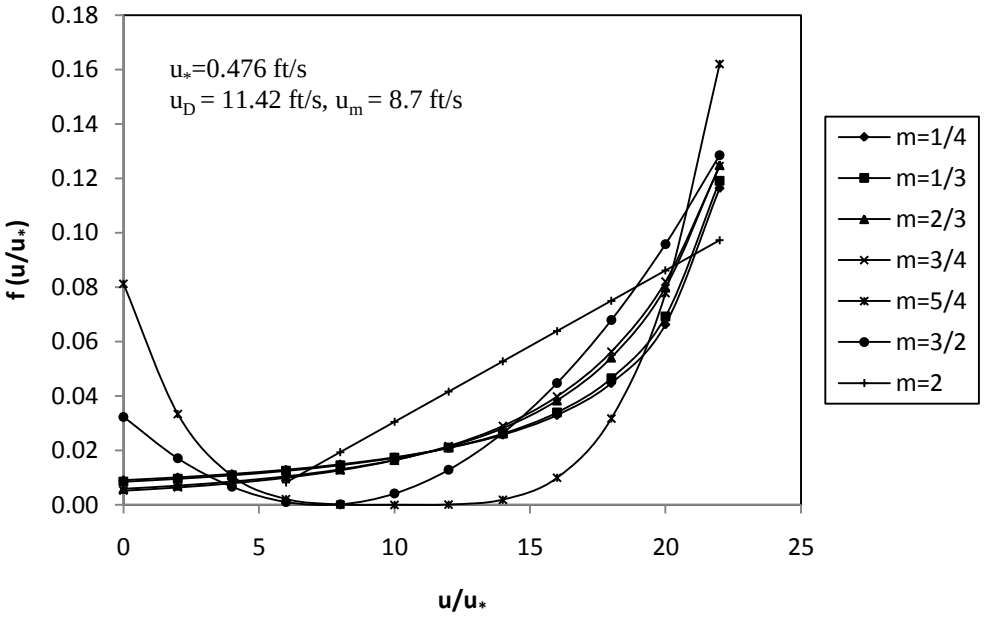

(b)

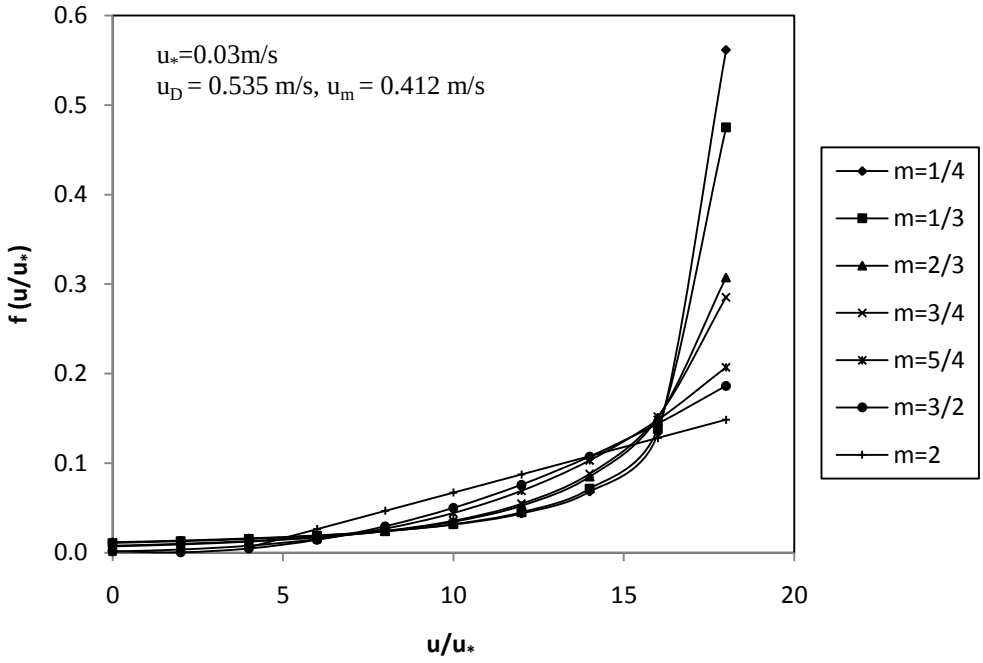

(c)

Fig. 7. continued

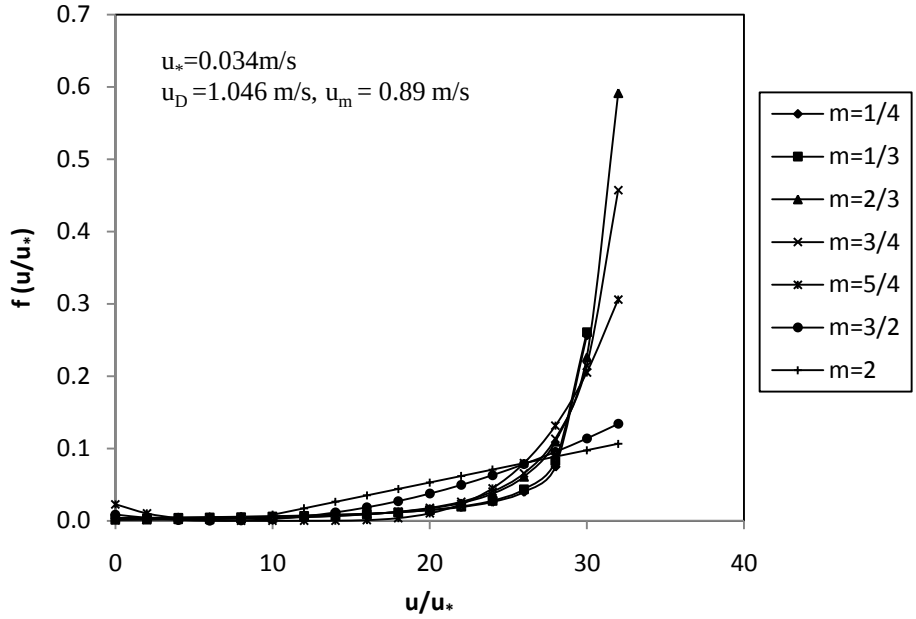

(d)

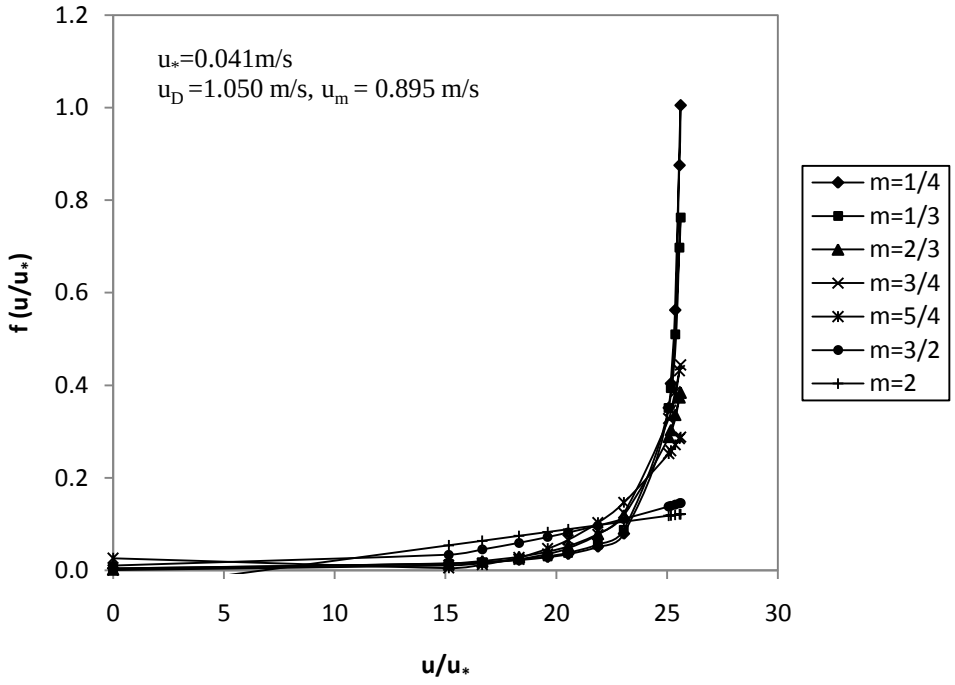

(e)

Fig. 7. continued

As we can see from Fig. 6 and Fig. 7 with the mean and maximum velocities given, the probability density function varies with the change of exponent parameter m, sometimes dramatically as shown in Fig. 6(a), Fig. 6(b), Fig. 7(a) and Fig. 7(b) . For the four sets of data, when *m* is within 0 to 1, as low as 1/4 and as high as 3/4 the probability density functions are all monotonically increasing against the velocity which corresponds with the previous observations that the probability density is not very sensitive to *m*. On the other hand, when *m* is larger than one, the plots do not show this trend steadily. As sown in Fig. 7(a) and (b), for *m*= 5/4 and 3/2 the probability density goes down with the increase of the velocity when the velocity is small which corresponds to the lower part of flows. When *m* tends to be its upper limit 2, the probability density turns to be a linear line, the simplest case which may make a simplification of the velocity equation possible so it may be interesting to further analyze this case in further research. Above all the variation of probability density with parameter *m* implies that overall the velocity distribution will not change dramatically with the change of parameter *m* within its possible range, the main differences will focus on the part close to channel bed and more details will be found out in the following sections.

2.4. Testing of Tsallis entropy based 1-D velocity distribution with different *m*

The reliability of Eq. (23) as a velocity distribution has been tested with experimental data collected by Einstein and Chien (1955) and field velocity data collected on rivers from Iran. The accuracy of velocity distribution equations can be investigated by evaluating the errors ε, defined as flows:

$$\varepsilon = \frac{u_{es} - u_{ob}}{u_{ob}} \tag{27}$$

in which u_{es}= velocity estimated using velocity equations, u_{ob}=observed velocity.

There is one parameter *m* in the Tsallis entropy based 1-D velocity equation that is required to be taken into account. For a given set of observed values or with the maximum and mean velocities given, there can be different sets of parameters based on the parameter *m* we choose. In order to numerically and visually compare which *m* value gives the best velocity simulation, parameters in the velocity equation are determined for different *m* values with the maximum and mean velocities given, and the corresponding velocity distributions are calculated. Parameters of the velocity distribution equation are given in Table 1. The Iran data were observed for the whole flow depth and so they are good to first test the overall performance of the derived equation in the full flow depth as shown in Fig. 8. The corresponding dimensionless velocity is also plotted, because there was some parameter estimation involved in the computation of dimensionless velocity, so it may be desirable to plot the actual velocity profile first.

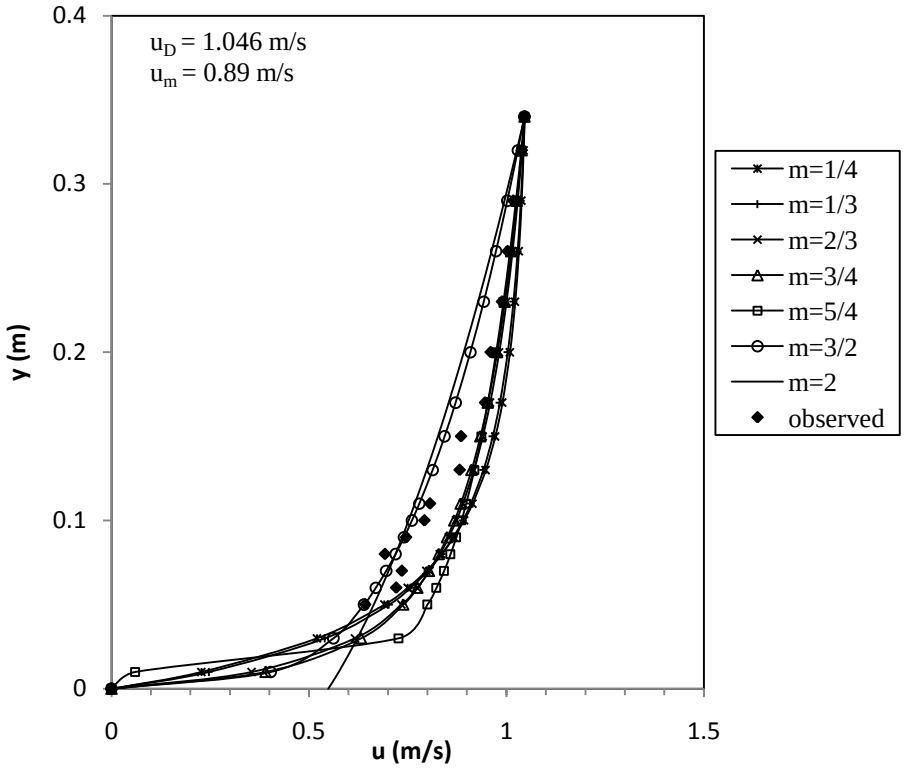

(a)

Fig. 8. Velocity profiles over the whole water depth for Iran Data 2. (a) velocity; (b) dimensionless velocity.

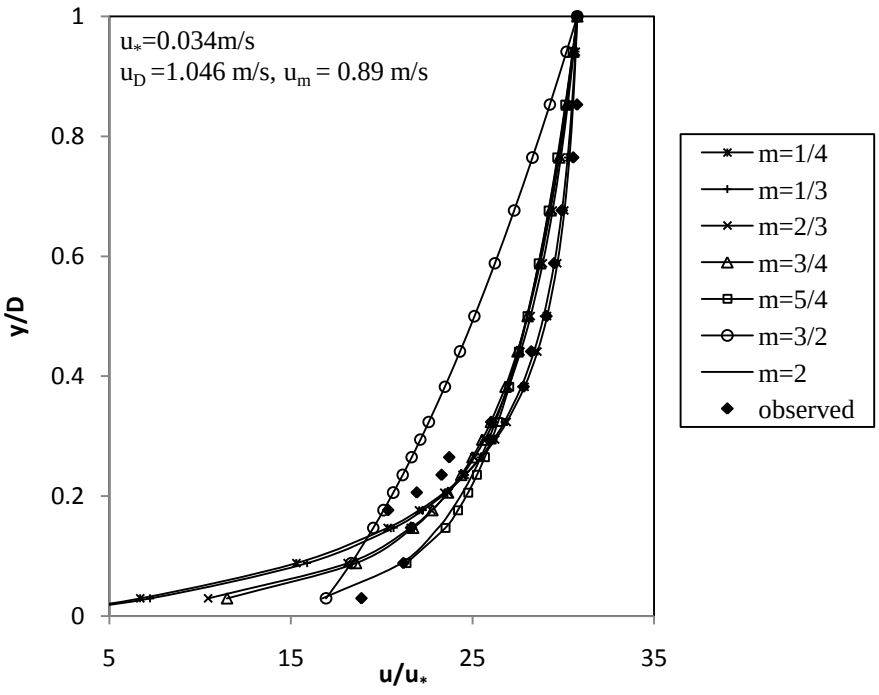

(b)

Fig. 8. continued

Generally, the velocity distribution given by Eq. (23) gives a good estimation of velocity for the whole water depth. But when $m>1$, plots begin to deviate from observed values, especially in the lower part of the water depth. It seems the probable value of m should be within 0 to 1. For m in this range, there are little differences between the plots based on different m values, whereas the estimation with $m=3/4$ is the closet to the observed values. The mean error ($\mu(\varepsilon)$) is found very close to zero and equal to 0.051 while the standard deviation ($\sigma(\varepsilon)$) is 0.096. To verify the value of m parameter, it is necessary for us to examine the performance of the velocity distribution close to the channel bed. The velocity distribution very close to the channel bed which is under the

influence of both sediment concentration (if sediment laden flow) and channel bed is always difficult to measure and hence is of great importance. Einstein and Chien (1955) used experimental methods to take measurements of velocity very close to the channel bed for different types of flow. Observations for S4 series were chosen here to show how the new velocity distribution works when it is very close to channel bed as shown in Fig. 9.

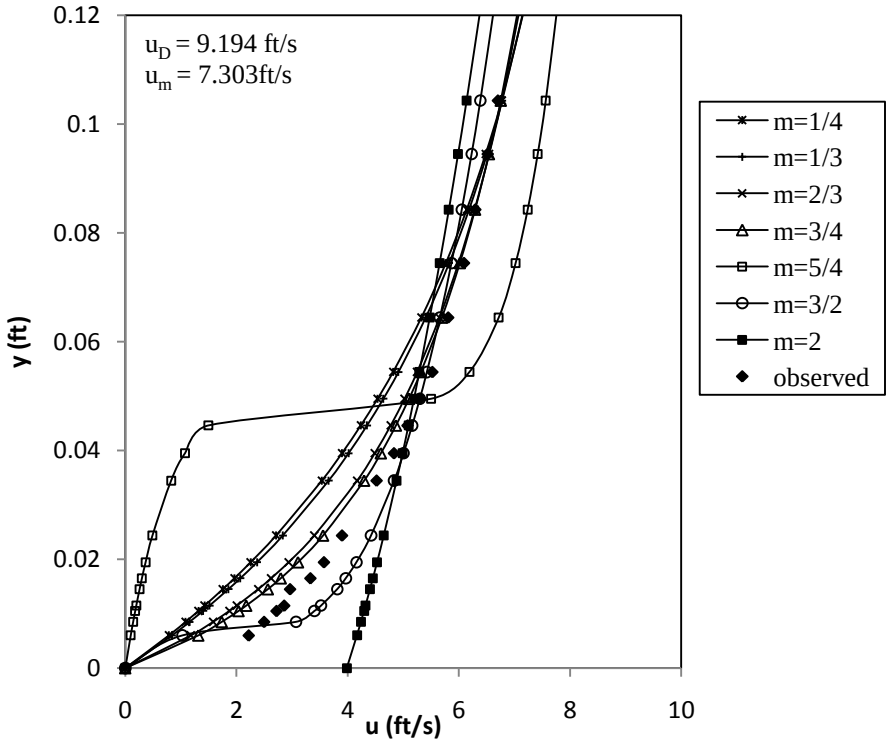

(a)

Fig. 9. Velocity distribution close to channel bed for S4 series.

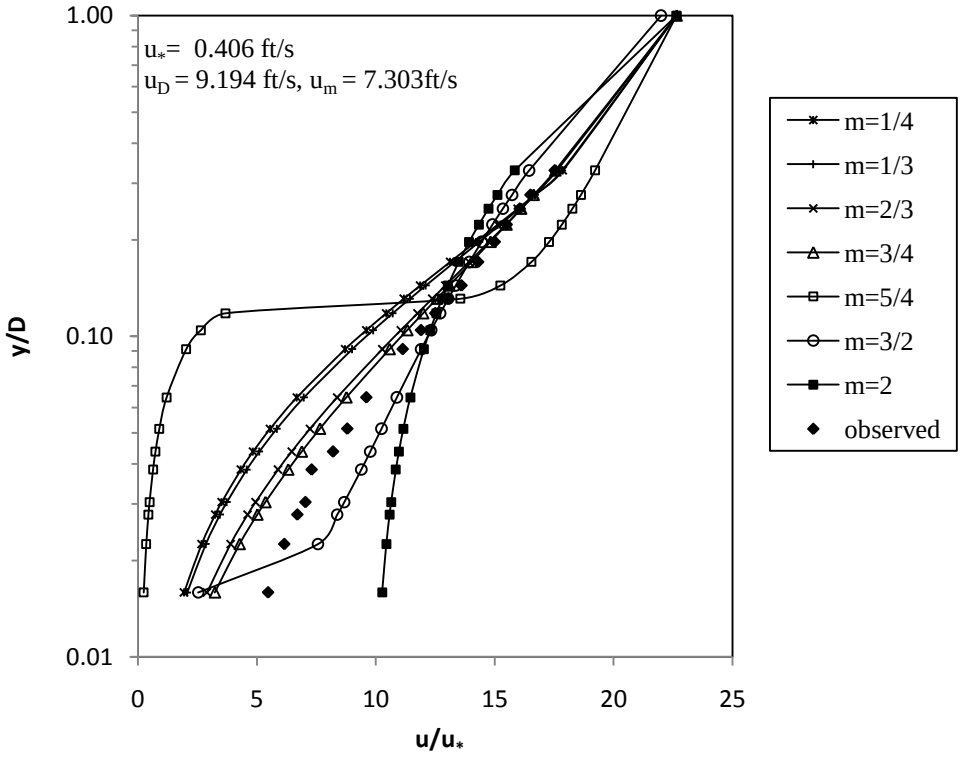

(b)

Fig. 9. continued

Table 2 shows the mean and standard deviation of the error given by Eq. (27) considering Eq. (23) for estimating velocity with different *m* for S4 series.

Table 2 Mean, μ(ε), and standard deviation, σ(ε), of error given by Eq. (27) considering Eq. (23) for estimating velocity with different *m.*

	m=1/4	*m*=1/3	*m*=2/3	*m*=3/4	*m*=5/4	*m*=3/2	*m*=2
μ	-0.247	-0.227	-0.131	-0.097	-0.457	0.122	0.186
σ	0.213	0.203	0.142	0.101	0.512	0.183	0.307

Based on the above computations and graphs, the possible range of *m* is from 0 to 2, but further testing shows that the values larger than 1 do not lead to stable performance. As seen from Fig. 8 and Fig. 9, in the region very close to channel bed, the plots with *m* values greater than 1 are not in agreement with the basic hypothesis that the velocity goes gradually up along the water depth and also exhibits a big gap with the observed values. On the other hand, the m values within the range between 0 and 1, as low as 1/4 and with the upper limit 3/4, and yield good predictions. Within this small range of *m*, a small change in m values does not make an appreciable difference in the plot. Overall *m*=3/4 gives the best prediction with the mean error (μ(ε)) as -0.097 (Table 2). Hence the following computations used *m*=3/4. In order to clearly see how good the velocity equation with *m*=3/4 works, the velocity was computed in comparison with two sets of observations and also the probability densities. The results are tabulated in Tables 3 and 4.

Table 3 Tsallis entropy based computed velocity in comparison with Einstein and Chien Data 1.

y	u (ft/s)		ε
(ft)	Computed	Observed	(%)
0.00	0.000	0.000	0.000
0.01	1.314	2.221	40.845
0.01	1.736	2.497	30.486
0.01	2.038	2.720	25.085
0.01	2.176	2.858	23.874
0.01	2.565	2.964	13.468
0.02	2.797	3.329	16.000

Table 3 (*continued*)

y (ft)	u (ft/s)		ε
	Computed	Observed	(%)
0.02	3.107	3.573	13.039
0.02	3.558	3.898	8.718
0.03	4.296	4.519	4.922
0.04	4.597	4.831	4.855
0.04	4.868	5.075	4.080
0.05	5.102	5.298	3.697
0.05	5.315	5.522	3.738
0.06	5.695	5.806	1.915
0.07	6.017	6.090	1.199
0.08	6.291	6.293	0.033
0.09	6.541	6.516	-0.372
0.10	6.754	6.699	-0.819
0.12	7.125	7.113	-0.171
Mean(μ(ε))			-9.703
Standard deviation (σ(ε))			10.10

Table 4 Tsallis entropy model based computed velocity in comparison with Iran Data 2.

y (m)	u (m/s)		ε
	Computed	Observed	(%)
0.01	0.390	0.512	23.768
0.03	0.632	0.540	-17.004
0.05	0.739	0.642	-15.009
0.06	0.775	0.721	-7.465
0.07	0.804	0.735	-9.368
0.08	0.829	0.692	-19.690
0.09	0.850	0.746	-13.921
0.10	0.868	0.792	-9.561
0.11	0.884	0.807	-9.625

Table 4 (*continued*)

y (m)	u (m/s)		ε
	Computed	Observed	(%)
0.13	0.912	0.882	-3.406
0.15	0.934	0.885	-5.527
0.17	0.953	0.946	-0.756
0.20	0.977	0.960	-1.713
0.23	0.996	0.989	-0.736
0.26	1.012	1.003	-0.933
0.29	1.026	1.017	-0.899
0.32	1.039	1.039	-0.001
0.34	1.046	1.046	-0.024
Mean(μ(ε))			5.114
Standard deviation (σ(ε))			9.622

The computed results were plotted against Iran data 2 in Fig. 10

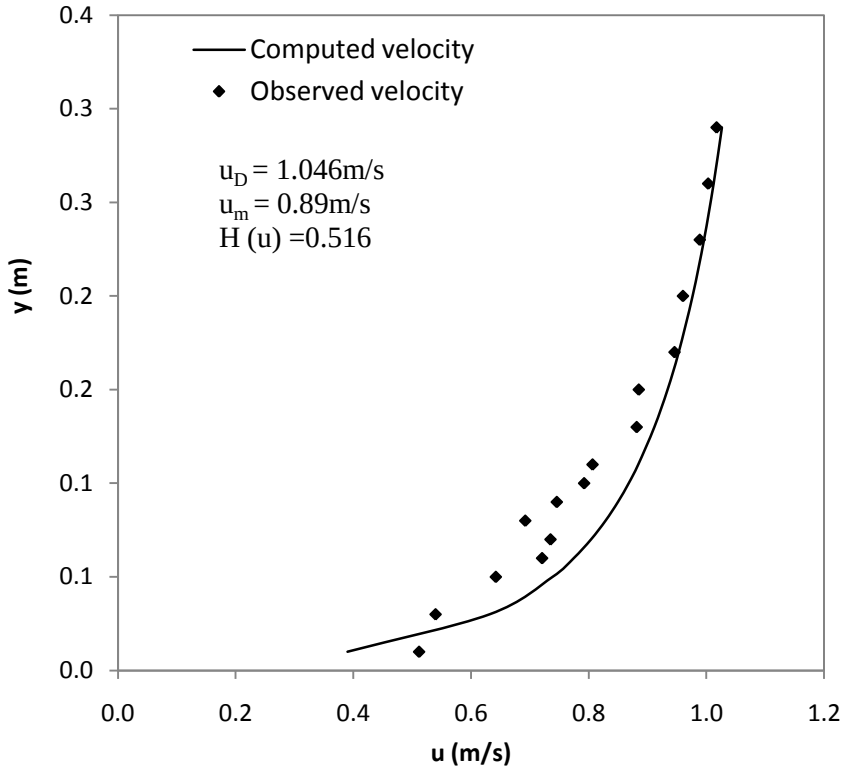

(a)

Fig. 10. Tsallis entropy based computed velocity in comparison with observed data (Iran Data 2) for the whole water depth and probability density function computed through Eq. (15) and observations.

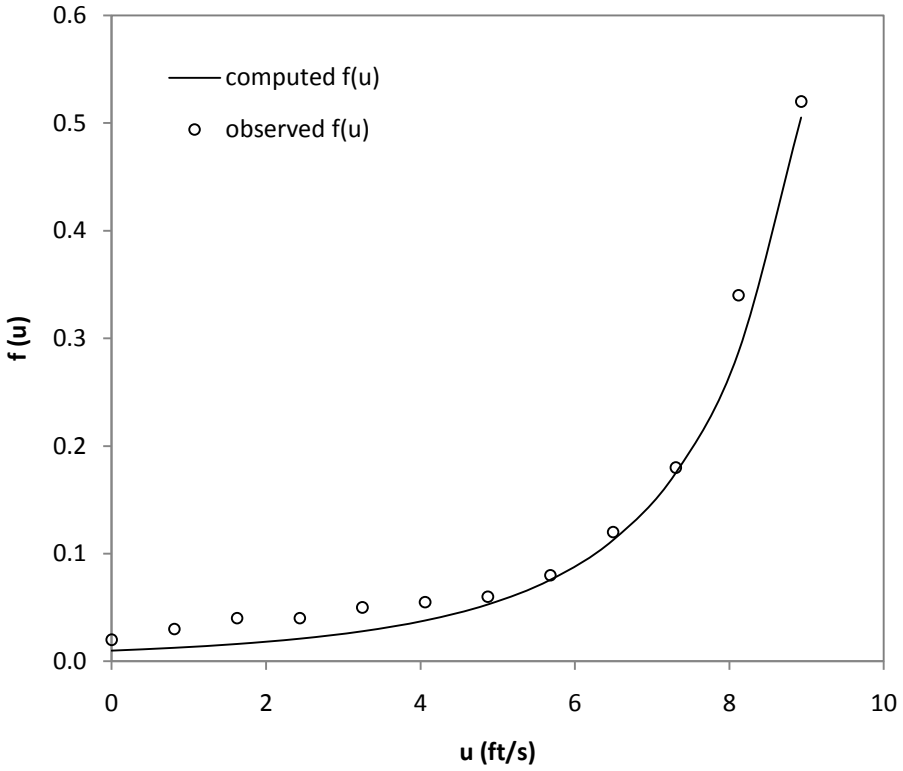

(b)

Fig. 10. continued

The computations were plotted against Einstein and Chien Data 1 in Fig. 11.

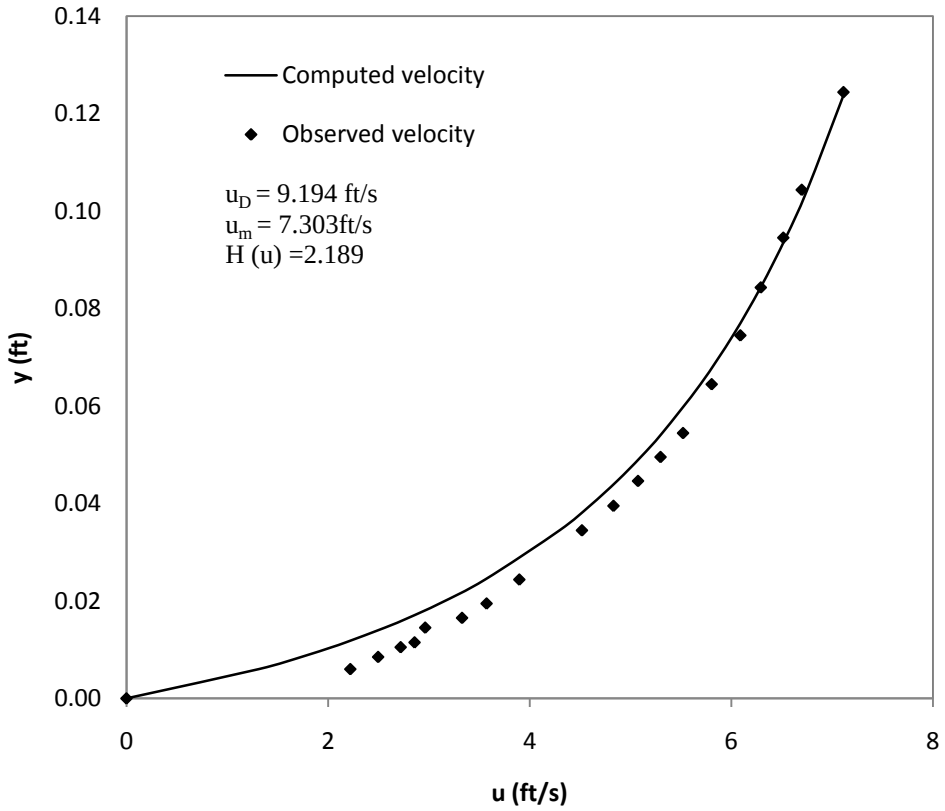

(a)

Fig. 11. Tsallis entropy based computed velocity in comparison with observed data (Einstein and Chien Data 1) near channel bed and probability density function computed through Eq. (15) and observations.

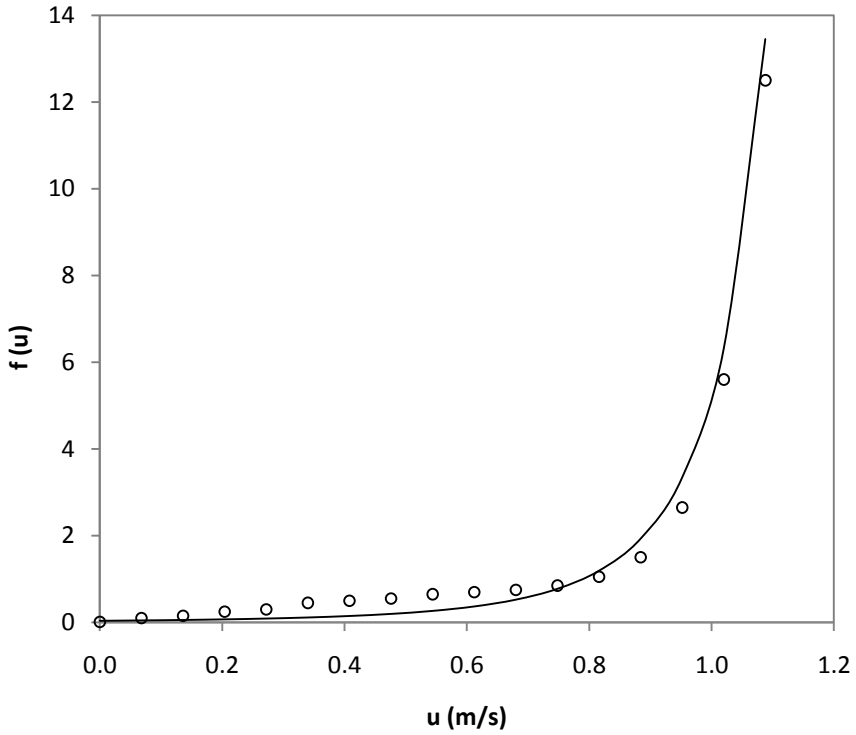

(b)

Fig. 11. continued

With the velocity distribution law as given by Eq. (23), velocity measurements between the channel bed and water surface according to a uniform density function $p(y)=1/D$ (i.e., the velocity in each distance dy has an equal probability of being measured) should result in a set of velocity data distributed according to the density function given by Eq. (14). This means that greater values of velocity have greater probabilities of getting measured. An experimental scheme based on an inspection of Fig. 10 and Fig. 11 would concentrate on the measurements on u_D, the maximum value of u. This is a great advantage made possible by the validity of Eq. (23) over the full range of

y from zero to D, such that the data points stay on or very close to the regression line based on Eq. (23), including the point where u=0 and y=0 even in sediment laden flows. These results indicate the sampling scheme depends on the mathematical models of the velocity and its underlying probability distribution to be used, and that applications of Eq. (23) greatly simplifies the velocity measurements.

2.5. Applications to different kinds of flows

2.5.1. Effects of sediment concentration near the bed on the velocity distribution

Since the turbulence which keeps the sediment in suspension is generated essentially at the bed, the local high sediment concentration naturally plays an important part in molding the turbulence pattern, resulting in a completely different flow as compared with that in clear water. It is imperative that the effects of heavy sediment concentration near the bed on the velocity distribution should be considered. The experimental data collected by Einstein and Chien (1955) which include velocity and sediment data from flows ranging from zero to heavy sediment concentration, over channel beds formed by coarse, medium, or fine sand was used here. The data include velocities measured very close to the channel bed. The relatively wide range of sediment concentrations, among other factors, makes the data attractive for the study. The validity of Eq. (23) was tested by actual data as shown in Fig. 12.

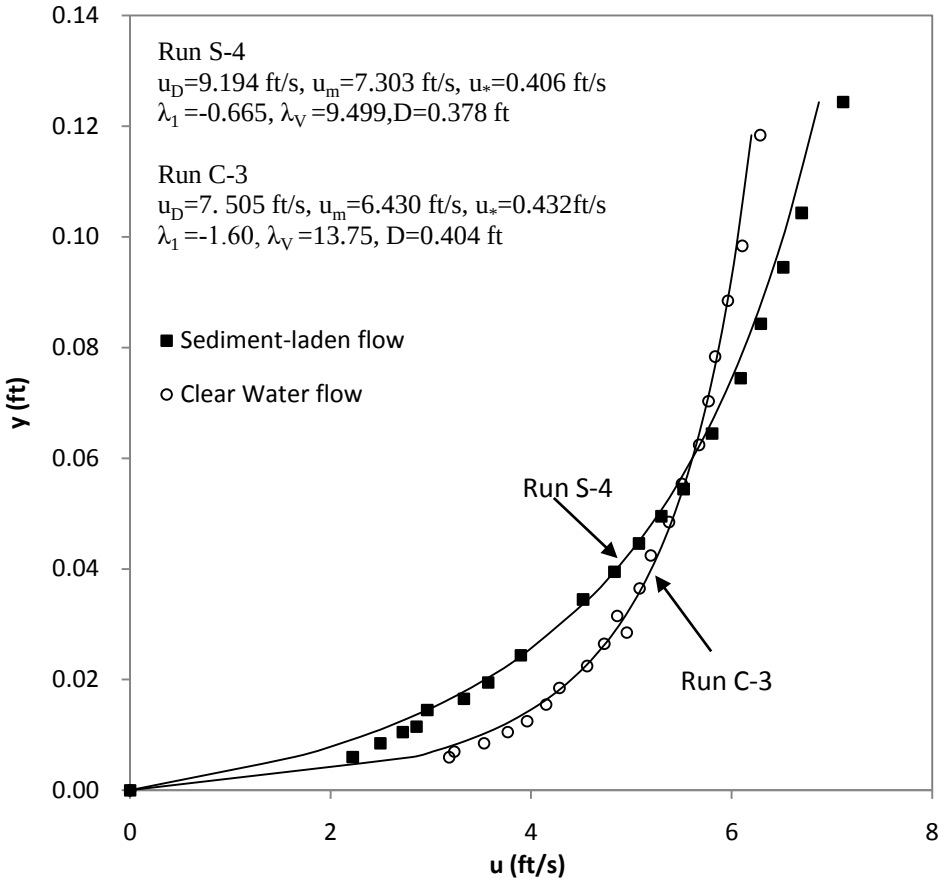

Fig. 12. Applicability of Eq. (23) near the bed in flows with and without sediments.

Eintein and Chien (1955) concluded that the sediment-laden flow can be divided into two different zones. One near the bed where both the sediment concentration and concentration gradient are large, and the other, the main part of the flow where either the sediment concentration is small, or the sediment are of such minute sizes that they do not interfere with the flow. Fig. 12 shows the validity of Eq. (23) in describing the velocity distribution near the bed in a flow of heavy sediment concentration as well as a clear water flow. The errors found in the two cases have an absolute value that did not exceed

0.45. The mean errors were 0.097 and 0.017, respectively while the standard deviation was not larger than 0.1 (also see in Table A1 and A3), respectively. The superiority of Eq. (23) is especially conspicuous near the bed. Though the errors were minor, more errors were fund in the sediment laden flow which also implicated the strong effect of sediment concentration played on velocity distribution.

2.5.2. Effects of suspended sediment on the open channel velocity distribution

River flows are part of the general class of bounded shear flows. Landweber (1953) and Coles (1956) have shown that in bounded shear flows the boundary layer above the viscous sublayer is composed of a near-boundary inertial region in which the velocity profile corresponds closely to a logarithmic equation, and a second region further from the boundary where the velocity profile gradually deviates, displaying velocities higher than those predicted by the logarithmic equation. This outer region has been termed the wake region by Coles (1956). The relative thickness of the inertial and wake regions appears to be related to the level of turbulence in the outer part of the boundary layer and in the free stream. Coleman presented the effect of suspended sediment on the velocity profiles by describing the behavior of the various terms in the complete boundary layer velocity profile equation in response to changes in suspended sediment concentration. First, Coleman measure velocity in clear water and then gradually added sediment. He measured the changes in the velocity field and in the sediment concentration distribution in the flow. Flow depths varied between 16.8 and 17.4 cm, and the channel width, W, is 35.6, giving an aspect ratio of around 2.

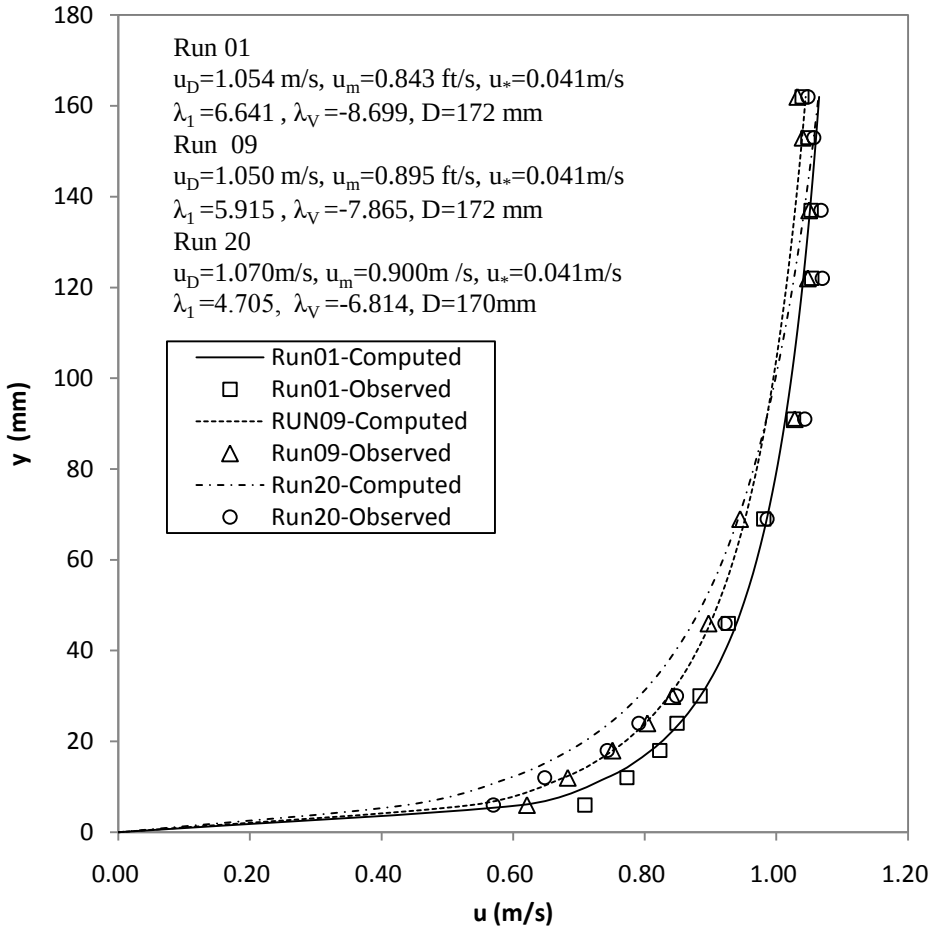

Fig. 13. Velocity profiles with different suspension sediment concentration from experimental series with 0.105 mm sand. Run 01: Q_S= 0 kg; Run 09: Q_S= 7.27kg; Run 20: Q_S= 17.27 kg.

Fig. 13 compares the clear water control velocity profiles and the velocity profiles with the medium sediment suspension and the capacity suspension comprising the beginning, the middle and the end of the series of experiments with 0.105-mm sand.

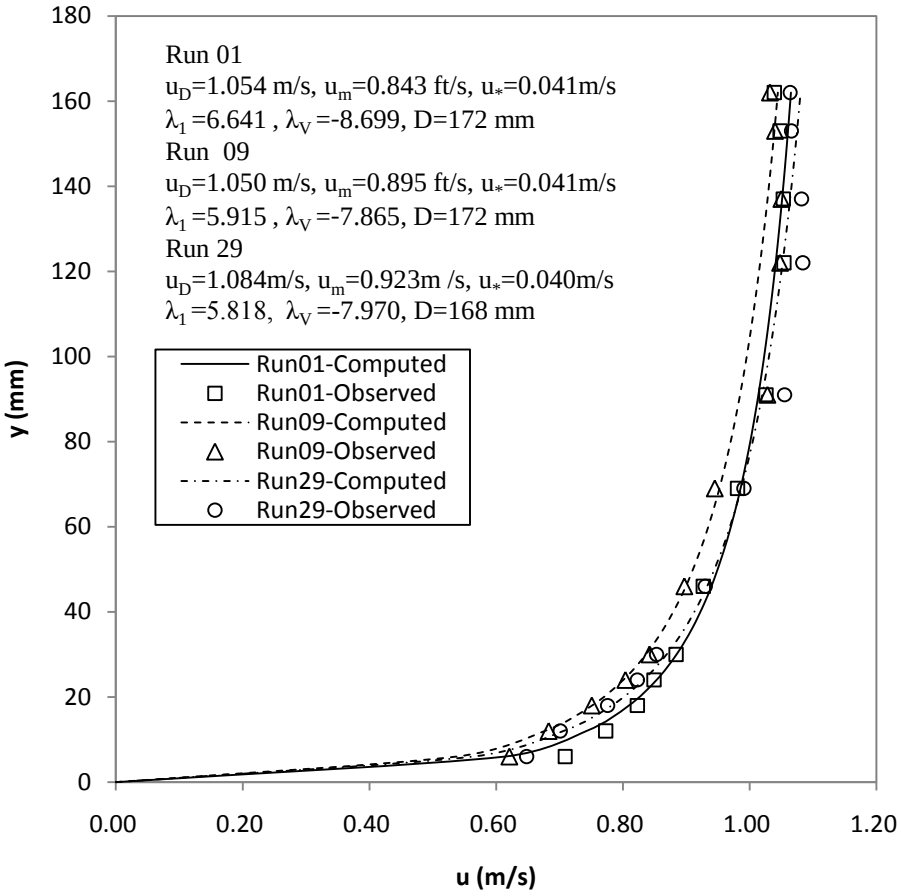

Fig. 14. Clear-water control velocity profile in comparison with velocity profiles with Q_S= 7.27kg with different particle size. Run 01: clear water; Run 09: D50= 0.105 mm; Run 29: D50= 0.210 mm.

Fig. 14 compares the clear water control velocity profiles and the velocity profiles with the same sediment suspension but different particle size.

The results obtained from the Eq. (23) for different profiles are compared with Coleman's (1986) experimental data and the errors are tabulated in Table 5.

Table 5 Mean, μ(ε), and standard deviation, σ(ε), of error given by Eq. (27) considering Eq. (23) for estimating velocity for flows with or without sediment. (Also see in Table A6 to A9).

	Run 01	Run 09	Run 20	Run 29
μ	-0.013	-0.019	-0.060	-0.012
σ	0.042	0.040	0.061	0.041

The mean errors and standard deviations are not substantially different for Run 01, Run 09 and Run 29 when the suspended sediment concentration did not change much, while the maximum errors happened in Run 20 with the maximum sediment concentration. Therefore, through this error analysis we can confirm the effect of sediment concentration on the velocity distribution. Parameters are also shown in the figure for different sediment concentration. With the increase of the sediment concentration the value of λ_1 decreased from Run 01 to Run 20, the similar trend can be found through Run 01 to Run 29, with the same sediment concentration λ_1 is almost the same. The advantage of Coleman's experiments is that the whole range of concentration up to the capacity transport could be covered with no stationary sand bed in the flume, while the virtual origin of the velocity profile remained at the flume channel bottom. Any tiny changes observed in velocity profiles could be attributed to increases in suspended sediment concentration alone and not to other factors such as changes in

channel roughness. The experiments were repeated with two sands with D_{50} of 0.105mm and 0.210mm. Apparently, the effect of the suspended sediment is to decelerate the flow in the high-concentration region near the channel bed. Continuity of mass then requires a compensating acceleration in the upper part of the flow (Coleman 1981, 1986). In the near-bed region, the sediment concentration is very high and eddy viscosity is increased when compared with clear water flow. Fig.13 and Fig. 14 show that the presence of suspended sediment causes a general reduction in the mean flow velocity and that the magnitude of this velocity reduction is positively related to the sediment size. In a free surface region, velocity profiles show little difference between measured and computed values.

2.5.3. Applicability in unsteady flows

The preceding discussion is all about steady flow or cases where time-averaged velocity can represent the flow quantity. Unsteady flows are those whose properties depend also on time if referenced to an Eulerian frame. In natural rivers most of the flows are unsteady. However, unsteady phenomena are worth studying only if they depart substantially from quasi-steady state, or if treated with steady flow theory, significant errors would arise, such as flows in mountain streams characterized by steep slopes and gravel beds.

In the past, some experiments had been carried out to study unsteady flow in open channels, for example, at the University of Canterbury, New Zealand, and at the EPFL, Switzerland. The researchers at these two institutions were concerned mainly with bedload transport in unsteady flow. Recently, Tu and Graf (1992) examined friction in

unsteady flow over gravel beds. Fig. 15 compared the computations with the measurements (Tu and Graf 1992) to test the performance of the Tsallis entropy based velocity distribution in unsteady case.

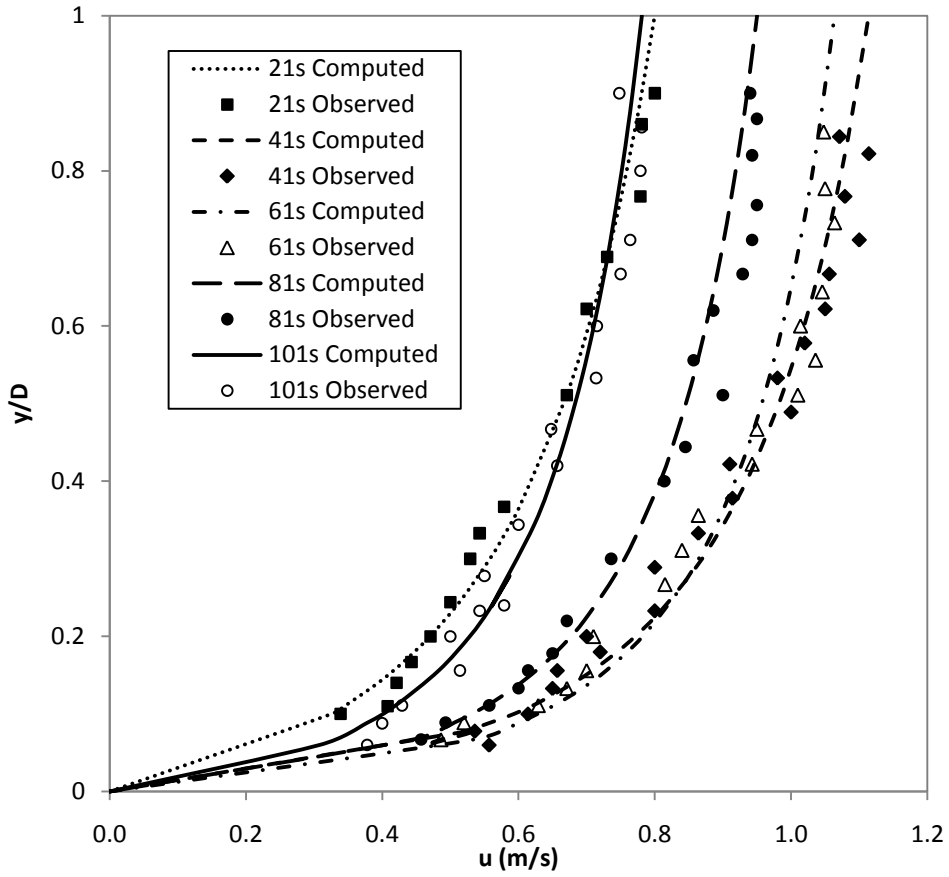

Fig. 15. The computed and observed evolution of vertical velocity profiles.

The evolution of the vertical velocity profiles during the passage of hydrograph NS 1(1), for several different time instants, is shown in Fig. 15. The velocity distributions at t=21s, 41s, 61s, 81s and 101s, being each 20 seconds apart, are selected here for

presentation. The corresponding hydraulic parameters and the parameters for Tsallis entropy based velocity distributions are summarized in Table 6.

Table 6 Hydraulic and Tsallis entropy based model needed parameters for the velocity profiles during the passage of hydrograph NS1 (1).

t (s)	D (cm)	u_{max} (m/s)	u_m (m/s)	λ_1	λ_V
21	12.2	0.800	0.606	3.359	-4.639
41	20.1	1.114	0.905	3.601	-5.946
61	20.7	1.064	0.889	4.293	-6.399
81	18.7	0.950	0.782	4.330	-5.936
101	15.5	0.781	0.628	4.475	-5.292

Table 7 Mean, $\mu(\varepsilon)$, and standard deviation, $\sigma(\varepsilon)$, of error given by Eq. (27) considering Eq. (23) for estimating velocity in unsteady flows. (Also see in Table A10 to A14).

	t =21s	t =41s	t =61s	t =81s	t =101s
μ	0.014	0.016	0.029	0.002	0.001
σ	0.111	0.081	0.077	0.058	0.086

As we can see from Fig. 15, during the passage of the hydrograph the velocity profiles tend to return towards the original shape. The data from unsteady flows over gravel bed and the previous data from steady open channel with flow with clear water or suspended sediment over smooth or rough bed can be simulated by Tsallis entropy based velocity distribution equations. The accuracy was verified using error analysis as shown in Table 7. As in Table 7, the errors for different time periods did not exceed 0.029,

while the maximum value of the standard deviation was about 0.111. More details can be found in Table A10 to A14.

2.6. Maximum entropy

Based on Eq. (12) with one constraint, the entropy can be determined by integration as:

$$H(u) = -4 \times \left\{ 1 - \frac{3}{2\lambda_1} \left[\left(\frac{1}{3(\lambda_V + \lambda_1 u_D)} \right)^2 - \left(\frac{1}{3\lambda_V} \right)^2 \right] \right\} \tag{28a}$$

and the maximum entropy of dimensionless velocity can be determined as

$$H(u/u_*) = -4 \times \left\{ 1 - \frac{3}{2u_*^{\frac{1}{4}}\lambda_1} \left[\left(\frac{1}{3(\lambda_V + \lambda_1 u_D)} \right)^2 - \left(\frac{1}{3\lambda_V} \right)^2 \right] \right\} \tag{28b}$$

Fig. 16 gives the relation between the entropy and u_D plus another important parameter λ_1, the equation relating entropy to u_D and λ_1 obtained from the regression analysis. 13 sets of data were investigated here, 2 of them are from Iran (Afzalmehr 2008), 8 are collected by Einstein and Chien (1955) and the other three are from Coleman's (1986) experimental data.

$$H = -0.67\lambda_1 + 2.12 \tag{29}$$

$$H = 3.50u_D + 0.95 \tag{30}$$

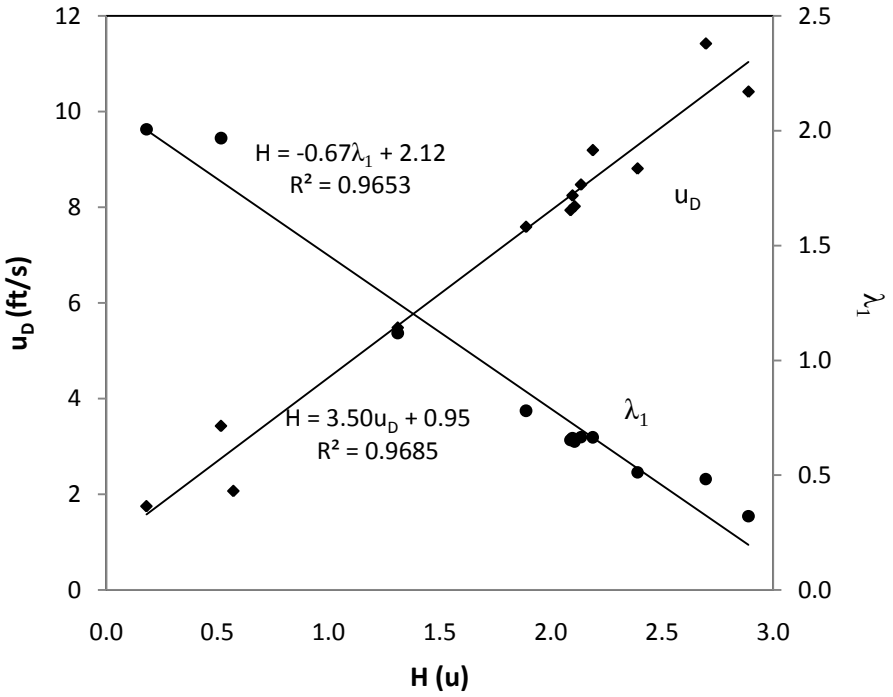

Fig. 16. Relation of *H(u)* to u_D and λ_1.

Based on the analysis, it is shown that parameter λ_1 can be taken as a new hydraulic parameter that can be used to characterize and classify open channel flows under the effects of both the coarseness of bed material and the sediment concentration. The data points in Fig. 16 at lower values of λ_1 and hence higher values of entropy represent flows over coarser channel beds and or with higher levels of sediment concentration. The considerably wide range of λ_1 in clear-water flows manifests the marked trend of λ_1 to decrease with the coarseness of bed material. For sediment-laden flows, the data points reflect the effects of both the coarseness of bed material and the sediment concentration. The high correlation coefficient R computed for λ_1 obtained from data and values of λ_1 given by the Eq. (29), indicates a high level of goodness of fit, hence, the strength of the

linear relation between λ_1 and H. Also plotted in Fig. 16 are the values of entropy H against u_D, in which u_D is the maximum velocity which happens at the water surface; physically the larger u_D and in turn H is, the more complexity is involved in the flow, the more likely the flow tends to be turbulent flow, hence, more uncertainty can be expected which is expressed as a linear relation.

3. 2-D VELOCITY DISTRIBUTION

3.1. Importance of 2-D velocity distribution model

The existing velocity distribution equations that are described in the 1-D case section are, however, applicable only to wide channels in which the velocity is assumed to increase monotonically in the vertical direction from the channel bed to the water surface. For flow in channels that are not wide with low aspect ratios that are < 7 and for most of the stream flow especially during flood events, they cannot be regarded as general or universal laws governing velocity distributions in open channels, since the velocity in an open channel cross section tends to vary also in the transverse direction, and the maximum velocity may occur below the water surface. Moreover, the maximum velocity usually occurs beneath the water surface during flood periods. The higher the water stage is, the deeper the location of maximum velocity (Chen and Chiu 2004). The fact that the maximum velocity may occur below the water surface is an important feature of open channel flows, and has attracted a great interest among civil engineers for at least 100 years (Stearns 1883). Even in a large river, such as Mississippi River, the maximum velocity occurs as much as one-third of the water depth below the water surface (Gordon 1992). The location of maximum velocity is linked to the ratio of the mean and maximum velocities, velocity distribution parameter, location of mean velocity, and probability density function underpinning a velocity distribution equation derived by applying the probability and entropy concepts. To determine the location and magnitude of maximum velocity, a velocity distribution equation is needed that is capable of describing all types of velocity distribution patterns, with maximum velocity

occurring on or below the water surface. To treat it analytically, a two-dimensional (2-D) analysis of velocity distribution is needed to deal with the geometry of isovels (lines of equal velocity) in a cross section. Applying probability concepts, Chiu and Chiou (1986) developed a technique that can be used to simulate velocity in rectangular open channels for any given set of values of discharge rate, slope, roughness, and width-to-depth ratio. All the work using the entropy concept reported in the literature has been done using Shannon Entropy. As a generalization of the Shannon entropy, the Tsallis entropy is applied for the first time to simulate the 2-D velocity distribution in this study.

There are regularities in open channel flows that, if detected, analyzed, and properly understood, can be used as the basis to simplify data collection and improve flow forecasting, and design and control of engineering systems. The regularities are natural laws governing flows, and their detection can be aided by theoretical analysis. Chiu and Said (1995) reported that nature maintains a constant ratio of mean to maximum velocities at a given section by adjusting the velocity distribution and the channel geometry and is invariant with time and discharge. Its relationship with the others in turn leads to the formation of a network of related constants characterizing regularities in open channel flows that can be used to ease discharge measurements and other tasks in hydraulic engineering. Applying the Tsallis entropy the related regularities have been investigated and a new entropy parameter M is introduced to facilitate the interpretation of relationship between different quantities.

The work presented here includes: (1) derivation by entropy maximization of an equation for two-dimensional velocity distribution in a channel cross section, which is

valid regardless of the location of maximum velocity; (2) derivation of equations for the location (on a vertical) of mean velocity in a channel cross section; (3) derivation of other equations, based on the maximum entropy principle, that can be used to provide additional descriptions of velocity distribution; and (4) investigation of a parameter of the entropy function, a new hydraulic parameter, which is a key to understanding and controlling open channel flows. The method can be applied in both high and low flows in rivers. Available laboratory flume and stream-flow data are used to illustrate the accuracy and reliability, and results show that this method can quickly and accurately estimate flow velocity.

3.2. Derivation of 2-D velocity distribution in open channel cross sections

In an open channel which is not "wide", the (time-averaged) velocity varies in both the vertical (y) and transverse (z) directions (Chiu and Lin 1983). The isovels curve up towards the water surface under the effects of, among other factors, the two sides of the channel. In modeling the velocity distribution it is, therefore logical first to transform the Cartesian y- and z- coordinates into another coordinate system, say, the s-r coordinate system, in which r has a unique, one-to one relation with a value of velocity, and s (coordinate) curves are their orthogonal trajectories. The idea of using the s-r coordinates is similar to that of using the cylindrical coordinates in studying flows in a pipe. The term u (time averaged velocity) is almost zero along an isovel that has an r value equal to r_0, which has a small value representing the channel bed (including the bottom and sides). In addition, u is u_{max}, the maximum values of u, at r equal to r_{max}, which may occur on or below the water surface. The velocity u increases monotonically

with the spatial coordinate r from r_0 to r_{max}, although it may not increase monotonically with y, the elevation from the channel bed. Therefore, Chiu (1987, 1989) expressed the function of velocity cumulative probability distribution in a channel cross section as:

$$F(u) = \int_0^u f(u)du = \frac{r - r_0}{r_{\max} - r_0} \tag{31}$$

Analogous to the derivation of 1-D velocity distribution, and the probability density function can be defined using Eq. (31) as:

$$f(u) = \frac{dF(u)}{du} = \frac{dF(u)}{dr}\frac{dr}{du} = [(r_{\max} - r_0)\frac{du}{dr}]^{-1} \tag{32}$$

With the probability density function given by Eq. (14), the velocity distribution, using one constraint, can be expressed as:

$$u = (\frac{m}{m-1})\frac{1}{\lambda_1}\left\{\left(\lambda_1 \frac{r - r_0}{r_{\max} - r_0}\right) + \left[(\frac{m}{m-1})\lambda_V\right]^{\frac{m}{m-1}}\right\}^{\frac{m-1}{m}} \tag{33}$$

By defining r in terms of coordinates in the physical plane, Eq. (31) and Eq. (33) can describe one- or two-dimensional velocity distributions. Eq. (31) indicates that $(r - r_0)/(r_{\max} - r_0)$ is equal to the cumulative distribution function, or the probability of velocity being less than or equal to u. Therefore, to identify an expression for r, the probability concept is needed. If a large number of r values are randomly generated within the range (r_0, r_{max}) and substituted into Eq. (33) to obtain a set of velocity samples, the probability of velocity being between u and $u+ du$ is $p(u)du$. Under such a concept, $(r - r_0)/(r_{\max} - r_0)$ is equivalent to the ratio of the area in which the velocity is less than or equal to $u(r)$ to the total cross-sectional area. For example, for a wide

$(r-r_0)/(r_{max}-r_0)$ =*(By)/(BD)* =*y/D*, where *B* is channel width, *D* is flow depth, and *y* is vertical distance from the channel bed. For an axially symmetric flow in a circular pipe, in which isovels are concentric circles, $(r-r_0)/(r_{max}-r_0)=1-r^2/R^2$, where *r* is radial distance from the pipe center; and *R* is pipe radius (Chiu et al. 1993). In such a way, $(r-r_0)/(r_{max}-r_0)$ may be defined to suit flows in various channels and conduits. In both cases r_0=0; r_{max}=1; and hence, $(r-r_0)/(r_{max}-r_0)=r$. Equations of $(r-r_0)/(r_{max}-r_0)$ for two-dimensional velocity distributions in the open channels are shown in Fig. 17.

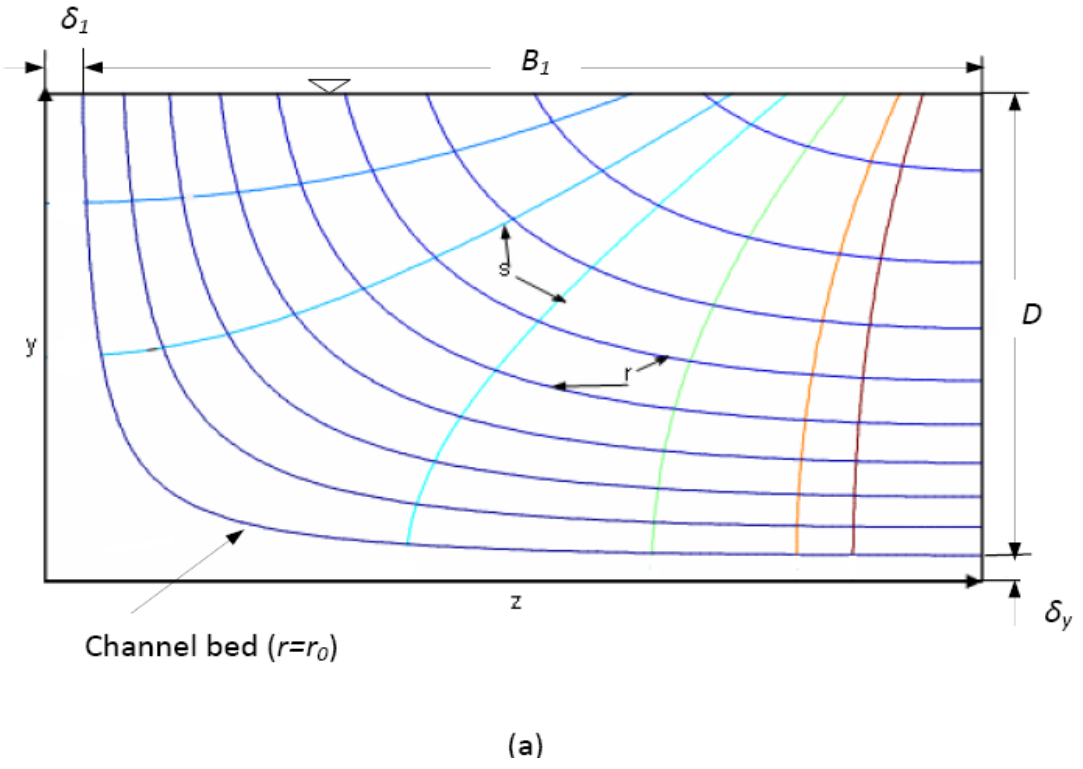

Fig. 17. Velocity distribution and curvilinear coordinate system. (a) *h*>0 and (b) *h*<0.

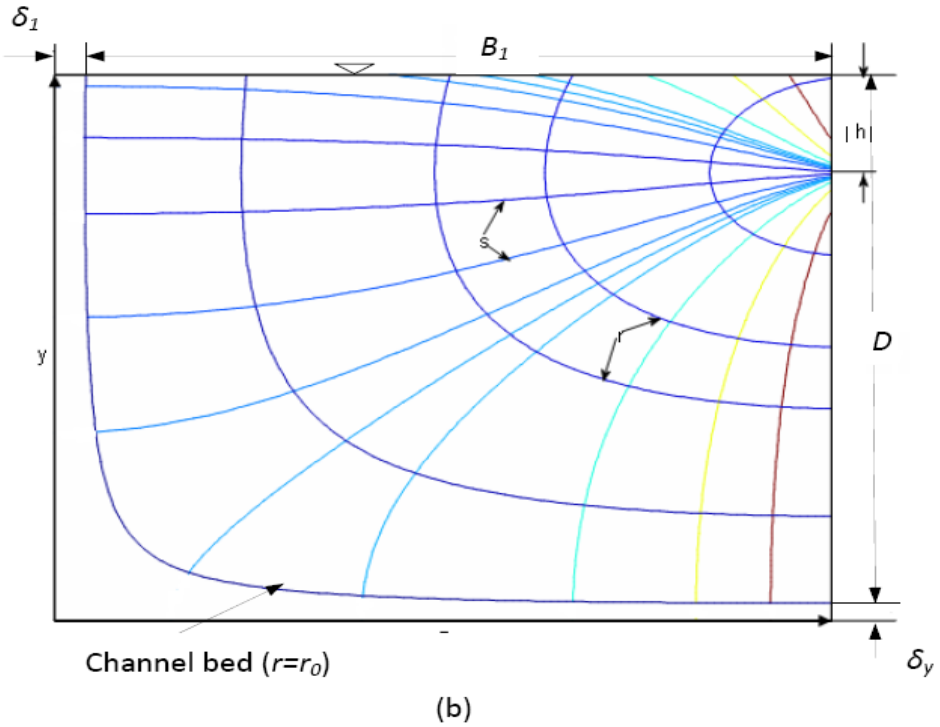

Fig. 17. continued

The following equations proposed by Chiu and Chiou (1986) are found to be suitable for the orthogonal curvilinear coordinates *r*-*s*.

$$r = Y(1-Z)^{\beta_i} \exp(\beta_i Z - Y + 1) \tag{34}$$

in which

$$Y = \frac{y + \delta_y}{D + \delta_y + h} \tag{35}$$

and

$$Z = \frac{|z|}{B_i + \delta_i} \tag{36}$$

Eq. (34) represents a family of isovels. Each isovel has a value of *r*. The channel bed itself is an isovel on which $r = r_0$. In Eq. (34) – Eq. (36), as shown in Fig. 17, *y* = the vertical coordinate measured from the channel bed along the *y* – axis, which is defined as the special vertical that passes through the point where the maximum velocity in the channel cross section occurs; *D* is the water depth at the y-axis; *z* is the coordinate in the transverse direction; B_i for *i* equal to either 1 or 2 is the transverse distance on the water surface; and $h, \delta_y, \delta_i,$ and β_i are parameters characterizing the isovel geometry. Among these parameters δ_y, δ_i approach zero, if the channel cross section tends towards the rectangular shape. They increase as the cross-sectional shape deviates from the rectangular. Parameter *h* controls the shape and slope of isovels, especially near the water surface and in the vicinity of the point of maximum velocity. *h* may vary from *–D* to +∞. If *h*<0, u_{max} occurs below the water surface and $|h|$ is the depth of u_{max} below the water surface; and, along the *y*-axis, velocity increases with *y* only up to *y=D-h*, and decreases with *y* in the region, *(D+h)* < *y* ≤ *D*. If *h* ≥ 0, u_{max} occurs at the water surface. If *h*=0, isovels are perpendicular to the water surface. If *h*>0, *h* is a parameter that can be used to fine-tune the slope of isovels. If the magnitude of h is very large, isovels are parallel horizontal lines such that velocity varies only with y and *r* approaches *y/D*. Such a situation tends to occur in very wide channels. The *s* curves shown in Fig. 17 are orthogonal trajectories of *r* curves, that can be derived from Eq. (34) as:

$$s = \pm \frac{1}{Z}\left(|1 - Z|\right)^{\beta_I \left[(D+\delta_Y + h)/(B_I + \delta_I)\right]^2} \exp\left[Z + \beta_i \left(\frac{D + \delta_y + h}{B_i + \delta_i} \right)^2 Y \right] \qquad (37)$$

in which s takes on the negative sign only when $y > D+h$ and $h<0$. In other cases, s takes on the positive sign. The network of r-s curves can be used as a coordinate system in modeling two-dimensional velocity and shear–stress distributions and related processes (Chiu and Chiou, 1986).

3.3. Determination of the y-axis

The y-axis, on which the maximum happens, is in the center of a channel cross section, if the section is in a straight reach and has a symmetrical shape. If a cross section a nonerodible channel has a symmetrical shape but is in a curved reach, the maximum velocity in it and, hence, the y-axis occur closer to the inner bank (Yen 1965). At a section in a curved reach of an erodible channel, however, the maximum velocity and y-axis occur closer to the outer bank. In any case, the location of y-axis can be ascertained by measured velocity distributions. The velocity data applied to determine the discharge that can be used to plot the isovels in the cross-section reveals the location of the y-axis (Z_y). The position of Z_y in a natural channel can be located anywhere in the cross-section. Fig. 18, plotted using conventional velocity data, shows isovel patterns of an open channel and indicates the position of Z_y, which is very stable and invariant with time, discharge and gauge height if the channel bed does not change drastically (Chen and Chiu 2004).

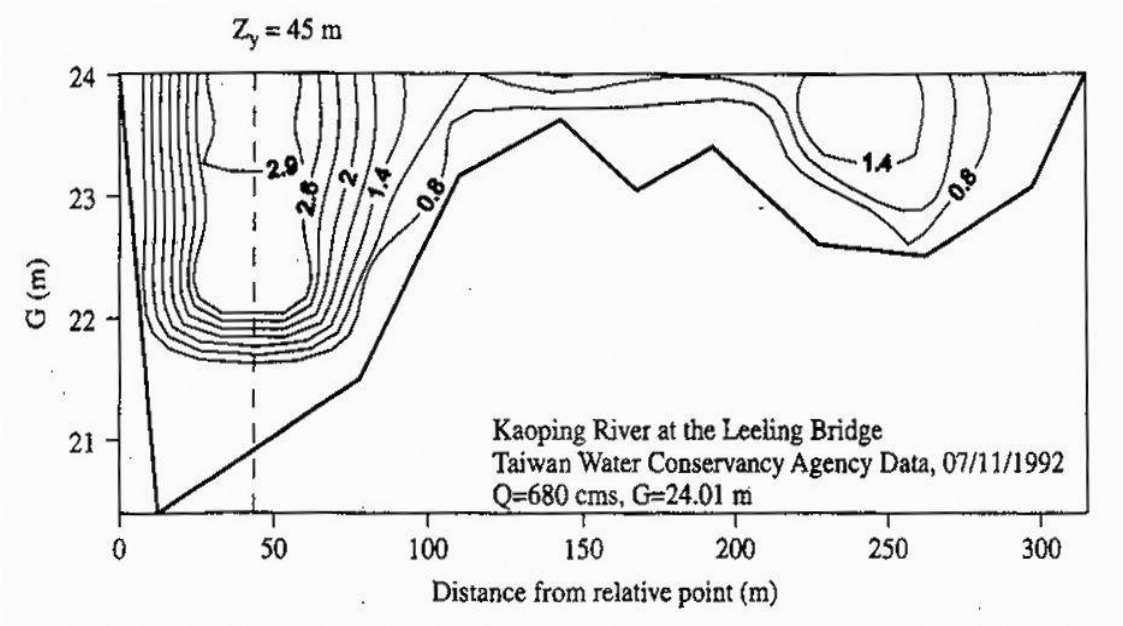

Fig. 18. Typical isovel pattern indication location Z_y (Chen and Chiu 2004).

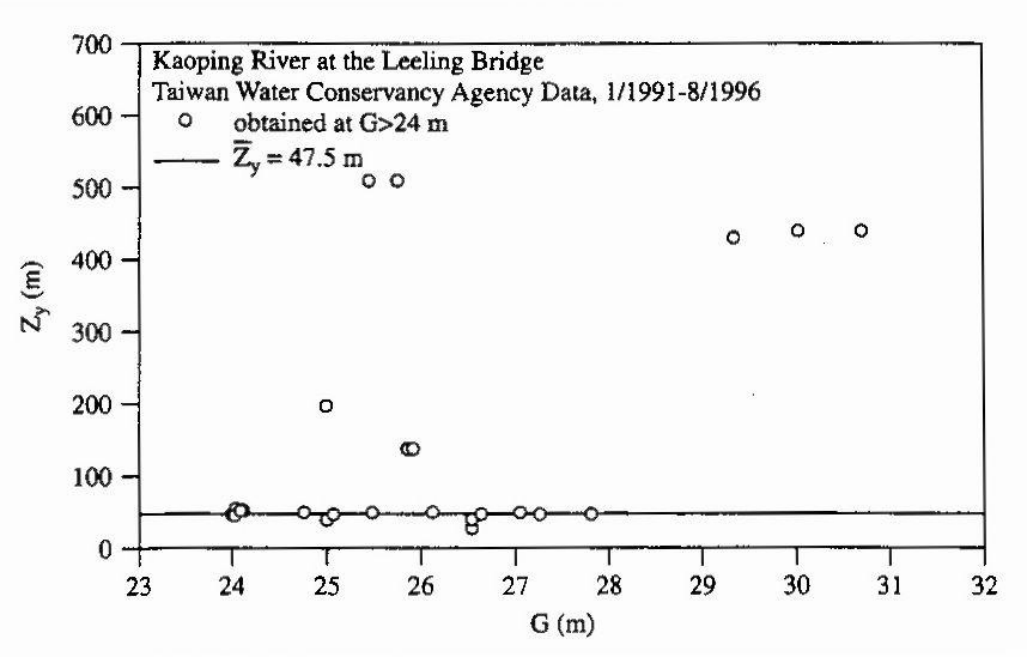

Fig. 19. Two locations of the y-axis in the Kaoping River at Leeling Bridge (Chen and Chiu 2004).

However, once the water exceeds a certain level, e.g., banks are overtopped and water spreads over the flood plain, Z_y in certain situations may shift to a new location. This kind of situation was illustrated in the Kaoping River at the Leeling Bridge (Chen and Chiu 2004) in Fig. 19.

The maximum velocity in the high-velocity region on the right-hand side is greater than that on the left-hand side when the water level is above 29 m (gauge height) but Z_y is found about 47.5 m from a reference point on the left bank when water flows in the main channel. Fig. 19 also shows that there are five anomalies between 25 and 26 m. The maximum velocities of the cross-section of the five flood events are very close to the maximum velocities on Z_y. Therefore the discharge of the five anomalies still can be estimated accurately on Z_y. Without records of data, Z_y may be estimated using floats thrown on to the water surface to determine the velocity profile on the water surface. During the flood period, the maximum velocity on the water surface can fairly indicate Z_y A slight shift of Z_y will not have much effect on the estimation of the maximum velocity (Chen, 1998). Therefore the maximum velocities can be estimated at the mean location of the *y*-axis ($\overline{Z_y}$). G denotes gauge height.

3.4. Derivation of velocity distribution along a particular vertical in a cross section

The key terms in an observed cross section are illustrated in Figure 20:

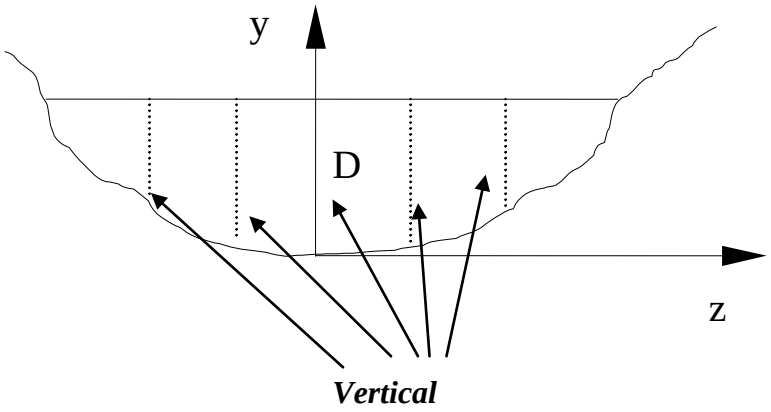

z = 0 (vertical were u_{max} occurs)

z < 0 (left side), z > 0 (right side)

depth = distance from the surface in m

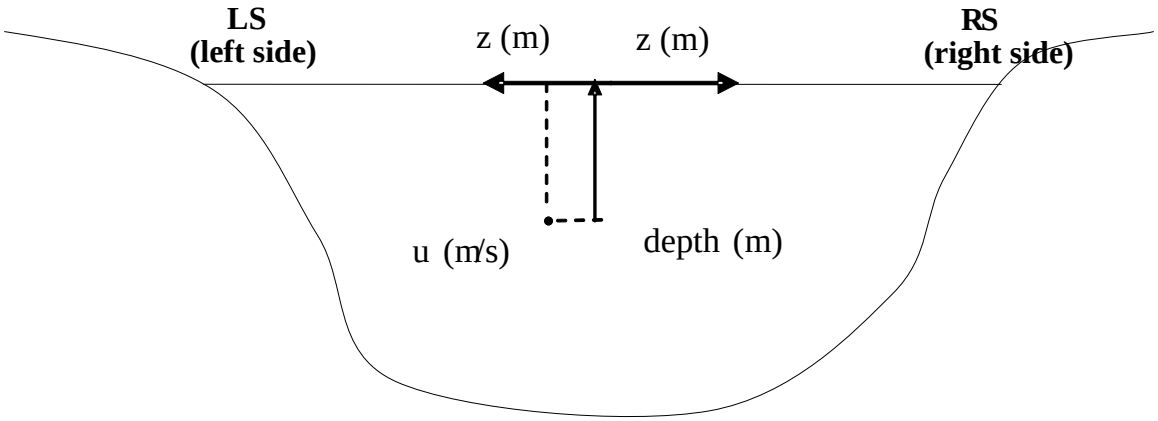

Fig. 20. Illustration of key terms at a typical cross section in an open channel.

In order to develop a practical and simple method for estimating flow velocity during high floods, it was assumed that the formulation of Eq. (34), written for the vertical where the maximum velocity occurs (z= 0) holds. For a particular vertical along the y-axis where z = 0. Eq. (34) to Eq. (36) gives:

$$r = \frac{y}{D+h}\exp(1-\frac{y}{D+h}) \tag{38}$$

as δ_y and δ_i is usually small (especially for a rectangular channel); and r_0=0.

If h<0, r_{max} and u_{max} occur at y=D+h, so that r_{max}=1 according to Eq. (38). Then, Eq. (38) gives:

$$\frac{r-r_0}{r_{\max}-r_0}=\frac{y}{D+h}\exp(1-\frac{y}{D+h}) \tag{39}$$

If $h\geq 0$, r_{max} and u_{max} occur at the water surface where y=D according to Eq. (38) :

$$\frac{r-r_0}{r_{\max}-r_0}=\frac{y}{D}\exp(\frac{1-\frac{y}{D}}{1+\frac{h}{D}}) \tag{40}$$

Eq. (34) with Eq. (39) or Eq. (40) depending on which case it belongs to and using Eq. (39) and Eq. (40) enhances the ability of Eq. (33) to refine the modeling of velocity distribution on the y-axis, regardless of whether u_{max} occurs on or below the water surface. For h< 0, the velocity distribution is :

$$u=(\frac{m}{m-1})\frac{1}{\lambda_1}\left\{\left(\lambda_1\frac{y}{D+h}\exp(1-\frac{y}{D+h})\right)+\left[(\frac{m}{m-1})\lambda_V\right]^{\frac{m}{m-1}}\right\}^{\frac{m-1}{m}} \tag{41}$$

If $h\geq 0$, the velocity distribution is determined as:

$$u=(\frac{m}{m-1})\frac{1}{\lambda_1}\left\{\left(\lambda_1\frac{y}{D+h}\exp(1-\frac{y}{D+h})\right)+\left[(\frac{m}{m-1})\lambda_V\right]^{\frac{m}{m-1}}\right\}^{\frac{m-1}{m}} \tag{42}$$

Based on Eq. (41) and Eq. (42) we can compute the velocity distribution for an arbitrary vertical with the maximum and mean velocities known. Note the probability density *f(u)* and the maximum entropy *H(u)* have the same form as in 1-D part.

3.5. Testing of the velocity distribution along a vertical and verification of parameter m

To test the validity of Eq. (41) and Eq. (42) as a velocity distribution model, the model computed data were compared with three sets of observed data. Two sets of field data that were collected from two verticals located at the left and right hand side of the *y*-axis of the cross-section at P. Nuovo gauged section of Tiber River in Central Italy (Moramarco 2008) during a flood event that occurred in June 1997 and laboratory data collected by Coleman (1986) for Run 16 were used here. Parameters of the velocity distribution function Eq. (41) or Eq. (42) are computed and summarized in Table 8.

Table 8 Parameters for Tsallis based 2-D velocity distribution with different *m*.

m	P.Nuovo Vertical No. 1		P.Nuovo Vertical No. 2		Coleman Data (for Run 16)	
	λ_1	λ_V	λ_1	λ_V	λ_1	λ_V
	u_D=2.48m/s, u_m=1.63m/s, h=-2.7m		u_D=2.72m/s, u_m=1.79m/s, h=-2.7m		u_D=1.074m/s, u_m=0.90m/s, h=-35mm	
2/3	0.74	-3.81	0.70	-3.94	3.87	-5.16
3/4	0.77	-4.91	0.72	-5.03	4.33	-6.48
5/4	0.80	2.87	0.72	2.80	7.09	-0.21
3/2	2.55	-2.62	2.22	-2.50	6.60	-1.50
2	0.61	0.05	0.51	0.04	7.03	-1.91

To evaluate how the *m* exponent influences simulation, the velocity was computed and is plotted in Fig. 21 based on different m values against the observed velocity profiles collected from Tiber River.

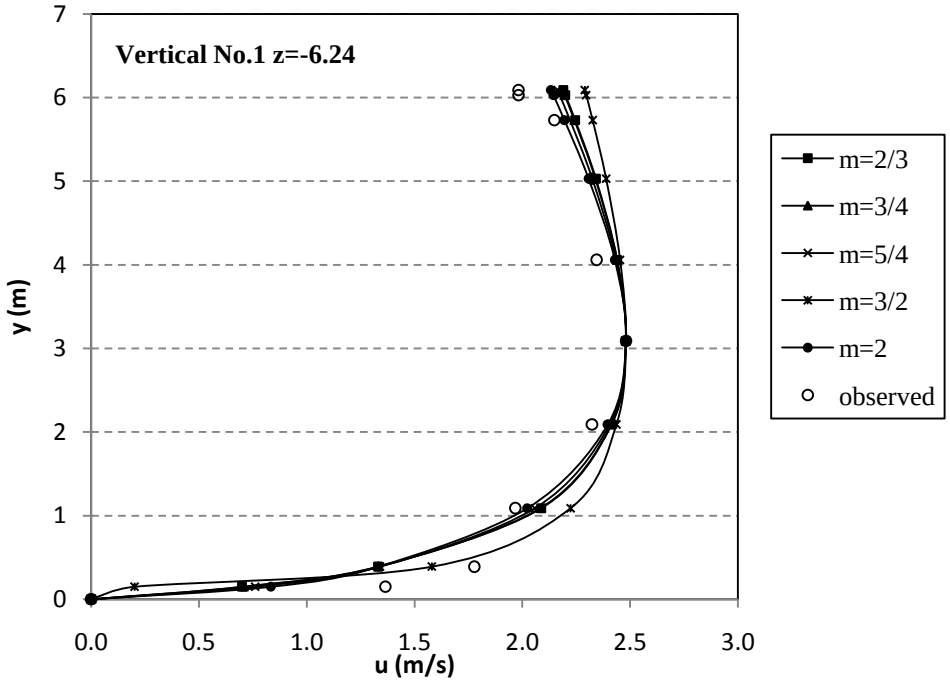

(a)

Fig. 21. Velocity profiles estimated by Tsallis entropy based 2-D velocity distribution, Eq. (41), plotted against velocity points sampled along two verticals at P. Nuovo gauged station during flood event that occurred in June 1997.

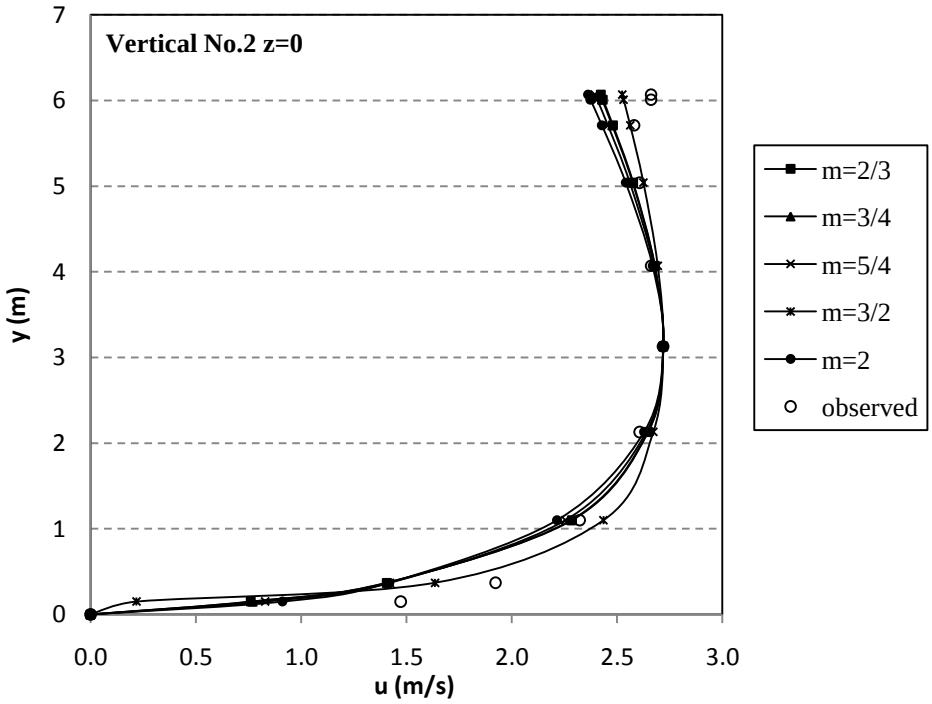

(b)

Fig. 21. continued

And the computations were also compared with experimental observations by Coleman (1986) in Fig. 22.

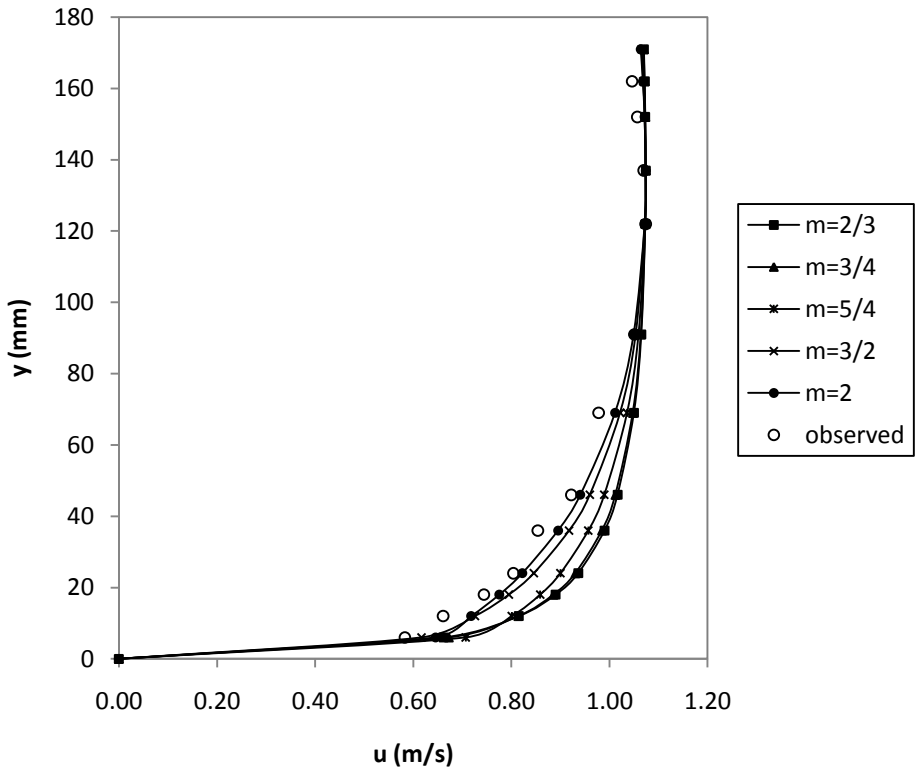

Fig. 22. Velocity profiles estimated by Tsallis entropy based 2-D velocity distribution, Eq. (41), plotted against experimental data for Run 16 by Coleman (1986).

Comparing the model estimated velocity profiles with both the field data collected during flood events and experimental data for non-wide channels, the accuracy of the Tsallis based velocity model has been validated especially in the lower region and also in the portion close to water surface where it is not possible to collect direct velocity measurements, especially during high floods. For all of the sampled velocity profiles, it is evident that the maximum velocity does not happen at the water surface, for the velocity sampled during a flood event in the P. Nuovo section the maximum happened 2.7 m below the water surface, and also for the experimental data collected for Run 16

(Coleman 1986) the maximum occurred at 35 mm below the water surface. They showed that the flow velocity profiles during flood events or for flow in non-wide channels the maximum velocity does not always happen at the water surface. The Tsallis entropy based 2-D velocity distribution combines the transformation of the coordinate system and the Tsallis entropy, in which the former shapes the velocity curve, and the latter enables the velocity equations satisfy the total probability and mass continuity, enhances the goodness of the model against the observed data, and helps guarantee that the maximum velocity happens below the water surface based on the curvilinear coordinate system.

3.6. Introduction of new parameter *M*

3.6.1. Mathematical definition of *M*

Based on the study using both field and experimental data, the feasible range of *m* is from 0 to 2 as indicated in Fig. 23 and Fig. 24.We can see that the velocity distribution changes little with the variation of *m* under the coordinate transformation mentioned previously, so the velocity distribution is not highly sensitive to exponent *m* within the feasible range. In another words, the velocity curves derived from different *m* values do not have significant differences between each other. Furthermore, we found that for fixing *m*= 2, the two parameters λ_1 and λ_V have simple analytical expressions obtained solving Eq. (17) and Eq. (19) in the previous section as:

$$\begin{aligned} \lambda_1 &= -\frac{12}{u_{\max}^3}(u_{\max} - 2u_m) \\ \lambda_V &= \frac{4 - \lambda_1 u_{\max}^2}{2u_{\max}} \end{aligned} \tag{43}$$

with u_{max} and u_m known, the two parameters can be easily obtained by substituting these two terms into Eq. (43). At this point, it is possible for us to make the velocity distribution equations much simpler by introducing a new dimensionless parameter *M* which is mathematically defined as:

$$M = \lambda_1 u_{\max}^2 \tag{44}$$

Based on the mathematical definition of parameter *M*, the mathematical range of it is in the interval (-12, 12). For most US rivers, the maximum velocity has been reported to be 25-50% larger than the mean (Leopold et al. 1995). Thus the *M* values for US rivers are between 4 and 7.2. *M* is directly linked to the ratio between mean and maximum velocity, serving as a new key hydraulic parameter, it can play an important role in understanding open channel flow. In order to find the physical range and hydraulic characteristics of *M*, further investigations using more data sets are presented here.

3.6.2. Investigations of *M* for typical channels

In Table 9 and Table 10, 42 pairs of maximum velocity and mean velocity that were collected for different verticals at Pontelagoscuro gauged section on the Po river during two flood events that occurred on February 2, 1985 and March 27, 1991 and at P. Nuovo gauged section during flood events that occurred on June 3, 1997 and November 18, 1996 (Moramarco and Singh 2004) were used to determine values of *M* for these rivers.

Table 9 Computation of M, λ_1 and λ_V based on u_m and u_{max} measured on the Po River (Italy) for different verticals at Pontelagoscuro gauged section during flood events that occurred on February 2, 1985 and March 27, 1991.

u_{max} (m/s)	u_m (m/s)	λ_1	λ_V	M	Event
0.38	0.27	36.08	-1.59	5.211	February13,1985 Po River
1	0.77	6.55	-1.27	6.549	
1.36	1.11	4.12	-1.33	7.618	
1.36	1.06	3.60	-0.98	6.662	
1.33	1.00	3.38	-0.75	5.985	
1.57	1.11	2.02	-0.31	4.968	
1.8	1.32	1.73	-0.44	5.600	
1.71	1.19	1.60	-0.20	4.678	
1.17	0.89	4.56	-0.96	6.236	
1.18	0.93	5.03	-1.27	7.006	
1.08	0.87	6.31	-1.55	7.358	
0.56	0.40	15.94	-0.89	5.000	
			mean	6.072	
0.80	0.56	7.97	-0.65	5.036	March 27,1991 Po River
1.26	0.86	2.85	-0.20	4.492	
1.35	1.02	3.33	-0.77	6.078	
1.42	1.10	3.30	-0.93	6.650	
1.44	1.17	3.64	-1.24	7.557	
1.49	1.17	3.13	-0.98	6.902	
1.80	1.29	1.58	-0.31	5.120	
1.80	1.41	2.08	-0.76	6.749	
1.44	1.10	3.13	-0.86	6.460	
1.37	1.04	3.31	-0.80	6.195	
1.32	0.89	2.41	-0.08	4.210	
1.07	0.79	5.09	-0.83	5.769	
0.56	0.35	8.62	1.13	2.733	
			mean	5.689	

Table 10 Computation of M, λ_1 and λ_V based on u_m and u_{max} measured on the Tiber River (Italy) for different verticals at P. Nuovo gauged section during flood events that occurred on June 3, 1997 and November 18, 1996.

u_{max} (m/s)	u_m (m/s)	λ_1	λ_V	M	Event
1.02	0.63	2.71	0.58	2.824	
1.83	1.18	1.04	0.14	3.475	
2.13	1.60	1.33	-0.48	6.028	
2.48	1.88	1.01	-0.44	6.194	June 3, 1997
2.72	2.20	1.00	-0.63	7.412	Tiber River
2.41	1.73	0.90	-0.25	5.228	
2.39	1.81	1.08	-0.46	6.176	
1.97	1.40	1.30	-0.27	5.056	
1.71	0.99	0.65	0.62	1.895	
			mean	4.921	
0.86	0.63	7.55	-0.92	5.581	
1.81	1.03	0.51	0.65	1.657	
1.98	1.46	1.45	-0.43	5.697	November 18,1996
2.13	1.67	1.50	-0.66	6.817	Tiber River
2.6	2.05	1.02	-0.56	6.923	
2.45	1.93	1.15	-0.59	6.906	
2.1	1.58	1.37	-0.49	6.057	
1.71	1.12	1.27	0.08	3.719	
1.49	0.87	0.91	0.67	2.013	
			mean	5.041	

M is found between 4.68 to 7.62 for different verticals at Pontelagoscuro gauged section on Po river and varies from 1.66 to 7.41 for verticals located at P. Nuovo gauged section on Tiber River. Though the M values computed for every single vertical is different at the same gauged section for the same flood event, but the cross-sectional

mean for the same gauged section tends to be constant for different flood events. We may therefore conclude that the dimensionless parameter *M* may signal the characteristics of the channel section, such as changes in bed form, slope and geometric shape and it does not fluctuate much according to the changes in characteristics of flood events.

Blaney (1937) also collected mean and maximum velocity data for typical canals which can be applied to our investigation on *M* as well as shown in Table 11.

Table 11 Bed width, depth, and mean maximum velocity for typical canals. Imperical Valley, 1918-1919 (Blaney 1937).

Name of canal	Location	B (ft)	D (ft)	u_m (fps)	u_{max} (fps)	u_m/u_{max}	M
Date	Meter Bridge	14	1.5	2.66	2.95	0.90	9.64
Lateral	Sharps Heading	4	1	1.58	1.74	0.91	9.79
Braw;eu	El Centro Road	14	6	3.66	4.12	0.89	9.32
No.5 Main	Yuma	23	4.8	3.52	4.25	0.83	7.88
No.5 Main	Allison	30	4.7	4.04	5.10	0.79	7.01
Central	Bounday	38	5.5	2.80	3.20	0.88	9.00
Dogwood	Meter Bridge	19	3.2	1.67	1.95	0.86	8.55
Alamitos	Sharps Heading	24	3.3	2.54	2.75	0.92	10.17
Briar	Ten foot Drop	11	2.3	2.76	3.30	0.84	8.07
Evergreen	Dahlia Heading	10	1.5	1.56	1.88	0.83	7.91
Elder	Five Gates	10	3.1	3.00	3.40	0.88	9.18
Encino	Flume	22	3.4	3.48	4.00	0.87	8.88

From the computations of parameter *M* using data from different kind of channels, the value of *M* is found to be as low as 0.537 and as high as 10.17, that means any value

within this range can be suitable for describing velocity profiles for certain kind open channel flow. The M value in the neighborhood of 9 represents channels of greater values of greater values of width-to-depth ratio and roughness and small slopes. An eodible channel generally tends to shape the channel and velocity distribution pattern so that u_m/u_{max} may fall between 0.85 and 0.9 at M between 8 and 11, as shown by the field data in Table 11.

3.6.3. Comparisons of parameter *M* in Tsallis entropy based 2-D velocity distribution and parameter *M* of Chiu's 2-D velocity distribution

In Chiu's work (Chiu 1987) based on Shannon entropy, he also introduced a hydraulic parameter *M* which is also the combination of the Lagrange multiplier and the maximum velocity. So there may be some interesting relationship between these two key parameters in two entropy-based equations. Comparison between the parameter *M* in the Tsallis entropy and the one used by Chiu for the Shannon entropy is tabulated in Table 12.

Table 12 Comparison of parameter *M* in the Tsallis entropy based equation with *M* in Chiu's Shannon entropy based equation. (Italy data and Blaney Data as in Table 9, Table 10 and Table 11).

	M	*M* (Chiu)	Diffence between M and M(Chiu)	Data
	6.07	1.95	4.12	Pontelagoscuro
	5.69	1.95	3.74	on Po River
	4.92	2.01	2.91	P. Nuovo on
	2.79	2.01	0.78	Tiber River

Table 12 (*continued*)

	M	*M* (Chiu)	Diffence between M and M(Chiu)	Data
	9.64	10.17	-0.53	Blaney (1937)
	9.79	10.87	-1.08	
	9.32	8.95	0.37	
	7.88	5.71	2.17	
	7.01	4.58	2.43	
	9.00	7.98	1.02	
	8.55	6.92	1.63	
	10.17	13.09	-2.92	
	8.07	6.02	2.05	
	7.91	5.77	2.14	
	9.18	8.49	0.69	
	8.88	7.66	1.22	
Average	7.80	6.51	1.30	
Standard Derivation	2.03	3.43	1.79	

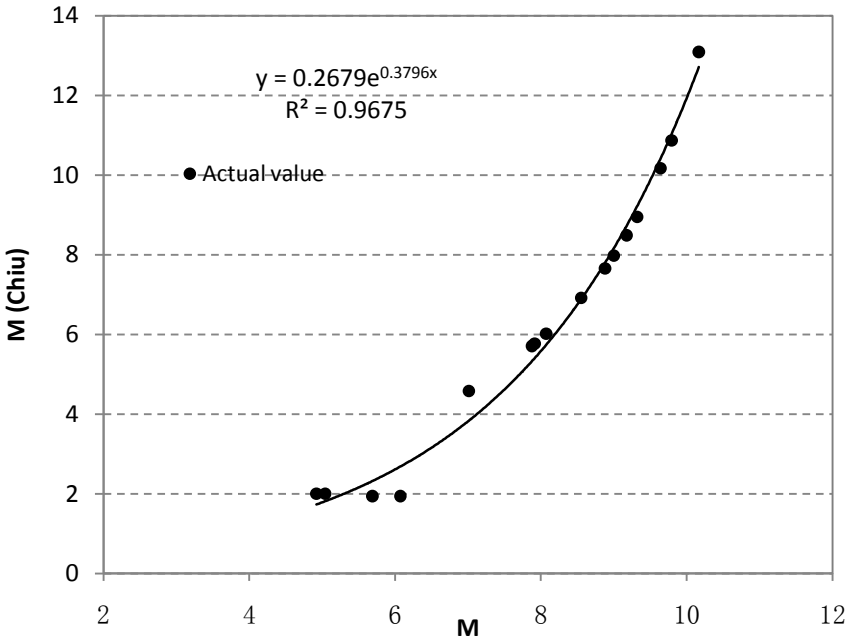

Fig. 23. Relationship of parameter *M* in Tsallis entropy based 2-D velocity distribution and Chiu's 2-D velocity distribution.

As shown in Fig. 23, the two *M* parameters almost obey a power law relation. This relationship needed to be confirmed with further studies with more data for different patterns of flow and channels. In Chiu's work, the *M* number has been found useful as an index for characterizing and comparing various patterns of velocity distribution and states of open channel flows. Based on Chiu's work plus the relationship between these two parameters, the relation between *M* number in the Tsallis entropy velocity distribution and open channel system factors, such as geometry, roughness, slope, sediment concentration and flow patterns may be explored in the future.

3.7. Velocity distributions with parameter *M*

3.7.1. Derivation of velocity distributions with parameter *M* for one vertical

Now replacing the two parameters λ_1 and λ_V in the velocity distribution function Eq. (42) with the new parameter *M*, the velocity distribution equation becomes to:

$$u = \frac{2u_{\max}}{M}\left[M\left(\frac{r-r_0}{r_{\max}-r_0}\right)+\frac{(4-M)^2}{16}\right]^{\frac{1}{2}}-\frac{(4-M)u_{\max}}{2M} \tag{45}$$

Therefore, the dimensionless velocity can be expressed in the form:

$$\frac{u}{u_{\max}} = \frac{2}{M}\left[M\left(\frac{r-r_0}{r_{\max}-r_0}\right)+\frac{(4-M)^2}{16}\right]^{\frac{1}{2}}-\frac{4-M}{2M} \tag{46}$$

As we can see from Eq. (45) and the term $(r-r_0)/(r_{max}-r_0)$ can be replaced with Eq. (39) or Eq. (40), so the velocity distribution with parameter *M* is linked with y in Cartisian coordinate system in the form as follows.

If the maximum velocity happens below water surface, i.e., $h<0$, the velocity and dimensionless velocity are determined as:

$$u = \frac{2u_{\max}}{M}\left[\frac{My}{D+h}\exp\left(1-\frac{y}{D+h}\right)+\frac{(4-M)^2}{16}\right]^{\frac{1}{2}}-\frac{(4-M)u_{\max}}{2M} \tag{47}$$

$$\frac{u}{u_{\max}} = \frac{2}{M}\left[\frac{My}{D+h}\exp\left(1-\frac{y}{D+h}\right)+\frac{(4-M)^2}{16}\right]^{\frac{1}{2}}-\frac{4-M}{2M} \tag{48}$$

If the maximum happens at the water surface, i.e., $h\geq 0$, the velocity distribution and dimensionless velocity can be expressed as:

$$u = \frac{2u_{\max}}{M}\left[M\frac{y}{D}\exp\left(\frac{1-\frac{y}{D}}{1+\frac{h}{D}}\right) + \frac{(4-M)^2}{16}\right]^{\frac{1}{2}} - \frac{(4-M)u_{\max}}{2M} \tag{49}$$

$$\frac{u}{u_{\max}} = \frac{2}{M}\left[M\frac{y}{D}\exp\left(\frac{1-\frac{y}{D}}{1+\frac{h}{D}}\right) + \frac{(4-M)^2}{16}\right]^{\frac{1}{2}} - \frac{4-M}{2M} \tag{50}$$

Eq. (47)- Eq. (50) with parameter *M* are the final form of the 2-D velocity distribution equations. Paramer *M* is the only parameter that need to be estimated, hence it is a key factor. In order to evaluate how the variation of *M* influences the velocity distribution, the dimensionless velocity distributions described in Eq. (48) are plotted in Fig. 24 for $h<0$.

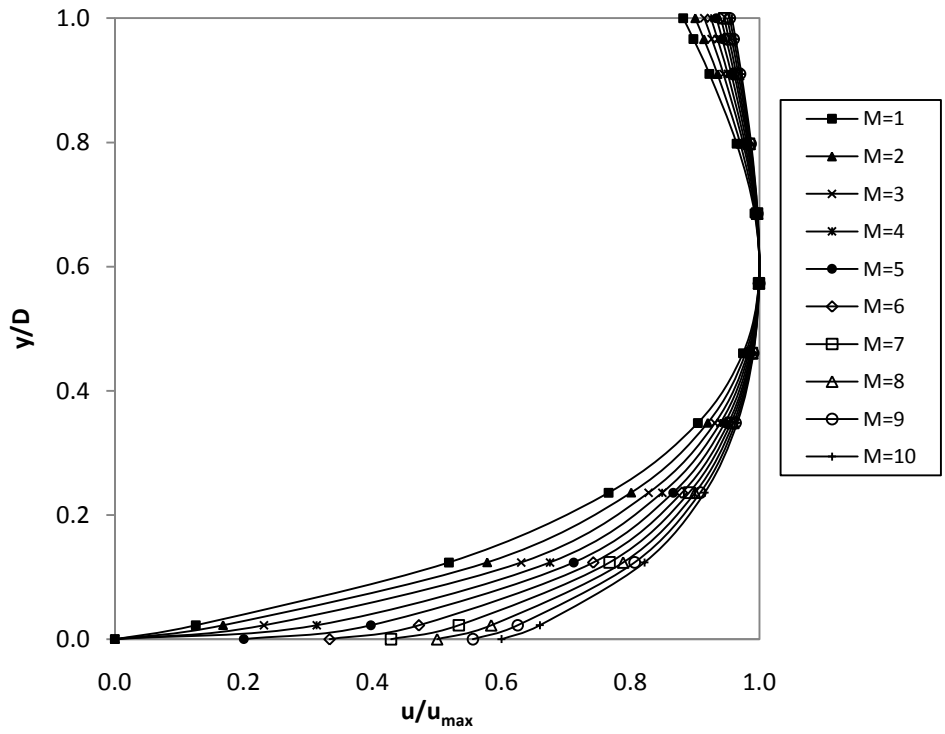

Fig. 24. Dimensionless velocity distributions at *h/D*=-0.4 and various *M* values.

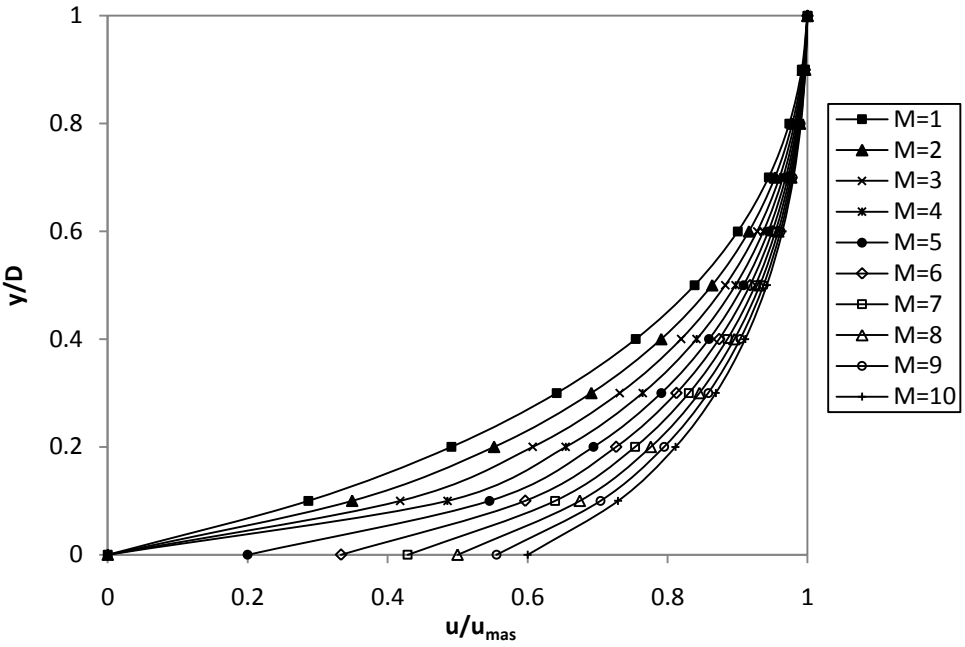

Fig. 25. Dimensionless velocity distributions at *h/D*=0.05 and various *M* values.

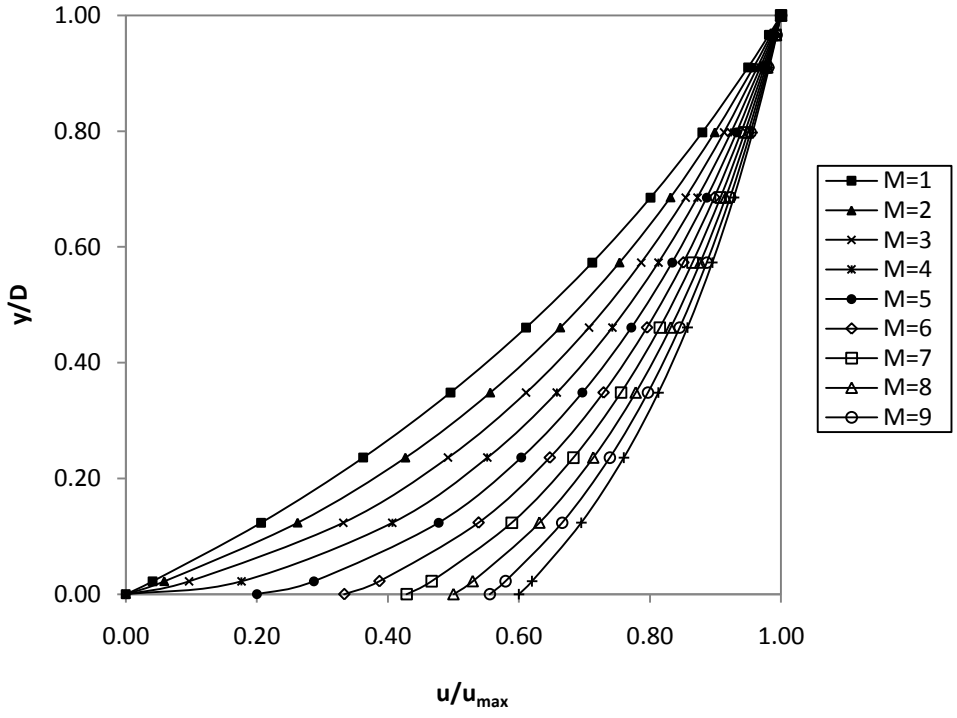

Fig. 26. Dimensionless velocity distributions at *h/D*=5 and various *M* values.

And the dimensionless velocity distributions described in Eq. (48) are plotted in Fig. 25 and Fig. 26 for $h \geq 0$. Fig. 24 to Fig. 26 describe velocity distributions given by Eqs. (48) and (50) with h/D= -0.4 ,0.05 and 5, respectively, and show the effects of M and h/D on the velocity distibution. These figures also show that Eq. (45) with r represented by Eqs. (39) and (40) can describe any velocity distribution pattern regardless of whether u_{max} occurs on or below the water surface.

As in Fig. 24 to Fig. 26, the velocity distribution curve changes gradually according to the change in parameter M, but not so dramatically; during the reasonable mathematical range of M, profiles with different M tend to the same shape. For h<0, the intersection of velocity profiles with different M is determined by h/D . The differences focus on the region close to the channel bottom.

Chiu and Chiou (1986) found an empirical relation between h/D and parameter M in his 2-D velocity distribution equation from 176 rectangular channels. He concluded that the h value can be significantly greater then zero only when the value of M is between 6 and 9, i.e., the ratio u_m/u_{max} falls between 0.84 and 0.89 which also corresponds to the M value in Tsallis entropy based 2-D velocity distribution is between 8.16 and 9.36. When the M value is between 8.16 and 9.36, the h value can be zero, smaller or greater than zero, so that isovels may or may not be perpendicular to the water surface. Both patterns of velocity distribution shown by Fig. 17 are possible. However, if M is outside the range of 8.16 to 9.36, the h value can only be zero or less than zero, and therefore, isovels tend to be perpendicular to the water surface. A small change in M will not lead to a remarkable change in the velocity distribution. For a given channel parameter M

does not change dramatically from vertical to vertical as disscussed in the previous section. The crossectional mean *M* seems acceptable to compute the velocity distribution. The velocity distributions at three verticals at gauged section P. Nuovo on Tiber River (Moramarco and Singh 2004) are plotted in Fig. 27 with the crosssectional parameter *M*=5.041 in comparison with the estimation using *M* computed for one particular vertical.

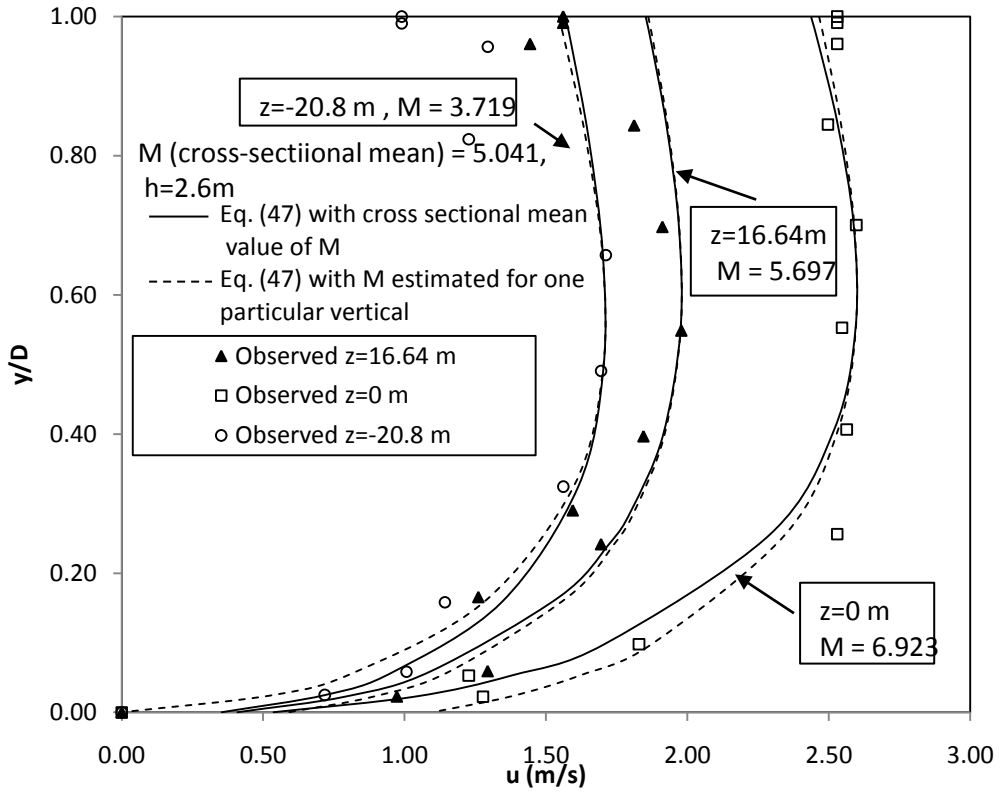

Fig. 27. Velocity profiles estimated by Tsallis entropy based 2-D velocity distribution, Eq. (47), using cross-sectional mean value of parameter *M* and *M* estimated for one particular vertical. Against velocity points sampled along three verticals at P. Nuovo gauged section during a flood event that occurred in November, 1996.

Table 13 Errors given by Eq. (27) considering Eq. (47) for estimating 2-D velocity distribution using cross-sectional mean value of parameter *M* (Mm) and *M* (Mi) estimated for one particular vertical.

Vertical	Mm		Mi	
	μ	σ	μ	σ
z=16.64 m	0.088	0.145	0.080	0.128
z=0 m	-0.028	0.077	0.027	0.104
z=20.8 m	0.192	0.243	0.139	0.281

Comparing velocity profiles estimated by Eq. (47) with the field data, it is obvious that Eq. (47) is accurate for the axis having the maximum velocity as well as for the region near the bank. The mean errors at the three verticals considering Eq. (47) for estimating velocity using parameter *M* estimated in two ways did not exceed 0.20. Fig. 28 also shows that though parameter *M* estimated from the maximum and mean velocity is different from vertical to vertical at the same section, there is no significant difference between the velocity profiles estimated by Eq. (47) using the cross-sectional mean of *M* and the *M* estimated particularly for the observed vertical. Obviously, comparison of errors shown in Table 13, the mean errors and standard deviations are not substantially different, while the estimation using parameter *M* for a particular vertical tends to be smaller. Though the differences are small, more differences are found in the lower portion of the velocity profiles and also in the region close to side walls, in this region the velocity profiles computed using *M* for this specific vertical have a higher accuracy. This aspect suggests that parameter *M* can be considered an indicator of the boundary effects on the velocity distribution. As in Fig. 27, *M* decreases when the vertical goes

away from the z-axis and get closer to channel bank, reaching the maximum of the cross section at the z-axis.

3.7.2. Velocity distributions (isovels) for a given cross section

For a given cross section, parameters of the isovels [Eq. (45) in combination with Eq. (34)-(36)] can be estimated directly from the actual velocity data or indirectly from discharge rate, slope, roughness, and cross section of the channel with reference to Manning's equation. The indirect method is a simulation technique that can be used to generate any number of velocity distribution data sets for wide ranges of discharge rate, slope, roughness, and cross sections of channels.

Fig. 28 shows isovel patterns simulated by Eq. (45) in conjunction with Eq. (34) - (36) for rectangular channels having various discharge rates and width-to-depth ratios, at the channel slope of 0.0016 and Manning's n of 0.015 and 0.03, respectively. For each of the channels (or velocity distributions) in the figure, the values of u_{max}, M, u_m and h/D are also indicated. The general trend for M varying with the width-to depth and channel roughness is vividly presented by the figures.

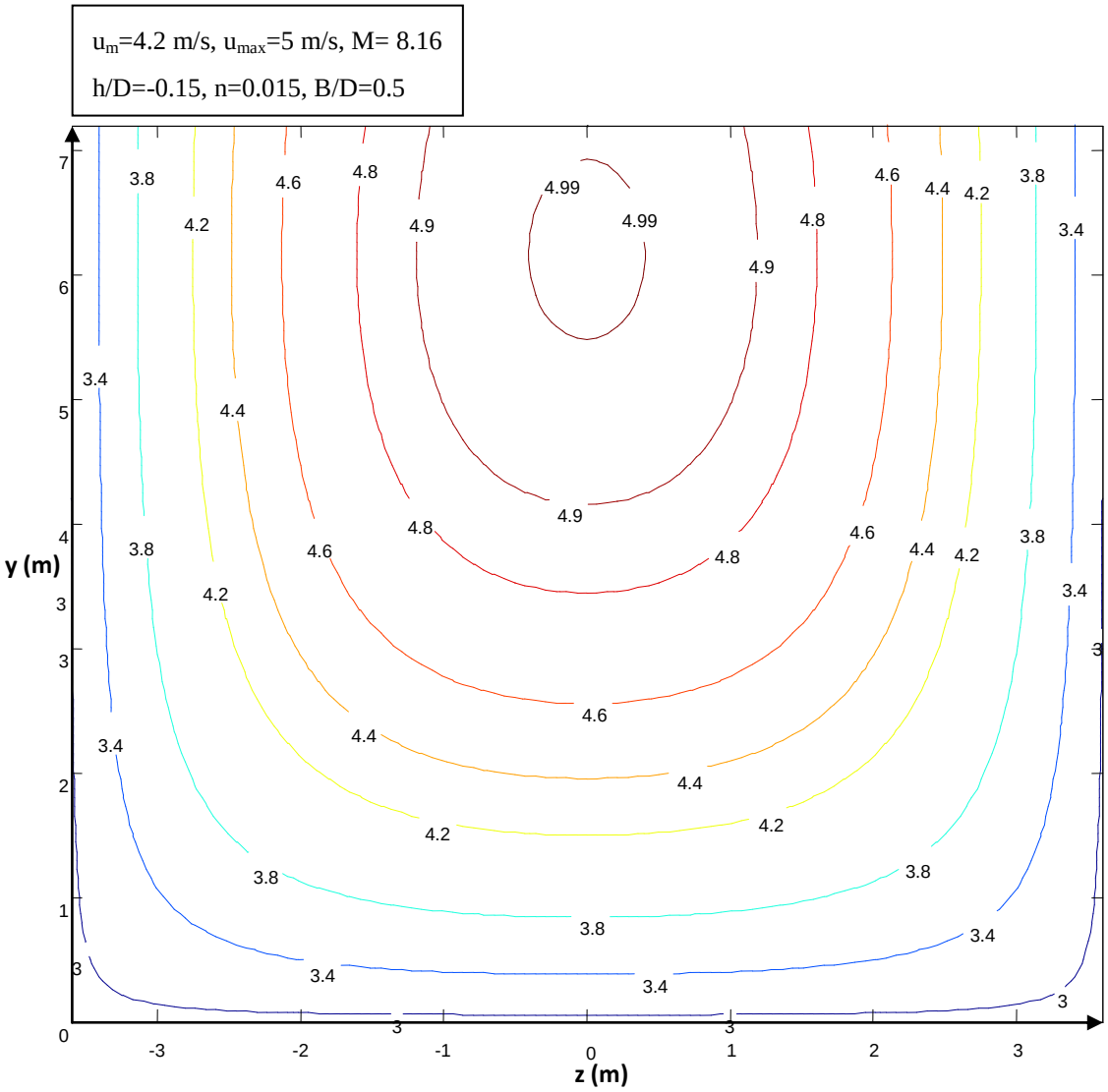

(a)

Fig. 28. Parameter *M*, *B/D* ratio, Manning's *n* and velocity distributions.

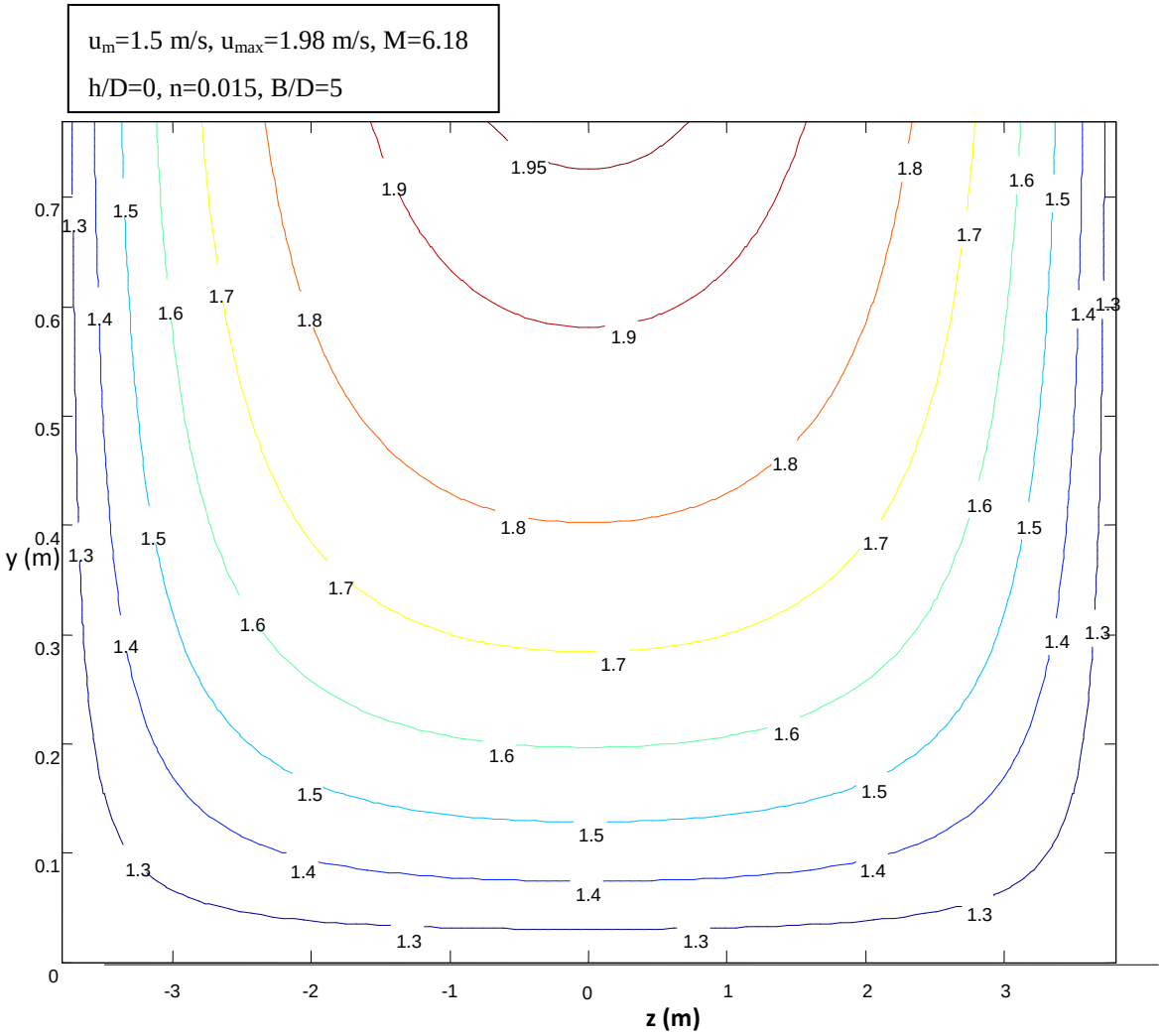

(b)

Fig. 28. continued

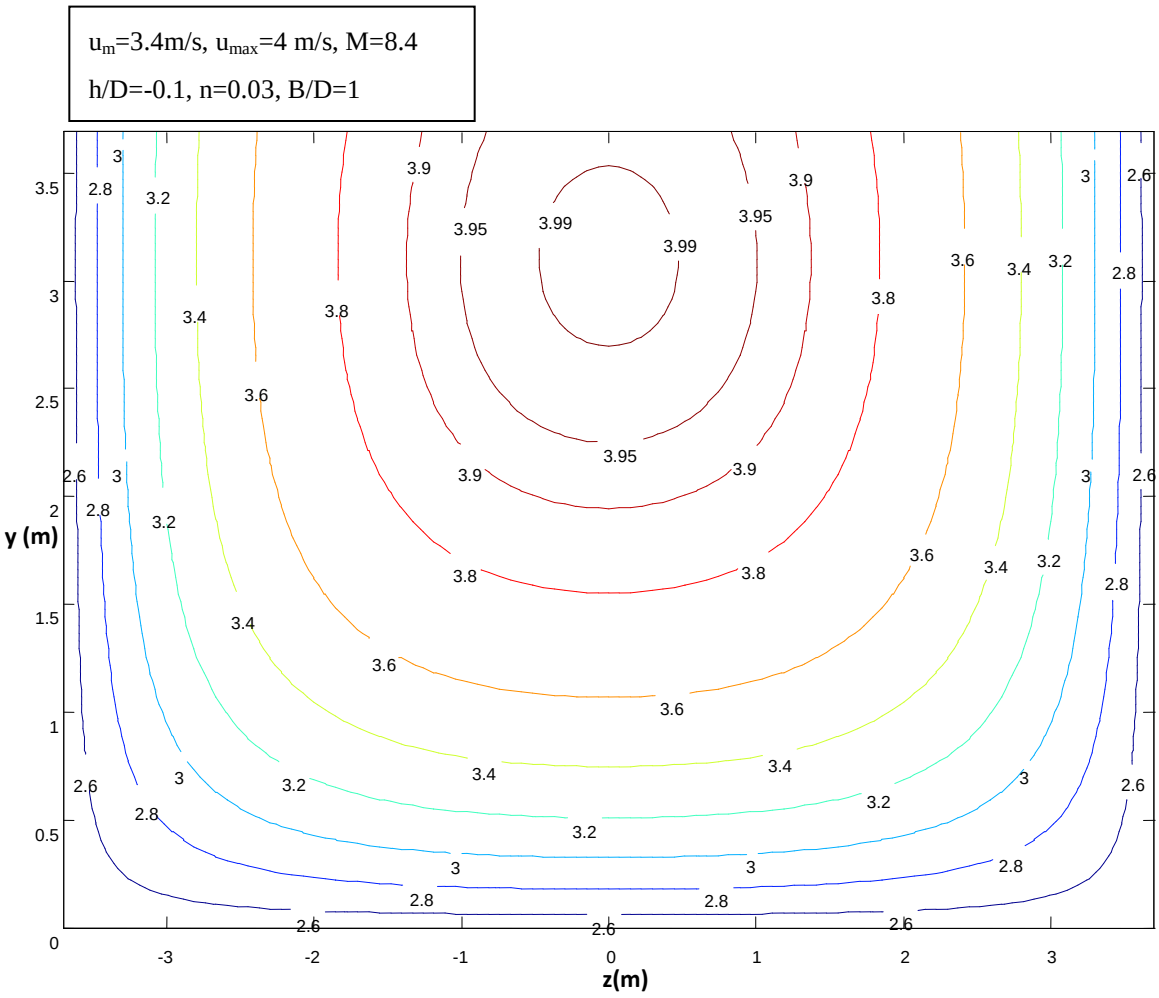

(c)

Fig. 28. continued

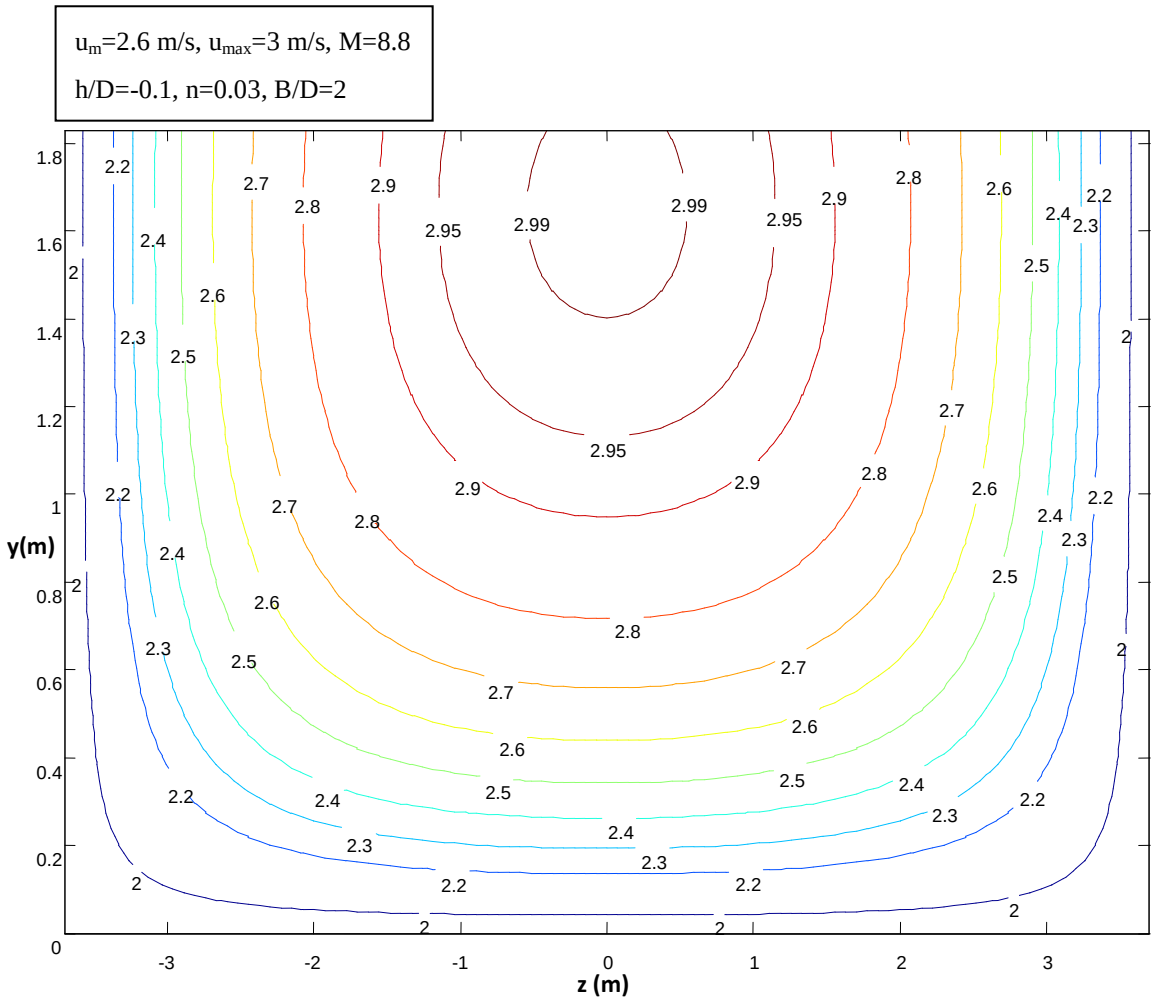

(d)

Fig. 28. continued

To determine how good the new model is it is applied to predict the cross-sectional velocity distribution. Based on the previous analysis, the cross-sectional mean value of *M* can be applied to simulate velocity profiles along different verticals for the whole cross section, so these values are also acceptable to simulate the isovels presented here.

But more details about how to accurately estimate *M* can be found in the latter sections. The isovels are also plotted in comparison with the field data collected at P. Nuovo gauged section on Tiber River during two flood events that occurred June, 1997, respectively in Fig. 29.

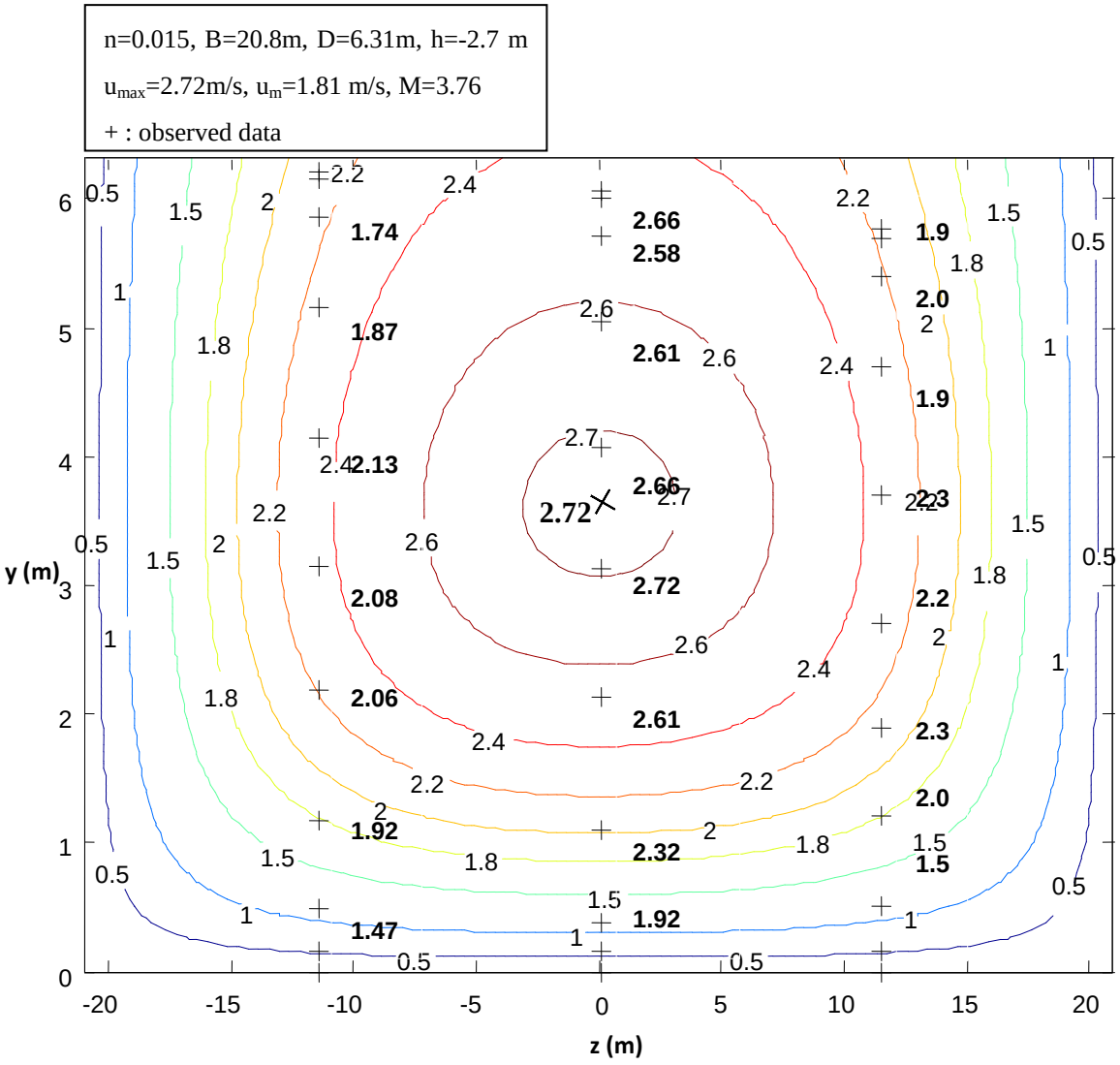

Fig. 29. Velocity distributions at P. Nuovo gauged section on Tiber River during flood events that occurred in June 1997.

3.8. Probability density function and maximum entropy of dimensionless velocity and velocity with *M*

The desired PDF, *f(u)*, can also be expressed with *M* as

$$f(u) = \frac{4-M}{4u_{\max}} + \frac{M}{2u_{\max}^2}u \tag{51}$$

The probability density function of dimensionless velocity $f(u/u_{max})$ can also be expressed with *M* as a parameter:

$$f(u/u_{\max}) = u_{\max} f(u) = \frac{4-M}{4} + \frac{M}{2}(u/u_{\max}) \tag{52}$$

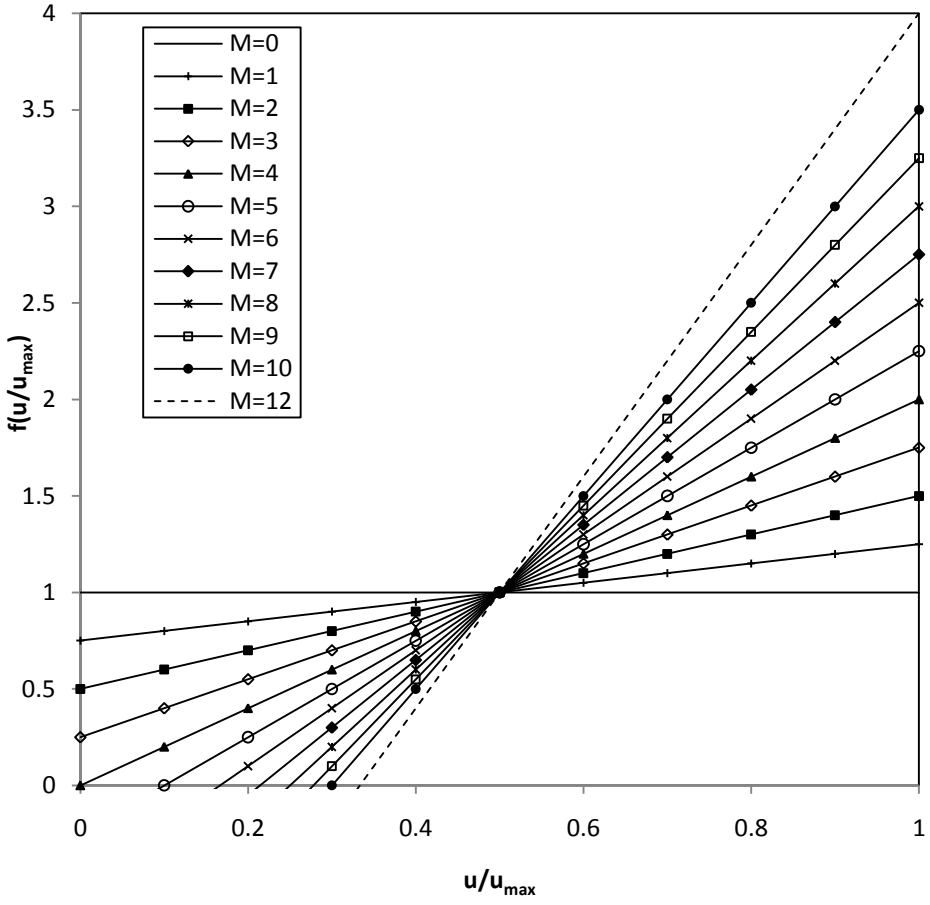

Fig. 30. Parameter *M* and probability density of dimensionless velocity $f(u/u_{max})$.

Eq. (52) shows the probability density and the dimensionless velocity u/u_{max} follows a simple linear relationship, and the slope of the lines are determined by the parameter M. Fig. 30 describes the function $f(u/u_{max})$ for various M values.

Using Eq. (51) and Eq.(52), integration of Eq. (4) gives the maximum entropy of velocity and dimensionless velocity u/u_{max}, denotes u/u_{max} as w:

$$H(u) = 1 - \int_0^{u_{\max}} f(u)du = 1 - \int_0^{u_{\max}} \left(\frac{4-M}{4u_{\max}} + \frac{M}{2u_{\max}^2} u \right) du = 1 - \frac{48 + M^2}{48u_{\max}} \tag{53}$$

$$\begin{aligned} H(u/u_{\max}) &= 1 - \int_0^1 f(w)dw = 1 - \int_0^1 \left(\frac{4-M}{4} + \frac{M}{2} w \right) dw \\ &= 1 - \frac{48 + M^2}{48} = -\frac{M^2}{48} \end{aligned} \tag{54}$$

From Eq. (54), the maximum entropy is always determined by the parameter M; similarly, Chiu (1988) also found that the maximum entropy of dimensionless velocity is a function of the parameter M in his 2-D velocity equation. In order to further explore the relation between the two M parameters, Chiu's function concerning M is also presented as Eq. (55a) and Eq. (55b):

$$H\left(\frac{u}{u_{\max}}\right) = 1 + \ln[\exp(M) - 1] - M\exp(M)[\exp(M) - 1]^{-1} - \ln M \tag{55a}$$

$$H(u) = H\left(\frac{u}{u_{\max}}\right) + \ln u_{\max} \tag{55b}$$

The maximum entropy of dimensionless velocity based on Eq. (54) and Eq. (55a) is plotted in Fig. 31(a) and (b) with various M values respectively.

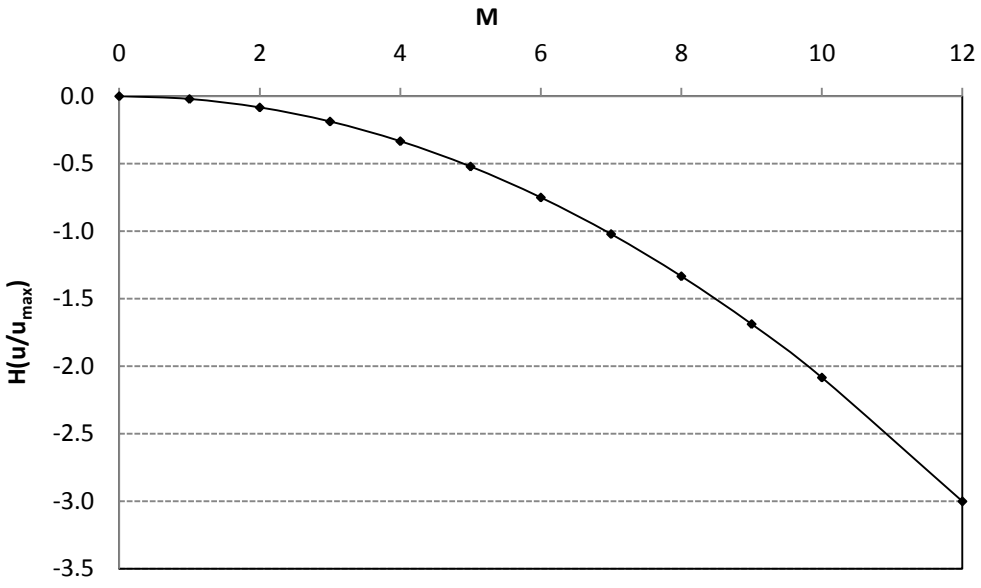

(a)

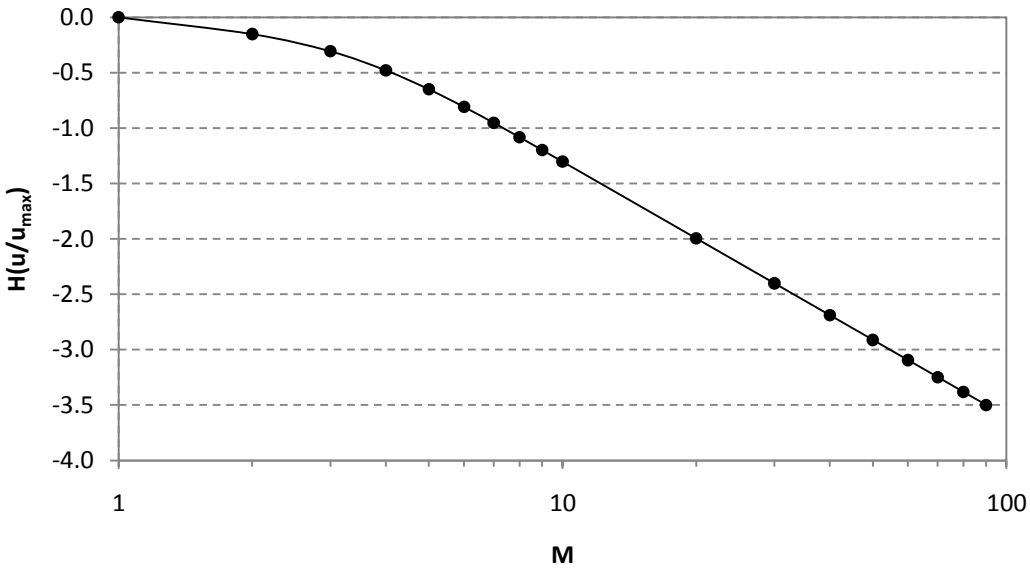

(b)

Fig. 31. Maximum entropy with various *M*. (a) Eq. (54); (b) Eq. (55a).

As we can see from Eq. (53) to Eq. (55b), the value of the maximum entropy of both Tsallis entropy based 2-D velocity distributions and Chiu's 2-D velocity distributions is determined by their hydraulic parameter *M* and the maximum velocity u_{max}. Apparently, *H(u)* increases with the increase of u_{max} as in Eq. (53) and Eq. (55b) which approves the argument we made earlier that the maximum entropy goes up with the increase of the maximum velocity. In order to investigate how parameter *M* in these two velocity distributions influences the maximum entropy, we need to exclude the effects of u_{max} and that is the reason we introduced the term $H(u/u_{max})$. As in Fig. 31, $H(u/u_{max})$ of the two velocity distributions is determined by their parameter M respectively and decreases with the increase of *M* in their possible range. Though Eq. (54) based on Tsallis entropy is much simpler that Eq. (55a), there is great similarity between the relation between the two *M* parameter and the maximum entropy which implies the similarity between their hydraulic characteristics. For an erodible channel, Chiu (1987) stated greater values of $H(u/u_{max})$ were from channels of greater values of roughness and width-to-depth ratio and smaller slopes. $H(u/u_{max})$ and *M* may be changed by adjusting the cross section (width, depth, and shape); slope; roughness; alignment; velocity distribution; and, perhaps, sediment transport. To increase the entropy $H(u/u_{max})$, a nonerodible channel can only adjust the water depth and the pattern of velocity distribution. Consequently, flows in artificial channels of rigid boundaries tend to have a relatively wider range of possible values. Based on the similarities found between *M* in Tsallis entropy based 2-D velocity distributions and *M* in Chiu's 2-D velocity distributions and their empirical mathematical relation presented in the previous section, the same conclusion can also be

applied to Tsallis entropy based 2-D velocity distributons, while *M* in Tsallis entropy based 2-D velocity distributions has a much smaller possible range than parameter *M* defined in Chiu's 2-D velocity distribution, maybe easier to estimate and therefore more applicable in engineering. The great similarities found between the key parameter M in the two velocity distributions verified that Tsallis entropy is a generalization of Shannon entropy again.

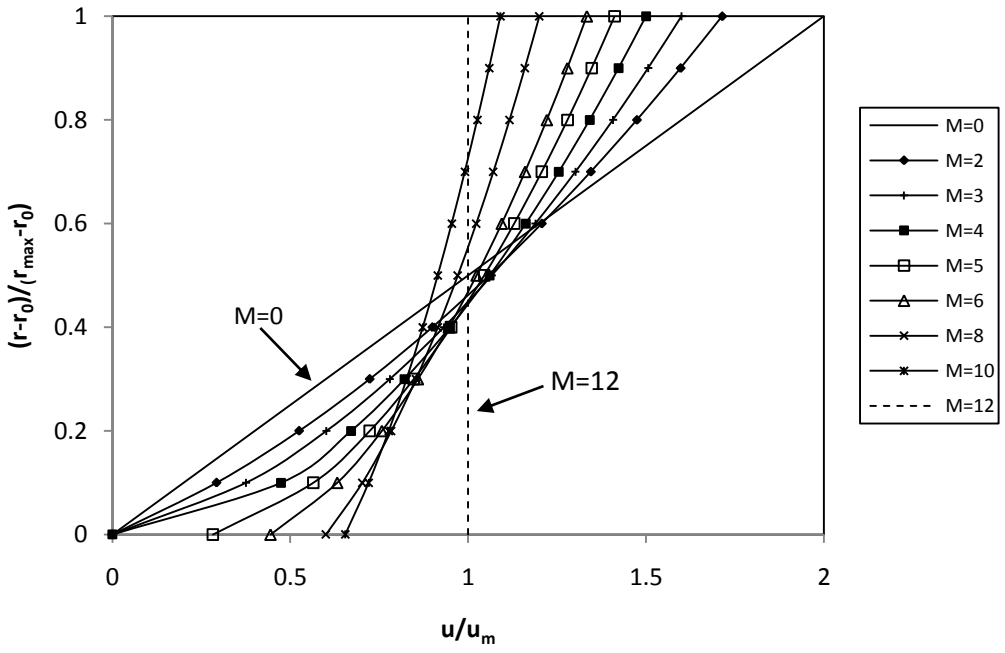

Fig. 32. Dimensionless velocity distribution and parameter *M*.

Fig. 32 shows that the gradient of probability density lines goes up from 0 to 5 and the upper limit is 6 (because the mathematical upper limit of *M* is 12 as mentioned earlier) and they intersect at the point (0.5, 1). For $M = 0$, $f(u/u_{max})$ is a constant equal to unity and represents a uniform distribution. It corresponds to the (theoretical) maximum value of entropy function $H(u/u_{max})$, which is equal to zero. In Fig. 32, the linear velocity

distribution, with velocity equal to zero at the bed and u_{max} at the water surface in wide channel, corresponds to M= 0 and hence the theoretical maximum entropy. Another extreme case is when M tends to 12, $f(u/u_{max})$= 4, this corresponds to the minimum entropy situation, in this case the velocity is constant. Since $f(u/u_{max})$ is determined by parameter M, the resilience or stability of it can be tested through either M or u_m/u_{max}, and can be used as a basis for using Eq. (45) for describing velocity distributions under varying u_{max}, u_m or discharge in flows with or without sediments. This provides the motivation to investigate u_m/u_{max} and M.

3.9. Maximum velocity and mean velocity

3.9.1. *M* and the relation of maximum velocity to mean velocity

In open channel hydraulics the mean velocity is needed in the governing equations for the transport of mass, momentum, and energy through a channel cross section. Therefore, the importance of determining the mean velocity is well known. To determine the mean velocity and discharge in rivers and streams, available methods include the use of empirical formulas and velocity samples. Originally derived for uniform flow, Manning's equation is a popular empirical formula but its application in unsteady nonuniform flow is questionable, because both the energy slope and Manning's *n* tend to vary with time and water depth from section to section along the flow direction. These temporal and spatial variations of energy slope and Manning's *n* are often irregular and pronounced in flows affected by such factors, as ice and wind, and tend to cause great uncertainties in flow forecasting (Crissman 1993).

To determine the mean velocity and discharge from velocity samples, the conventional method requires a great amount of time and measurements, and, hence, is unsuitable for unsteady flows and (Kalman) filtering schemes are used to reduce uncertainties in flow forecasting (Crissman 1993). What is needed for unsteady flows and filtering schemes is an efficient method to quickly determine discharge and flow resistance that may change rapidly.

In comparison with mean velocity, the maximum velocity in a channel cross section had never been considered important enough to receive special attention until Chiu (Chiu 1991) explored the relationship between the mean velocity and the maximum velocity using one entropy parameter M (different from the M in Tsallis entropy based 2-D velocity distribution) which can be expressed as:

$$\frac{u_m}{u_{\max}} = \frac{e^M}{e^M - 1} - \frac{1}{M} \tag{56}$$

It is considered worthwhile to make special efforts for measurement, analysis and modeling of maximum velocity and determining the relation of maximum velocity to the mean velocity. The maximum velocity may be considered as a "signal" that is measurable and contains useful information about the open channel flow. First of all, the maximum velocity gives the range of velocity in a channel cross section, which is an important piece of information about the velocity distribution and mean velocity.

On an isovel where $r=r_m$ and $u=u_m$, Eq. (46) becomes:

$$\frac{u_m}{u_{\max}} = \frac{2}{M}\left[M\left(\frac{r_m - r_0}{r_{\max} - r_0}\right) + \frac{(4-M)^2}{16} \right]^{\frac{1}{2}} - \frac{4-M}{2M} \tag{57}$$

On the other hand, based on the definition of M and its relationship with the two parameters, we obtained:

$$\Phi(M) = \frac{u_m}{u_{\max}} = \frac{12 + M}{24} \tag{58}$$

It is obvious that in Chiu's work, the ratio of mean and maximum velocity is an exponential distribution of the entropy parameter *M* from the Shannon entropy based 2-D velocity model (Chiu 1989). While the relation found based on Tsallis based 2-D velocity distribution is following a linear distribution with *M*. The ratio of mean and maximum velocity (i.e.Φ(*M*)) is plotted against various *M* for both Tsallis entropy based velocity distribution and Chiu's velocity distribution in Fig. 33.

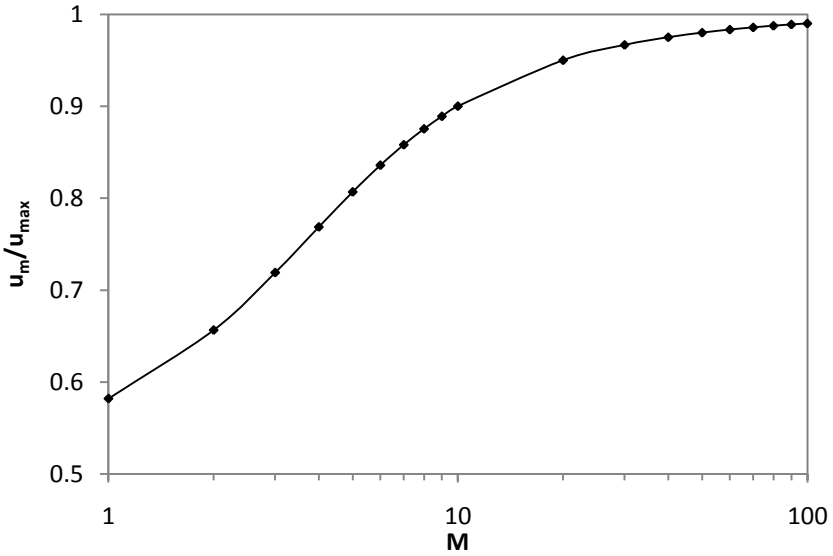

(a)

Fig. 33. u_m/ u_{max} versus various M . (a) Eq. (56); (b) Eq. (58).

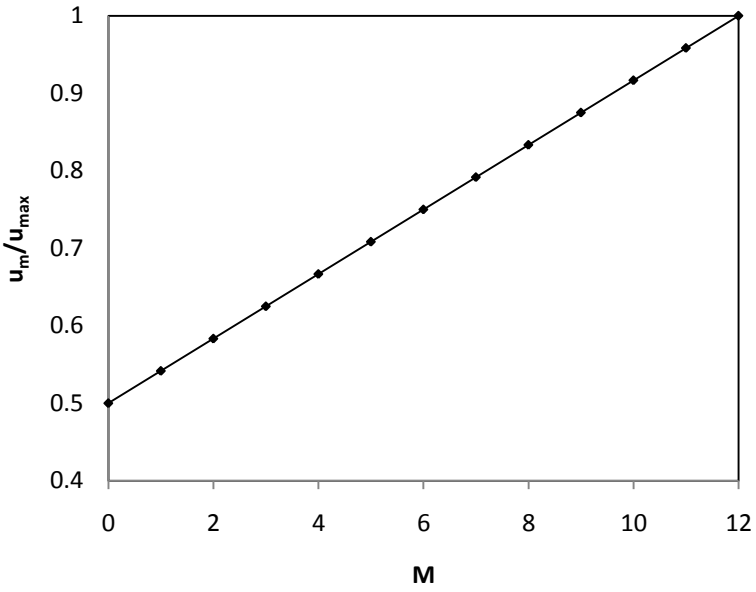

(b)

Fig. 33. continued

Eq. (56) and (58) show that if a sample of pairs (u_m, u_{max}) is given, first $\Phi(M)$ can be estimated and then the entropy parameter M .The parameter M in Chiu's 2-D velocity distribution has a larger possible range compared with the parameter in Tsallis entropy based velocity distribution .

Fig. 34. Upper Tiber River basin with location of river gauging stations.

To test the relationship between the mean velocity and the maximum velocity in a channel cross section, the velocity data collected during a period of 20 years were analyzed for four gauged sections, three of them are located along the Tiber River at 68 km (S. Lucia), at 109.2 km (P. Felcino) and at 137.4 km (P. Nuovo) and one section along the Chiascio River, a tributary of the Tiber River at 85 km (Rosciano). Fig. 34

shows a cartographic map of the upper Tiber basin along with locations of the gauged sections investigated.

The number of velocity measurements and the flow characteristics are summarized in Table 14. The selected sections are equipped with a remote ultrasonic water level gauge, while the velocity measurements are made by current meter from cableways. In particular, depending on the cross-sectional flow area, the number of verticals carried out changes from 4 up to 10 and for each vertical at least 5 velocity points are sampled.

Table 14 Flow characteristics, discharge, *Q*, and maximum water depth, *D*, of the available velocity measurements, *N*, for four gauged sections in the upper Tiber River basin.

Location	N	Q (m^3s^{-1})	D (m)
S. Lucia	42	1.5-215	0.9-5.2
P. Felcino	34	2.3-412	0.8-6.2
P. Nuovo	51	5.4-537	1.1-6.7
Rosciano	38	3-160	1.3-3.3

Comparing the velocity points sampled along different verticals and applying the well-known velocity-area method (Herschy 1985), the maximum and mean velocities were estimated (Chiu and Said1995; Xia 1997). Generally, the true maximum velocity is unknown, but for each vertical, the maximum value in the data set of velocity points sampled can be assumed for it (Chiu 1988). Topographical surveys of the gauged

sections were also available for different years of sampling, showing that there were no substantial changes in the cross-sectional shape.

Using pairs of u_m and u_{max} collected at the four gauged sections, the best-fit mean velocity, u_{bf}, was calculated. The values of $\Phi(M)$ were estimated and are shown in Fig. 35(a)-(d), wherein is also reported the correlation coefficient, R^2.

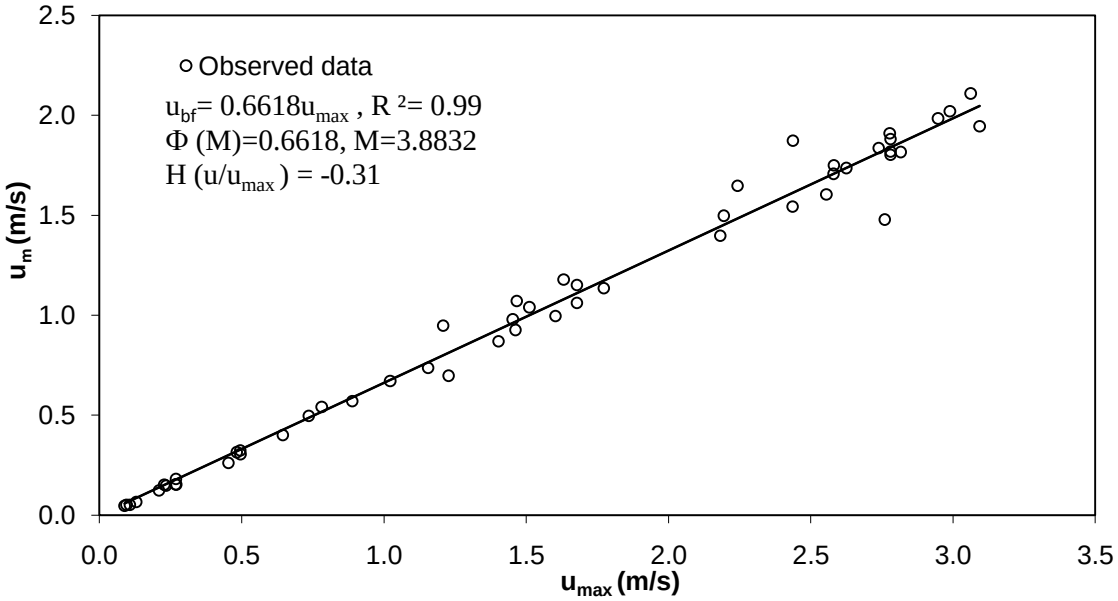

(a)

Fig. 35. Relation between mean and maximum velocities at selected gauged river sections. (a) S. Lucia (b) P. Felcino (c) P. Nuovo (d) Rosciano.

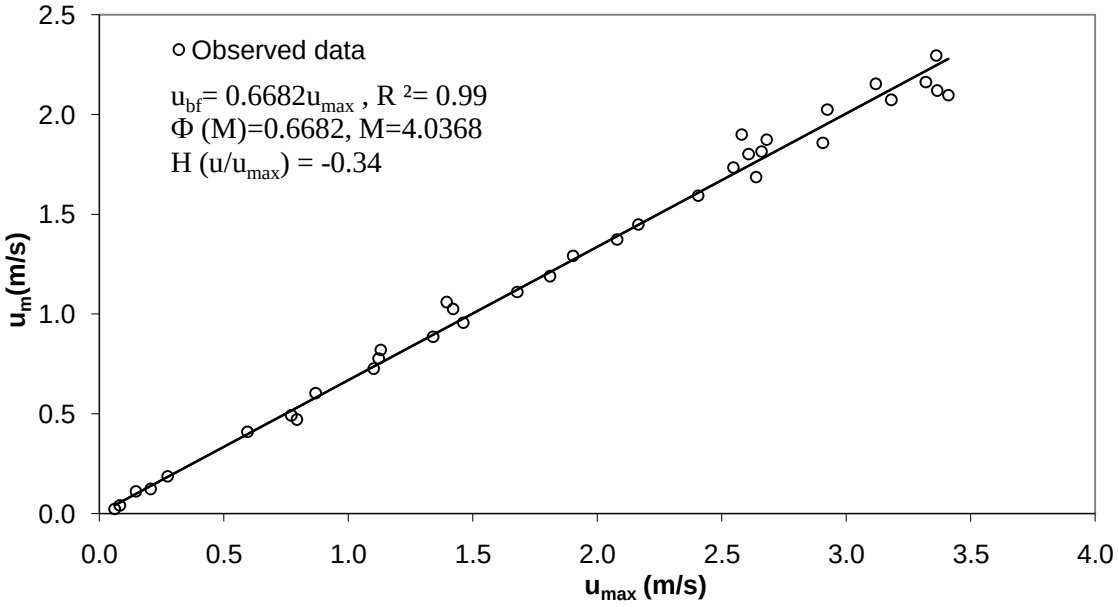

(b)

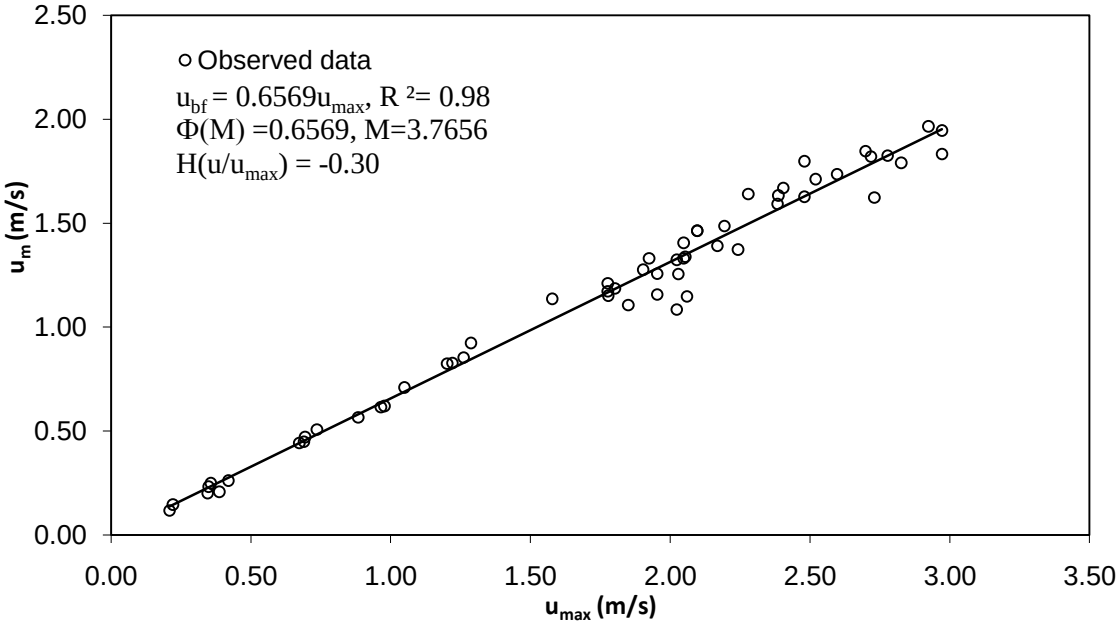

(c)

Fig. 35. continued

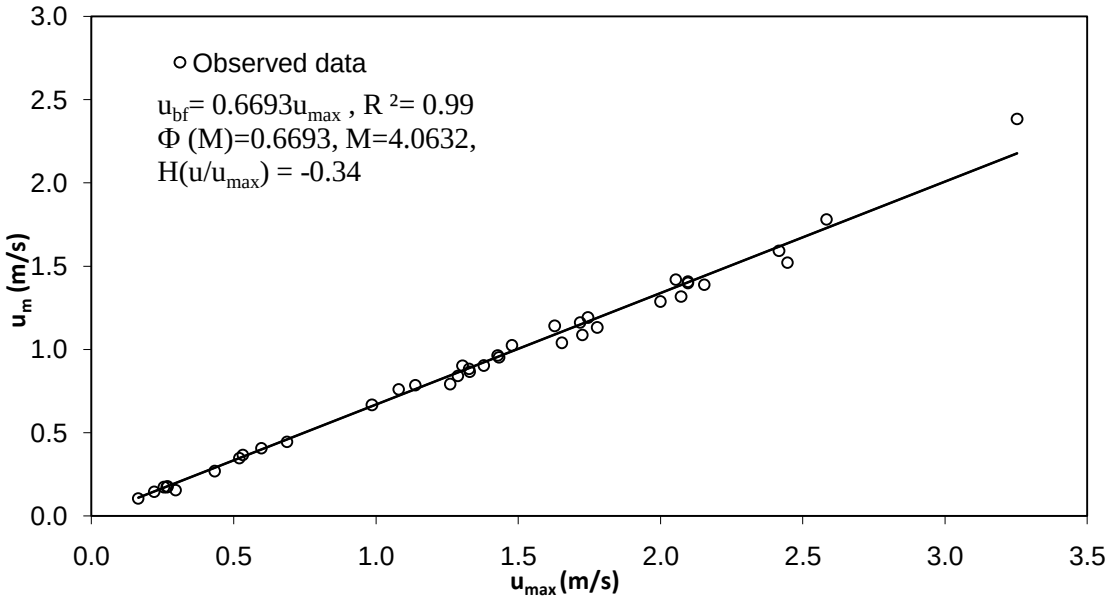

(d)

Fig. 35. continued

Therefore, Φ(*M*) can be assumed constant for the four gauged sections, confirming the results obtained by Xia (1997) for the Mississippi River. This means that the same linear relationship between the mean and maximum velocities can be surmised at any cross-section within the river reach between S. Lucia and P. Nuovo section and along the Chiascio River downstream Rosciano section. In order to test this assumption the best-fit line relative to the mean and maximum velocity data set of the four gauged sections was estimated as plotted in Fig. 36.

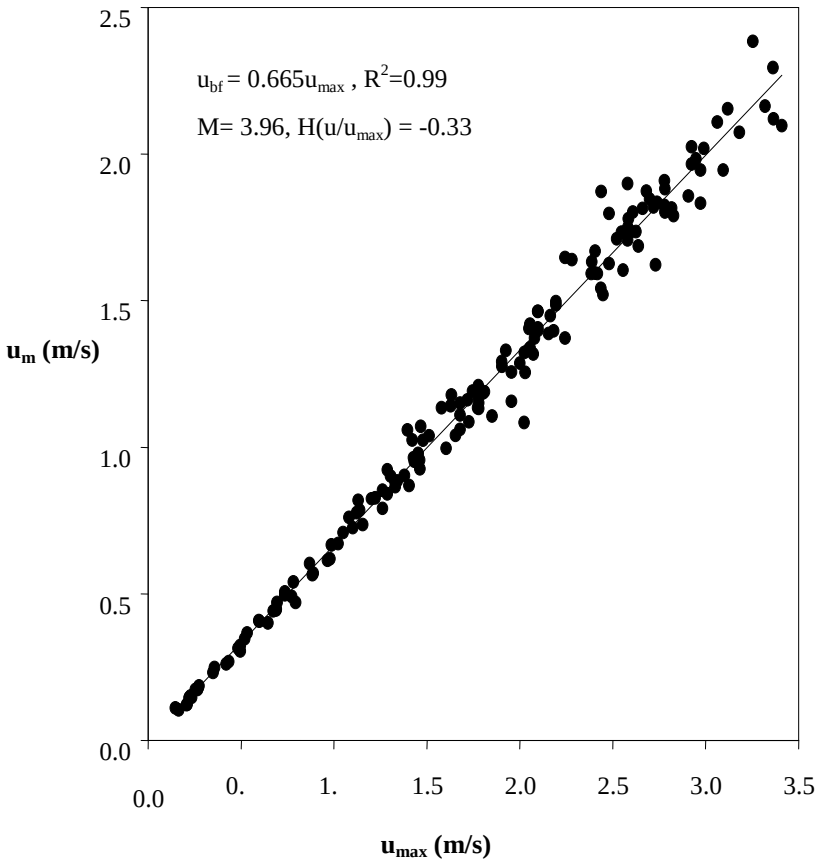

Fig. 36. Relation between mean and maximum velocities for data sets from four gauged sections.

As can be seen, the linear relationship based on Eq. (58):

$$u_{bf} = 0.665\, u_{max} \tag{59}$$

has a high correlation coefficient showing that parameter $\Phi(M)$= 0.665 and then M=3.96 can be assumed constant within the two river reaches investigated. This means M is constant for each channel section and invariant with the discharge or water depth. The excellent, linear relation and correlation between u_{max} and u_m obtained at a channel

section at a value of discharge should be accurate and valid at other values of discharge. However, a given plot such as that in Fig. 35 or Fig. 36 is desirable for determining M in the least-squares sense, to offset likely errors in a single pair of u_{max} and u_m. In Fig. 35 and Fig. 36 each value of u_m was obtained from a given discharge; and u_{max} from velocity samples.

Fig. 35 shows that under a wide range of flow conditions, as characterized by discharge, water depth, and other flow properties, a channel section has a propensity to establish and maintain an equilibrium state that corresponds to a value of M and, hence, a value of the entropy of the distribution $f(u/u_{max})$. To establish an equilibrium state and the corresponding M value, an erodible channel section adjusts the channel characteristics as represented by the bed form and material, roughness geometrical shape, slope, and alignment, under various values of discharge and water depth. A nonerodible or well-established channel section maintains the equilibrium state and the corresponding M and entropy by adjusting the velocity distribution through modifying u_{max} and h when the flow condition changes (Chiu and Said 1995).

So far we come up with three methods to estimate parameter M when the problem is to estimate the velocity distribution along a single vertical of on a cross-section. First, if the mean and maximum velocities along the objective vertical are available, M can be estimated using Eq. (58). Second, if enough velocity samples along several verticals are available, M can be estimated for the known verticals and then get the cross-sectional mean of M, as tested in the previous section, the cross-sectional mean is safe to use to predict the velocity distribution along any vertical with the maximum given or known.

Third, based on the previous analysis on $\Phi(M)$ and M, they tend to be constants for a particular river reach and do not change much during different time periods. That means if the historical records of the mean and maximum velocities at a cross-section are available, $\Phi(M)$ can be estimated from the least square method and then M can be obtained based on Eq. (58). Fig. 37 presented the velocity profiles plotted using M estimated in the three ways above for three verticals at P. Felcino gauged section during the flood event that happened in April, 1997. The values of M parameter estimated in the three ways are listed in Table 15.

Table 15 M for different verticals at P. Felcino on Tiber River and estimated in three ways. Mm denotes M taken as the cross-sectional mean, Mh is M derived from historical value, Mi is M estimated using the data for the objective vertical.

z (m)	Mm	Mh	Mi
-14.66	5.23	4.04	3.38
0.00	5.23	4.04	6.36
7.34	5.23	4.04	5.87

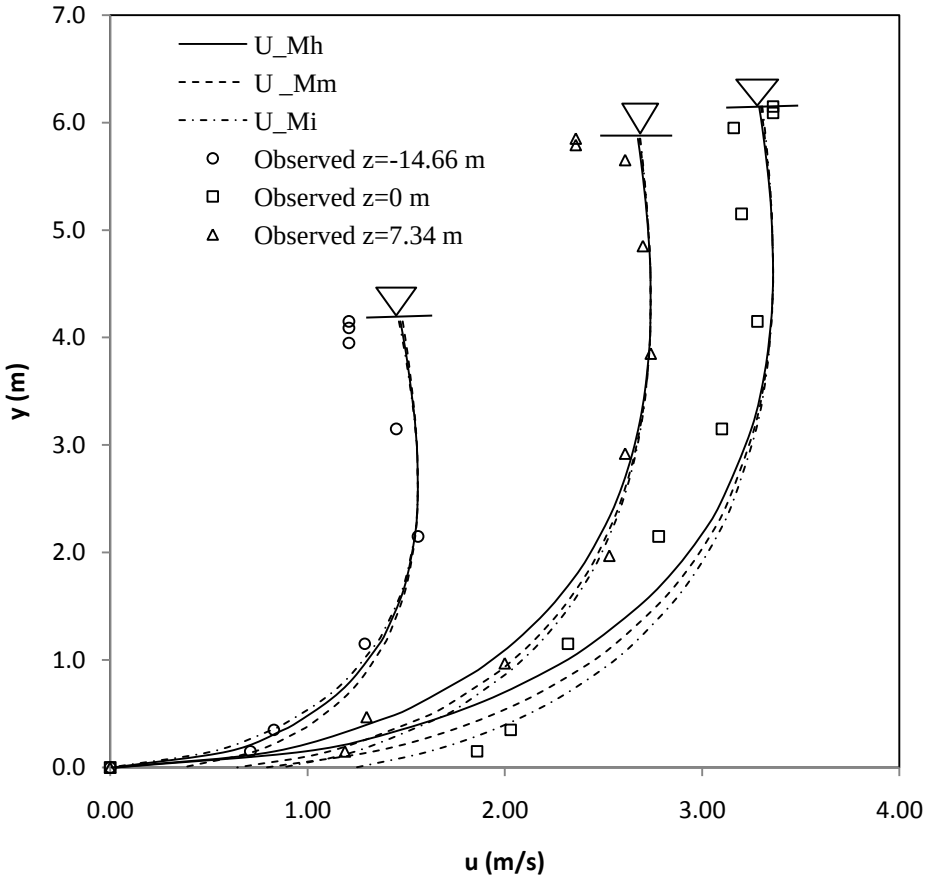

Fig. 37. Velocity profiles estimated by the Tsallis entropy based 2-D velocity distribution. U_Mh denotes velocity estimated using *M* derived from historical methods; U_Mm denotes velocity estimated using *M* obtained from cross-sectional mean value of *M*; U_Mi denotes velocity estimated using *M* obtained from velocity samples along the objective vertical.

Though we can see from the Table 12, the values of *M* computed in three ways are not the same, there is no major difference found between the velocities profiles plotted

using *M* estimated using different ways as shown in Fig. 37 and Table A24 to Table A26. More significant differences concentrated in the region close to the channel bed, for this area velocity estimation using *M* parameter for this particular case is the best against the observations. Based on the results, the three methods to estimate the *M* parameter are acceptable to use, but usually enough samples along one vertical is hard to get and many verticals needed to be taken into account to estimate the cross-sectional mean so both of these methods will rely on the available data. Based on the conclusion that *M* is a hydraulic parameter that holds constant and that is always historical data for the gauged section, *M* is handy and recommended to get in the third way.

3.9.2. Location of mean and maximum velocity

From Eq. (57) and (58), the location of mean velocity can be obtained as the ratio is computed and plotted for various *M* values in Fig. 38:

$$\frac{r_m - r_0}{r_{\max} - r_0} = \frac{1}{M}\left[\left(\frac{M^2}{48}+1\right)^2 - \frac{(4-M)^2}{16}\right] \tag{60}$$

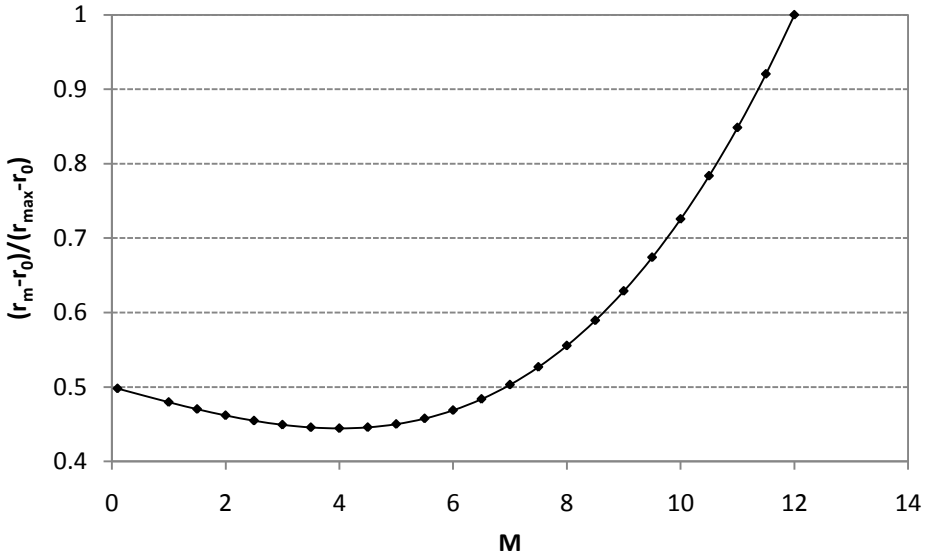

Fig. 38. $(r_m-r_0)/(r_{max}-r_0)$ versus M.

As shown in Fig. 38, $(r_m-r_0)/(r_{max}-r_0)$ (for wide channels this term can be approximated as y/D) decreases slowly and reaches the lowest value 0.44 when M=4. Once M exceeds 4, the ratio increases very quickly and reaches the maximum as unity when M=12, this is consistent with the previous statement that M=12 corresponds to the constant velocity case. As mentioned earlier, parameter h controls the shape and slope of isovels, especially near the water surface and in the vicinity of the point of maximum velocity. If $h< 0$, u_{max} occurs below the water surface and $|h|$ is the depth of u_{max} below water surface. h/D can be determined using the least square method.

The velocity distribution is plotted in Fig. 40 using Eq. (47) in comparison with the observed data for two verticals in Pontelagoscuro gauged section on Po River during the

flood event that occurred in March, 1991, the locations of maximum and mean velocities are also shown.

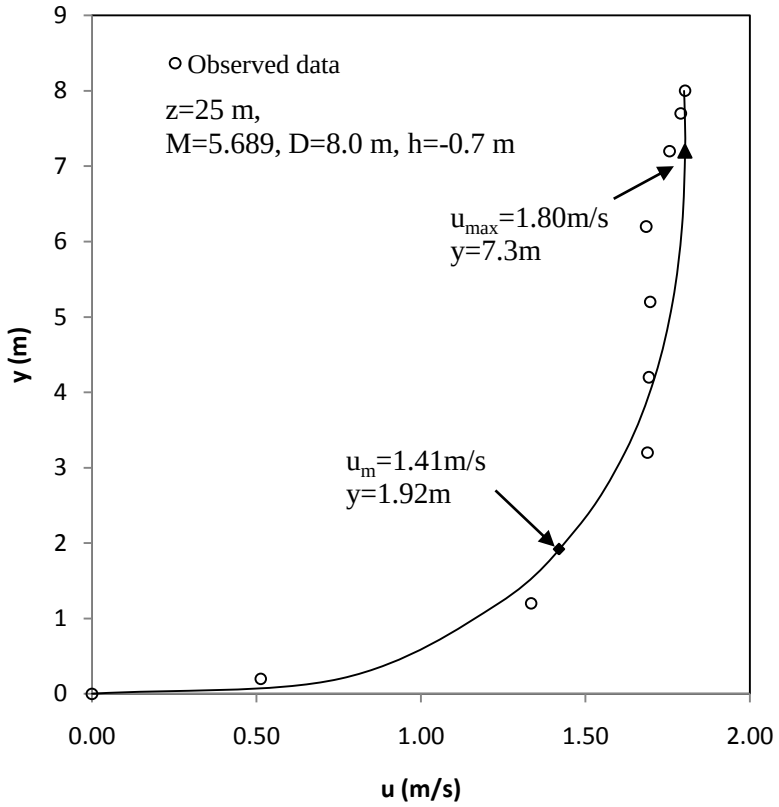

(a)

Fig. 39. Velocity profiles plotted against the observed data collected from Pontelagoscuro gauged section on Po River during the flood event that occurred in March, 1991 and the locations of maximum and mean velocity.

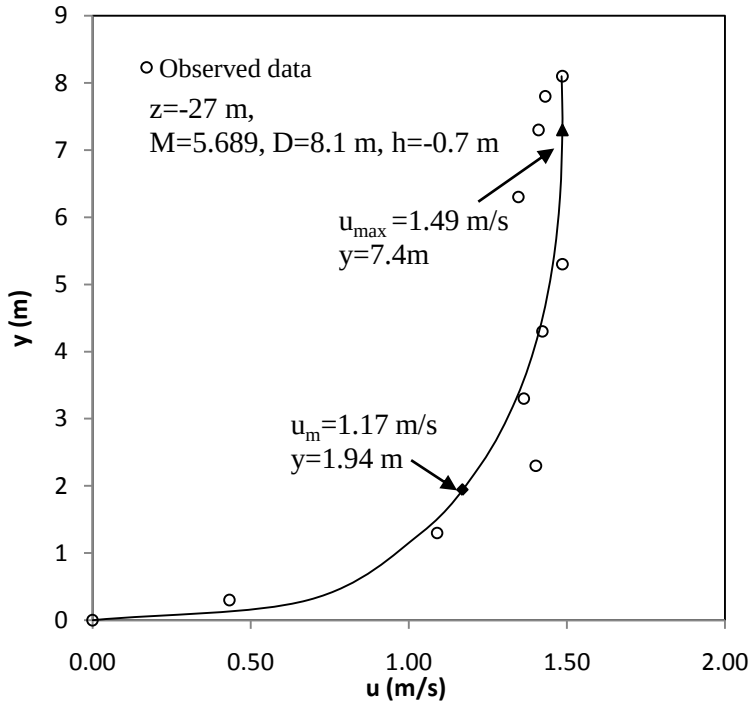

(b)

Fig. 39. Continued

Based on the maximum entropy, the four functions giving $u_m/u_{max,}$ $(r_m-r_0)/(r_{max}-r_0)$, $H(u/u_{max})$, and $f(u/u_{max})$ have one common parameter, M, providing different ways for describing a velocity distribution in a channel cross section. The term u/u_{max} as given by Eq. (46) and (48) describe the spatial distribution of velocity; u_m/u_{max}, $(r_m-r_0)/(r_{max}-r_0)$, and $H(u/u_{max})$ are measures of homogeneity (or uniformity) of spatial distribution of velocity. Since these quantities are functions of M, they are constant at a given channel section and represent regularities that exist in various flow patterns. These regularities also support and connect to each other in open channel flows such that if one is known the rest can be determined from it. These diagrams can be used to facilitate the task of

describing velocity distributions and the field work dealing with natural and man-made channels, such as discharge measurements.

The preceding results show that entropy parameter *M* is an effective measure of the overall characteristics of a channel section, as represented by the bed form and material, slope, shape, and alignment, and can be used to classify various channel sections and their equilibrium states. Even in a nonerodible or well-established channel, Manning's *n* at a channel section tends to vary with discharge, u_m or water depth, while *M* remains constant. Therefore, *M* is a better representative of a channel section than Manning's *n*. Periodic reevaluations of the *M* value of a channel section can be conducted to detect any significant changes in the channel characteristics due to man's activities, such as construction of dams, bridges, and other structures that tend to upset the equilibrium state of the channel section. Most importantly, the *M* value can be used in Eq. (58) to facilitate the estimation of u_m from u_{max}, or u_{max} from u_m. To determine u_m, u_{max} determined from a velocity profile on the y-axis can be used. u_{max} can be determined without velocity data, if the discharge or u_m is known. .

3.10. Application to different cases

The Tsallis entropy based 2-D velocity equation is tested using various sources of data in this section to evaluate the performance of Tsallis entropy based 2-D velocity equation in steady uniform flows, nonuniform flows, high flood events, unsteady flows.

3.10.1. Applicability to uniform and nonuniform flows

In hydraulics, uniform flows are defined as flows with the depth average flow velocity (integrated over depth), area flow cross-sections constant everywhere along the channel.

For uniform flows, the energy grade line slope, water surface slope, and channel bed slope are all equal. The assumption of a uniform flow is the simplest model (and the least accurate) to solve a hydraulic problem. The principal advantages of a uniform flow assumption are speed and simplicity. Spreadsheet applications for normal depth analysis are either readily available or easily written. The disadvantages are loss of accuracy in water surface profile calculations and the potential to over- or under-design the storm sewer or small channel, depending on the topography of the site. This simplification may be adequate for some applications, but it can include significant error in the storage-outflow estimate. Uniform flow assumptions may be employed when the engineer believes that more complex, rigorous methods will not generate sufficient additional hydraulic accuracy or result in sufficient cost reductions in the engineering design. There are generally few instances in river hydraulic analysis when the engineer assumes uniform flow for the solution of an open channel modeling problem. More practical and frequently happening in natural channel is nonuniform flows, so it may be interesting to test the performance of Tsallis entropy based velocity distribution in both steady uniform and nonuniform flows. Data collected by Guy (1966) were for a steady and uniform flow in a rectangular flume. The velocity profiles plotted here were on the y-axis (i.e., a single vertical that passes through the point where u_{max} occurs). Data along a steady, nonuniform flow in a rectangular flume is also used here to see how the model works for a nonuniform case.

Fig. 40(a) and (b) compare velocity estimated by Tsallis entropy based 2-D velocity equation and velocity samples collected on the y-axis for two rectangular channels.

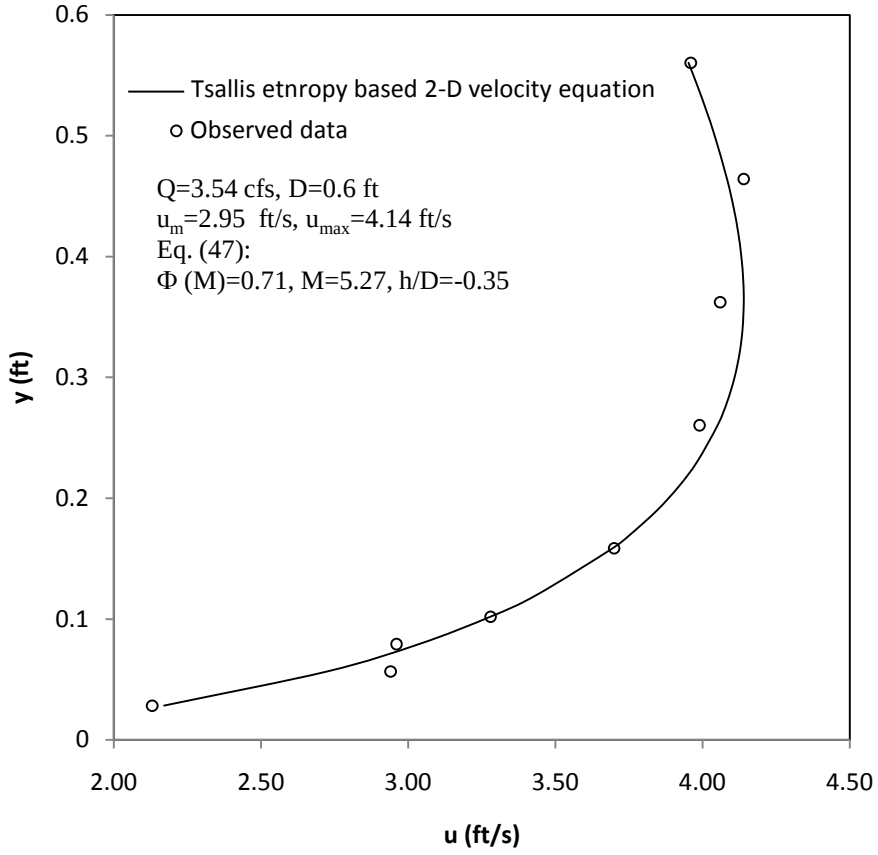

(a)

Fig. 40. Velocity profiles on *y*-axis of rectangular channels. (a) Uniform flume flow (Guy 1966); (b) Nonuniform flume flow (Guo 1990).

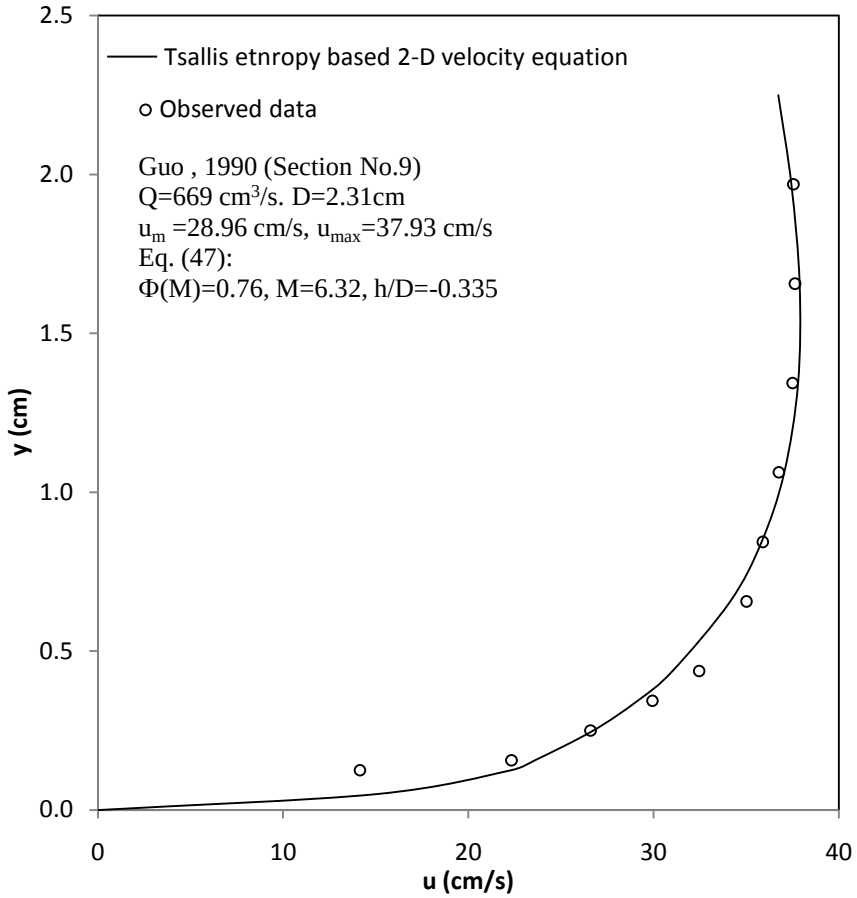

(b)

Fig. 40. continued

Fig. 40(a) shows velocity samples on the *y*-axis at a channel section, 2ft wide, 0.60 ft deep and u_m =2.95 ft/s (Run7, Guy 1966) and the computed values using Tsallis entropy based velocity equation. Fig. 40(b) shows the velocity distribution on the *y*-axis of a rectangular channel, 10 cm wide and 2.31 cm deep (Guo 1990). Good agreement is found between the velocity samples and the velocity profiles estimated by the Tsallis entropy based equation. For Fig. 40(a) the flow condition is uniform and ideal, and the case in Fig. 40(b) the flow is nonuniform and more complicated and realistic in natural

rivers and streams. The entropy based velocity equations predict velocity in both uniform and nonuniform steady flows with high accuracy. The accuracy was verified with error analysis and the mean errors were 0.022 and 0.060, respectively, while the standard deviation did not exceed 0.05. More details about the data and errors are tabulated in Tables A29 and A30.

3.10.2. Application to clear water control flows and sediment laden-flows

As stated for the 1-D case, the 1-D entropy based method can simulate both clear water flows and sediment-laden flows in the lower region of the flow when it is very close to channel bed where lots of factors have effects on the velocity distribution. The two dimensional velocity equation is proposed for channels that are not wide, where that the maximum velocity does not always happen at the water surface. Therefore, a more universal distribution is described by Eq. (47) and Eq. (49) by transforming the Cartesian coordinate system (*y*-*z*) to curvilinear coordinate system (*r*-*s*). The 2-D velocity distribution law can be treated as a generalized velocity law and its applicability to sediment-laden flow and clear water control flow is tested here using Coleman's experimental data (Coleman 1986).

Fig. 41 shows a clear-water control velocity profile and the capacity suspension profile comprising the beginning and end of the series of experiments with 0.105-mm sand.

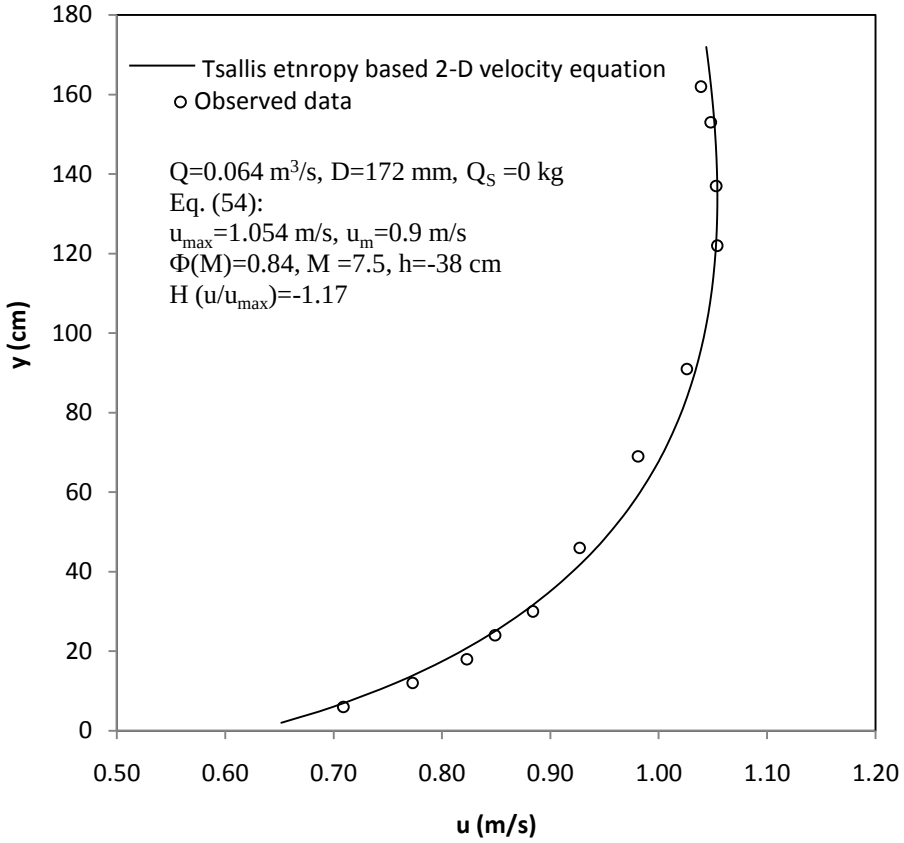

(a)

Fig. 41. Clear water control velocity profile and the capacity suspension profile from the experimental series with 0.105 mm sand. (Run 1 and 20, respectively).

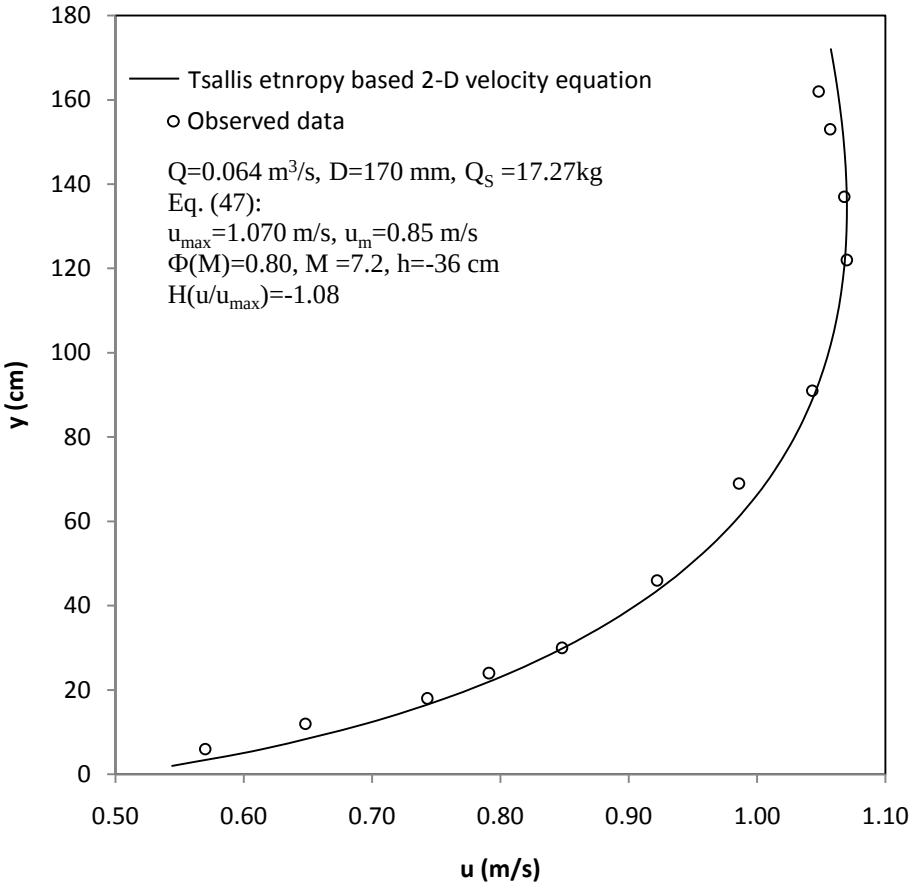

(b)

Fig. 41. continued

The other hydraulic factors that can affect the shape of the velocity profiles are constant, such as the channel geometry, discharge and alignment. Apparently parameter *M* decreases with the increase in the sediment load and hence the maximum entropy $H(u/u_{max})$, with the maximum velocity being almost constant that means the mean velocity of the profile decreases. The location of the maximum velocity and then the term *h/D* that helps shape the velocity profile can be obtained by the least square method. The simulations using the Tsallis entropy based 2-D velocity equation are found to be

accurate in both the regions close to water surface and the lower part of the flow which is under the influence of high sediment concentration and shear stress with mean errors as -0.001 and 0.02 for Run 01 and Run 20, respectively. More details about the data can be found in Tables A31 and A32.

3.10.3. Applications to high and unsteady flows

The linear relationship between the mean and the maximum flow velocities is found to be accurate at four gauged river sections in the upper Tiber River basin in Central Italy in the previous section. The value of parameter could be surmised to be constant at any site within the two river reaches investigated and is acceptable to use to predict the velocity distribution along any vertical at the selected gauged section. The simple method developed for reconstructing the velocity profiles at a river section based on Tsallis entropy based two-dimensional velocity distribution (Eq. (47)) is tested here against the velocity samples on three verticals located at P. Nuovo gauged section and also the isovels for the cross section was plotted.

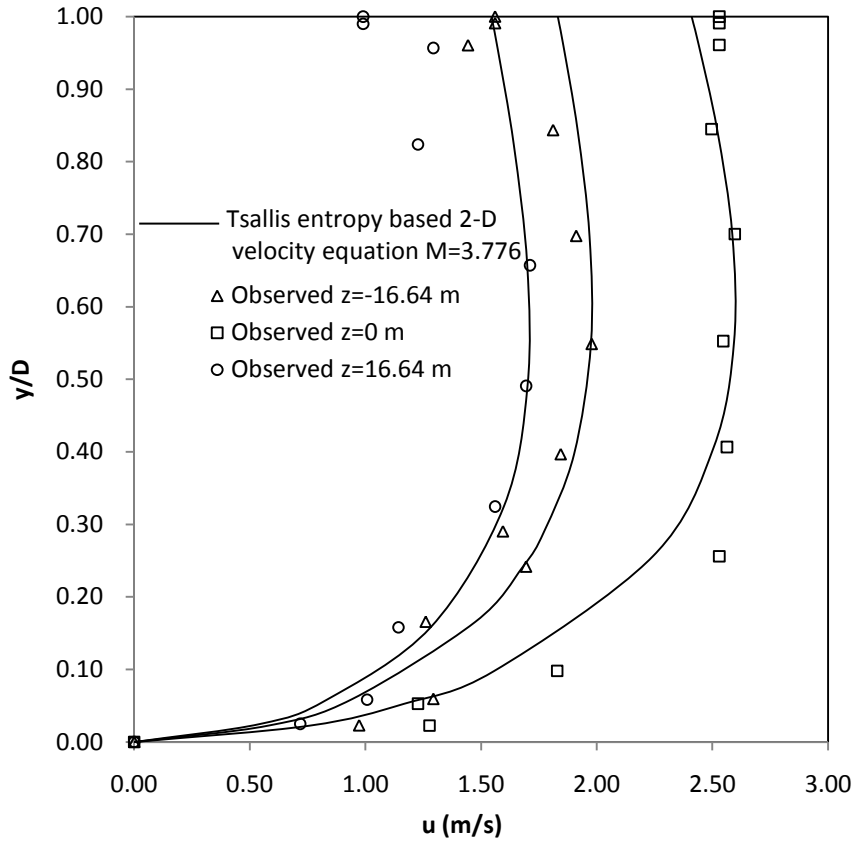

(a)

Fig. 42. Velocity distributions estimated using the Tsallis entropy based 2-D velocity distribution. (a) velocity samples and computed velocity distribution on selected verticals and (b) simulated 2-D velocity distribution using the Tsallis entroy based 2-D model in the rectangular channel section.

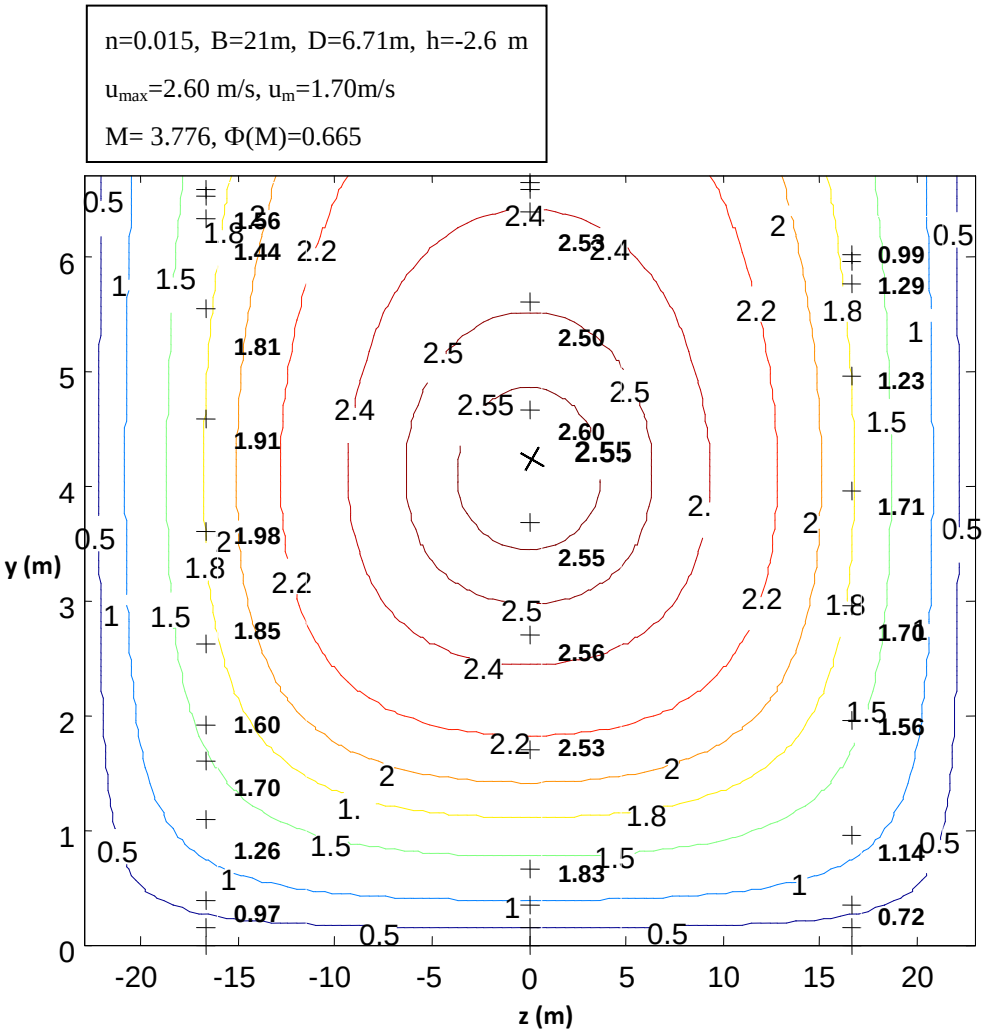

(b)

Fig. 42. continued

The Tsallis entropy based 2-D velocity distribution is found to be capable of estimating with a reasonable accuracy when compared with the sample of the observed velocity profiles for high flood events with mean errors between -0.03 to 0.05 and the maximum value of standard deviation was about 0.046. Therefore, through the analysis we can confirm the Tsallis entropy based velocity equation can be applied locally.

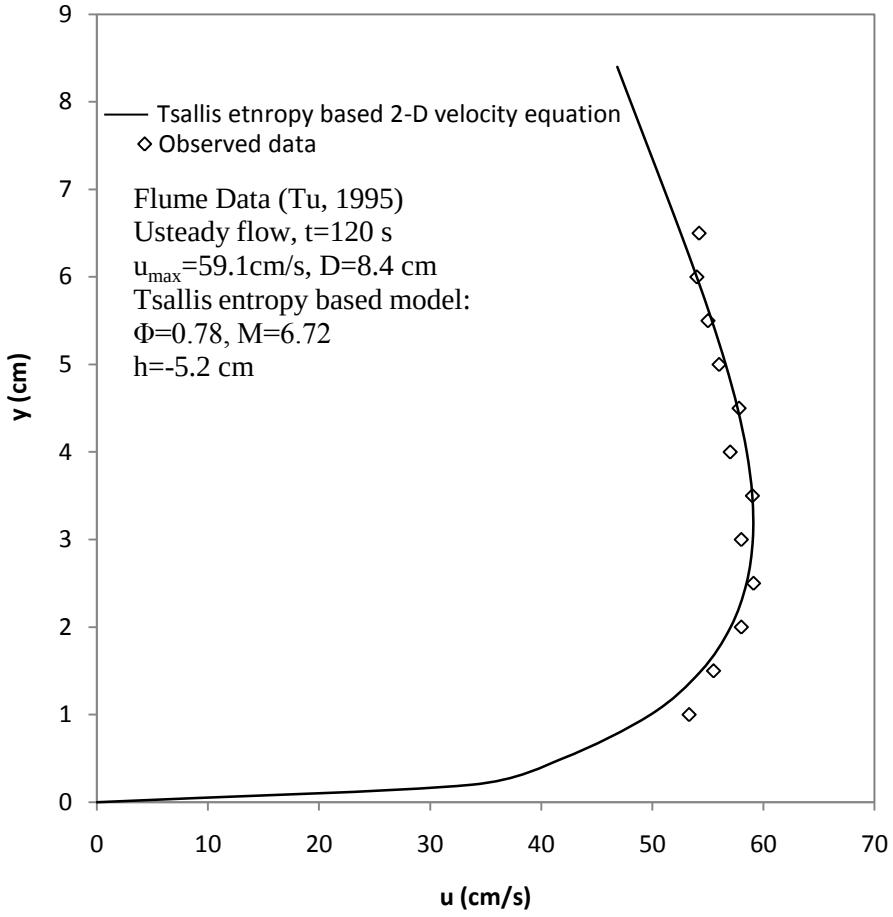

Fig. 43. Velocity distribution of unsteady flows.

Available laboratory flume data are used to illustrate accuracy and reliability of the Tsallis entropy based 2-D velocity equation in unsteady flow cases in Fig. 43. The laboratory flume data (Tu 1995) are used to evaluate and verify the applicability of the 2-D velocity distribution model. The results on comparison with observations with a mean error as -0.007 and standard deviation as 0.024 show that the new velocity equation can quickly and accurately estimate velocity distribution in unsteady flows. The maximum velocity usually occurs beneath water surface during flood periods. The

higher the water state is the deeper the location of maximum velocity. Fig.43 shows the velocity distribution of unsteady flows with the maximum as 59.1 cm/s, and the maximum velocity occurs beneath the water surface at around 0.6 depths.

The probability law describing the velocity distribution at a channel section in rivers and streams is resilient and invariant with time and discharge. This is based on the observation that its parameter *M*, the average ratio of the mean and maximum velocities, is invariant with time, discharge, and water level. This in turn can serve as the basis for an efficient method of discharge measurements in rivers and streams. The method is applicable in both steady and unsteady flows in rivers, and can be used with any velocity-measuring equipment to drastically reduce the time and cost of discharge measurements. Its most important utility, however, is its applicability in unsteady, high flows to collect data that are essential in critical situations, such as flow forecasting, but cannot be measured by conventional methods.

4. COMPARISION OF VELOCITY EQUATIONS

4.1. Other 1-D velocity distributions

The velocity distribution given by Eq. (23) differs from the Shannon-entropy based velocity distribution derived by Chiu (1988):

$$u = \frac{u_*}{k_1} \ln[1 + \{\exp(k_1 \frac{u_D}{u_*}) - 1\} \frac{y}{D}] \tag{61}$$

and the widely used Prandtl-von Karman universal velocity distribution:

$$u = \frac{u_*}{k} \ln \frac{y}{y_0} \tag{62}$$

where k_1 is a parameter, k is the von-Karma universal constant, y_0 is a very small (almost unmeasurable) value of y at which the shear velocity (u_*) happens, u_D is the velocity at the water surface, u_* is the shear velocity equal to $\sqrt{gDS}$, where g is the gravitational acceleration, D is the flow depth, and S is the channel slope. The probability distribution function of Prandtl-von Karman velocity distribution is:

$$F(u) = \frac{k \exp(-ku/u_*)}{u_*[\exp(k) - \exp(-ku_D/u_*)} \tag{63}$$

Based on the probability density function $f(u)$, its maximum entropy is determined as:

$$H = \ln[\exp(k) - \exp(-ku_D/u_*)] + \frac{k}{u_*} u_m - \ln(k/u_*) \tag{64}$$

Furthermore y_0 can be estimated using the relation that:

$$y_0 \exp(ku_D/u_*) \approx D \tag{65}$$

We used the 12 sets of data collected by Einstein and Chien (1955) to test how Eq. (65) works as shown in Fig. 44. The data was chosen since the other parameters needed

to estimate D were available in their report. In order to guarantee the validity of Eq. (65) more data should be used to test it in the future.

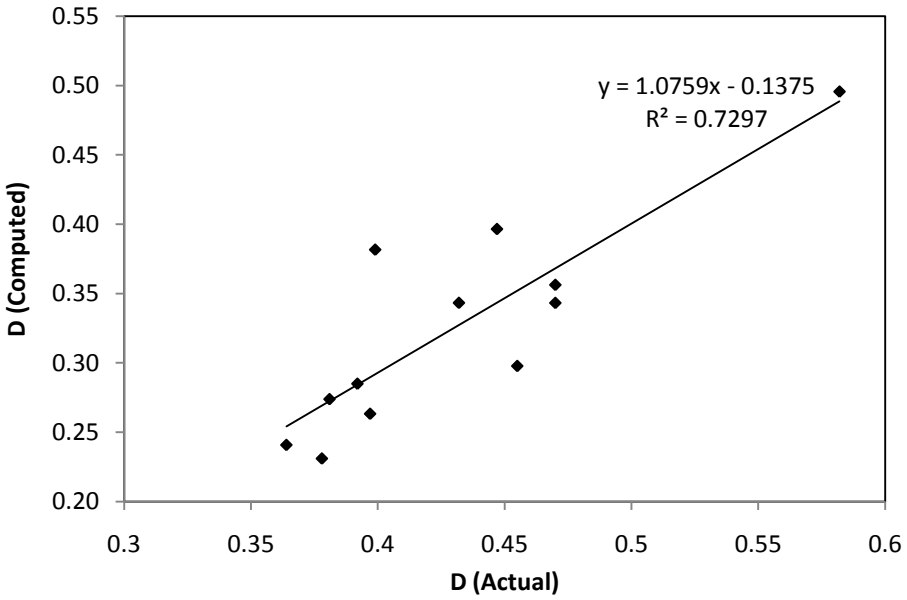

Fig. 44. Testing of Eq. (65) using the data collected by Einstein and Chien (1955).

Though the estimated values of water depth using Eq. (65) cannot strictly overlap the actual values, the ratio between the computed values and the actual data is almost unit and the R^2 value is 0.73, which means the relation given by Eq. (65) is acceptable to use to estimate y_0 with the other parameters easily estimated and given.

Another well-known velocity distribution law is power law. The power law velocity distribution in open channels can be expressed as:

$$u = ay^b \tag{66}$$

or

$$\frac{u}{u_D} = (\frac{y}{D})^{1/n} \tag{67}$$

where *a*, *b*, and *n* are parameters (Karim and Kennedy 1987). Exponent n is usually determined by the frictional resistance at the bed, and is, in practice, not known but can be determined using the least square method, if observed velocity profiles are available.

Using Shannon entropy the exponent parameter n can be estimated as:

$$n = \frac{1}{\ln u_D - \overline{\ln u}} \tag{68}$$

and its maximum entropy can be determined as:

$$H = (n+1)\ln u_D - n\overline{\ln u} \tag{69}$$

Parameter n can also be determined using regression analysis (least square method), Fig. 45 presents how the two methods works for the data collected by Einstein and Chien (1955).

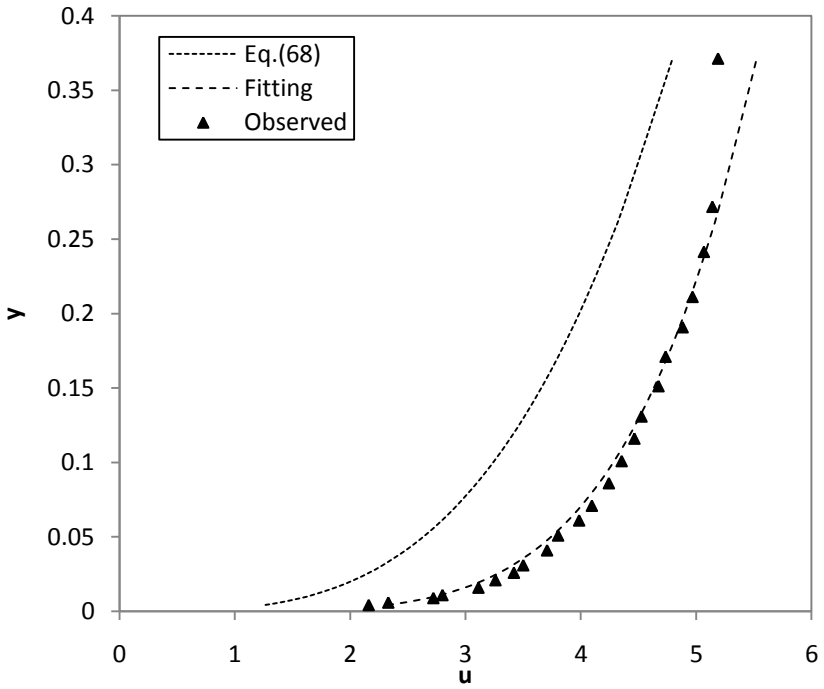

Fig. 45. Comparison of different method of estimating parameter *n*. (Data from C5 series (Einstein and Chien 1955)).

We found in Fig. 45 the velocity distribution using the method of mathematical fitting is strictly in agreement with the observed data. It may be interesting to examine the relation between the parameter values estimated by the two methods. 10 sets of data collected by Einstein and Chien (1955), 2 sets of field data from Iran and 3 Coleman's data are examined here and the *n* values estimated in two ways are found to follow a linear relationship. In practice, the estimation using Eq. (68) is easier to handle, it is possible to use the relation presented in Fig. 46 to obtain a more accurate value of parameter *n*.

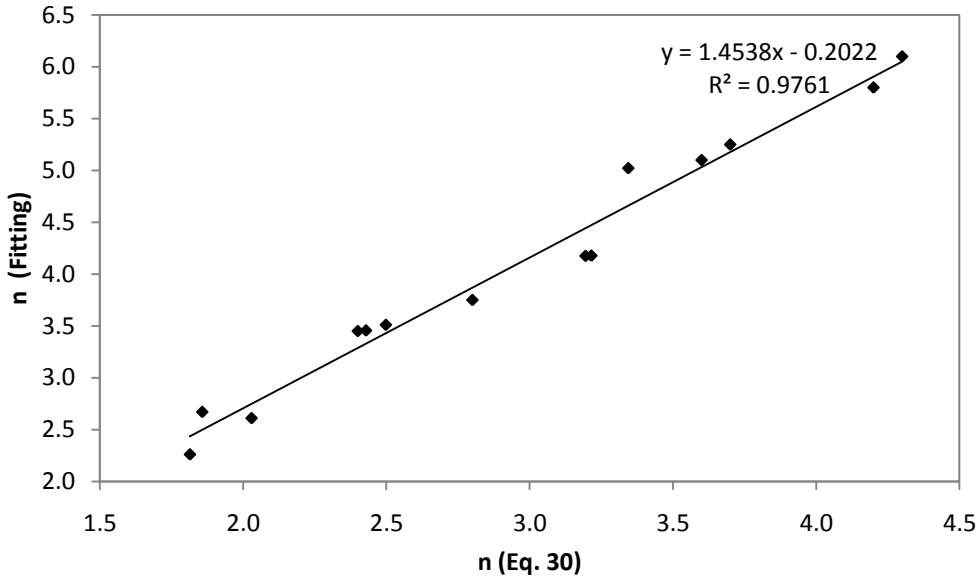

Fig. 46. The relationship between exponent parameter *n* derived from Eq. (68) and *n* from regression.

4.2. Comparison between Tsallis entropy based velocity distribution and other velocity distributions using field data and laboratory data

The reliability of Tsallis based entropy velocity distribution equation as a velocity distribution law, and any special features it may have relative to the Prandtl-von Karman universal velocity distribution law, Shannon Entropy based velocity law, Power velocity distribution law have been tested here. In order to see how these four different velocity distributions perform in simulating natural rivers and laboratory flume, the observations collected from natural rivers in Iran and experimental data collected by Einstein and Chien (1955) and Coleman (1986) were used to justify the results.

Comparison of the four velocity distributions and corresponding dimensionless velocity distributions along the whole water depth against Iran river velocity data are presented in Fig. 47.

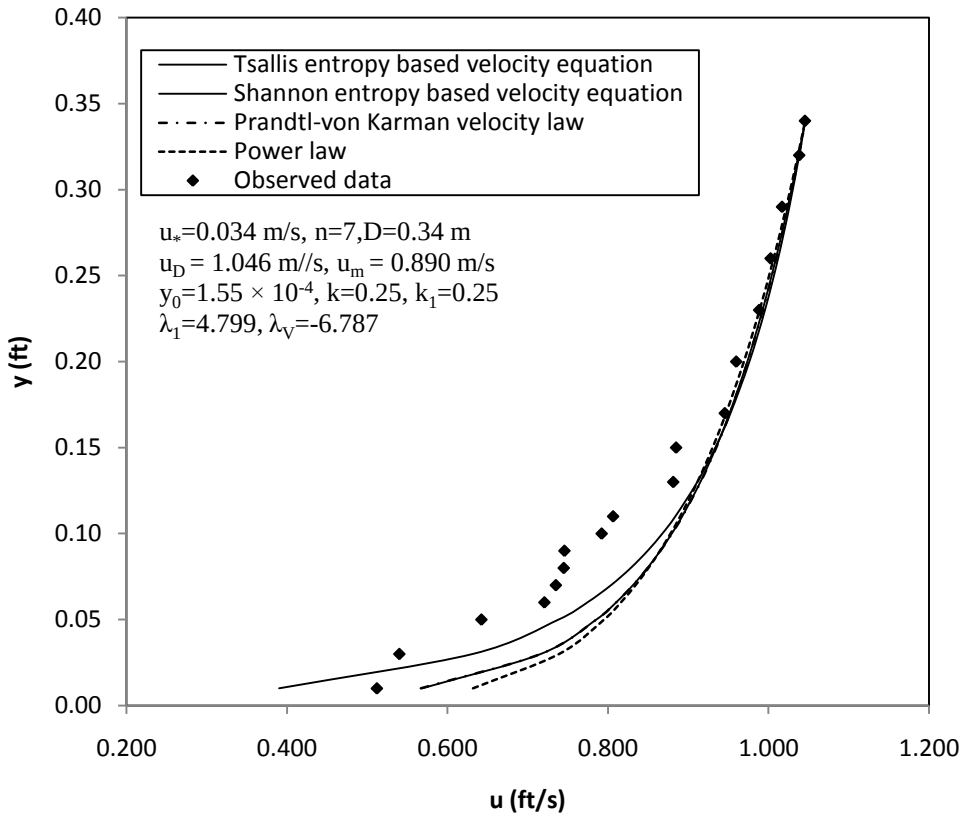

(a)

Fig. 47. Comparison of Tsallis entropy-based velocity distribution with observed velocity and velocity distributions based on Shannon entropy and Prandtl-von Karman universal velocity distribution and power law velocity distribution (Iran data 2). (a) velocity distribution; (b) dimensionless velocity distribution.

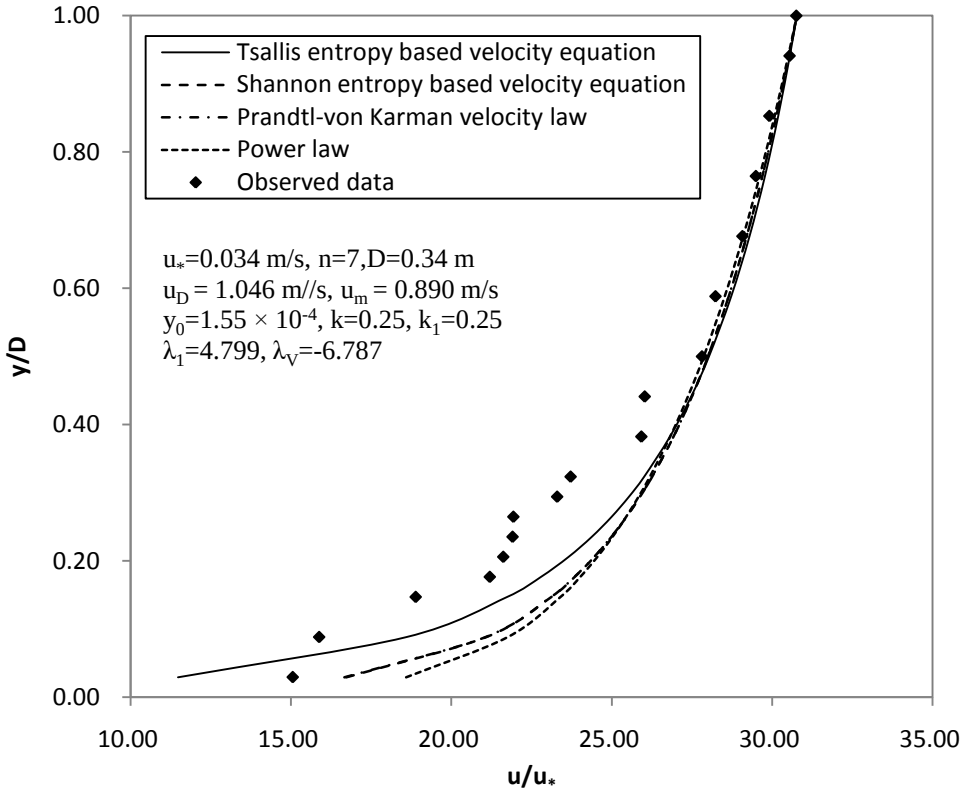

(b)

Fig. 47. continued

And the computations and observations were tabulated in Table 16.

Table 16 Comparison of Tsallis entropy-based velocity distribution with observed velocity and velocity distributions based on Shannon entropy and Prandtl-von Karman universal velocity distribution and power law velocity distribution (Iran data 2).

y (m)	u (m/s)				
	Tsallis	Shannon	Prandtl-von Karman	Power law	Observed
0.01	0.390	0.568	0.567	0.632	0.512
0.03	0.632	0.716	0.716	0.739	0.540

Table 16 (*continued*)

y (m)	u (m/s)				
	Tsallis	Shannon	Prandtl-von Karman	Power law	Observed
0.05	0.739	0.786	0.786	0.795	0.642
0.06	0.775	0.810	0.810	0.816	0.721
0.07	0.804	0.831	0.831	0.835	0.735
0.08	0.829	0.849	0.850	0.851	0.745
0.09	0.850	0.865	0.866	0.865	0.746
0.10	0.868	0.880	0.880	0.878	0.792
0.11	0.884	0.893	0.893	0.890	0.807
0.13	0.912	0.915	0.916	0.912	0.882
0.15	0.934	0.935	0.935	0.931	0.885
0.17	0.953	0.952	0.952	0.947	0.946
0.20	0.977	0.974	0.974	0.970	0.960
0.23	0.996	0.993	0.993	0.989	0.989
0.26	1.012	1.010	1.010	1.007	1.003
0.29	1.026	1.024	1.025	1.022	1.017
0.32	1.039	1.038	1.038	1.037	1.039
0.34	1.046	1.046	1.046	1.046	1.046

Table 17 Mean, $\mu(\varepsilon)$, and standard deviation, $\sigma(\varepsilon)$, of error given by Eq. (27) considering Tsallis entropy-based velocity equation, Shannon entropy and Prandtl-von Karman universal velocity distribution and power law velocity distribution (Iran data 2).

	Tsallis	Shannon	Prandtl-von Karman	Power law
μ	0.046	0.087	0.087	0.096
σ	0.091	0.090	0.090	0.106

As in Fig. 47, when *y/D* is below 0.5, the simulation lines of four velocity distribution began to deviate away from the actual values, all the four velocity distributions led to higher values than the measurements. The reason lies in the fact that in the lower part of the channel, especially alluvial channel, the sediment concentration tends be higher and the sediment movement tends to be more complicated which leads to a deceleration of the flow velocity. Therefore, a larger gap was found in the lower region that is close to the channel bed, whereas with the mean and maximum velocity measured or given the Tsallis entropy based velocity equation obtained the simulation closest to observations amongst the four velocity distributions with the minimum mean error as 0.046 and the standard deviation about 0.091 as shown in Table 17. One thing noted is that as low as *y/D* was 0.03, the Prandtl-von Karman velocity law generated almost the same simulation as the Shannon entropy based velocity equation.

And comparison of the four velocity distributions and corresponding dimensionless velocity distributions for the whole water depth against experimental data (Coleman 1986) are presented in Fig. 48.

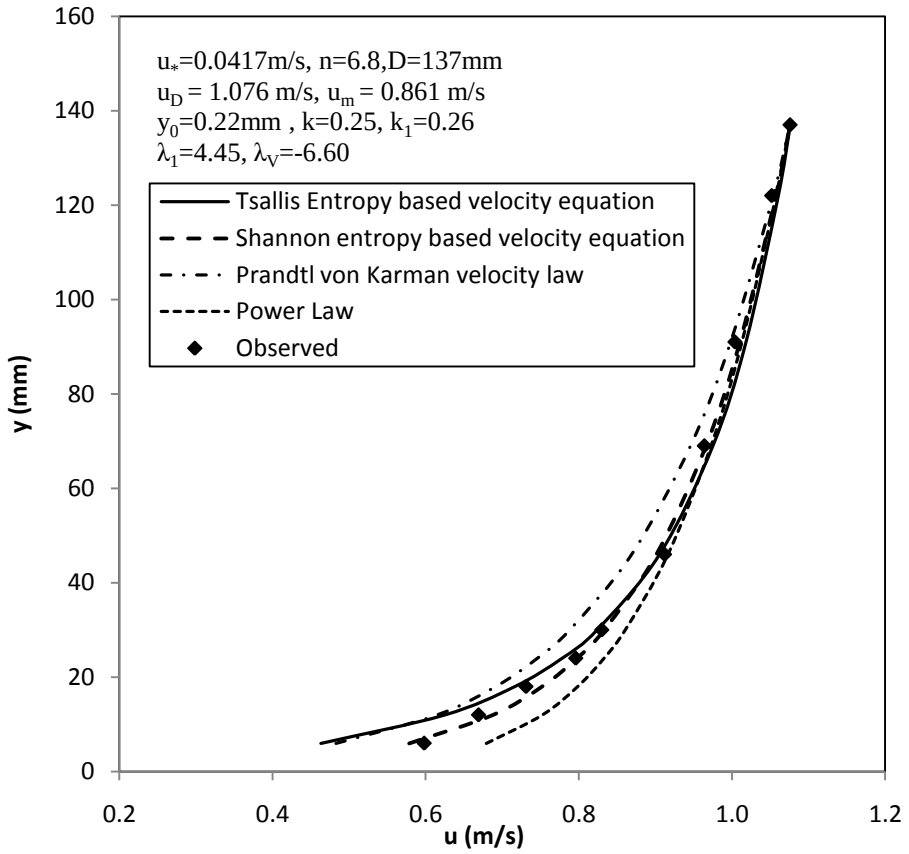

(a)

Fig. 48. Comparison of Tsallis entropy-based velocity distribution with observed velocity and velocity distributions based on Shannon entropy and Prandtl-von Karman universal velocity distribution and power law velocity distribution (Data from Run 12, Coleman 1986). (a) velocity distribution; (b) dimensionless velocity distribution.

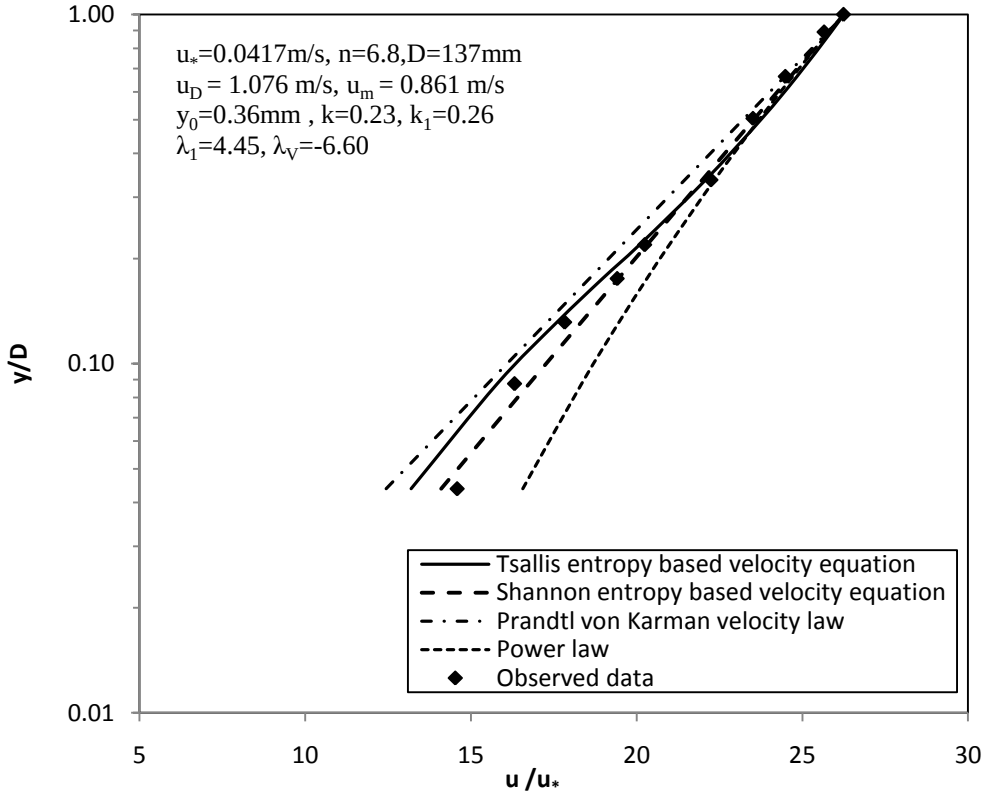

(b)

Fig. 48. continued

Furthermore, comparison of the four velocity distributions and corresponding dimensionless velocity distributions near channel bed against experimental data (Einstein and Chien 1955) are presented in Fig. 49.

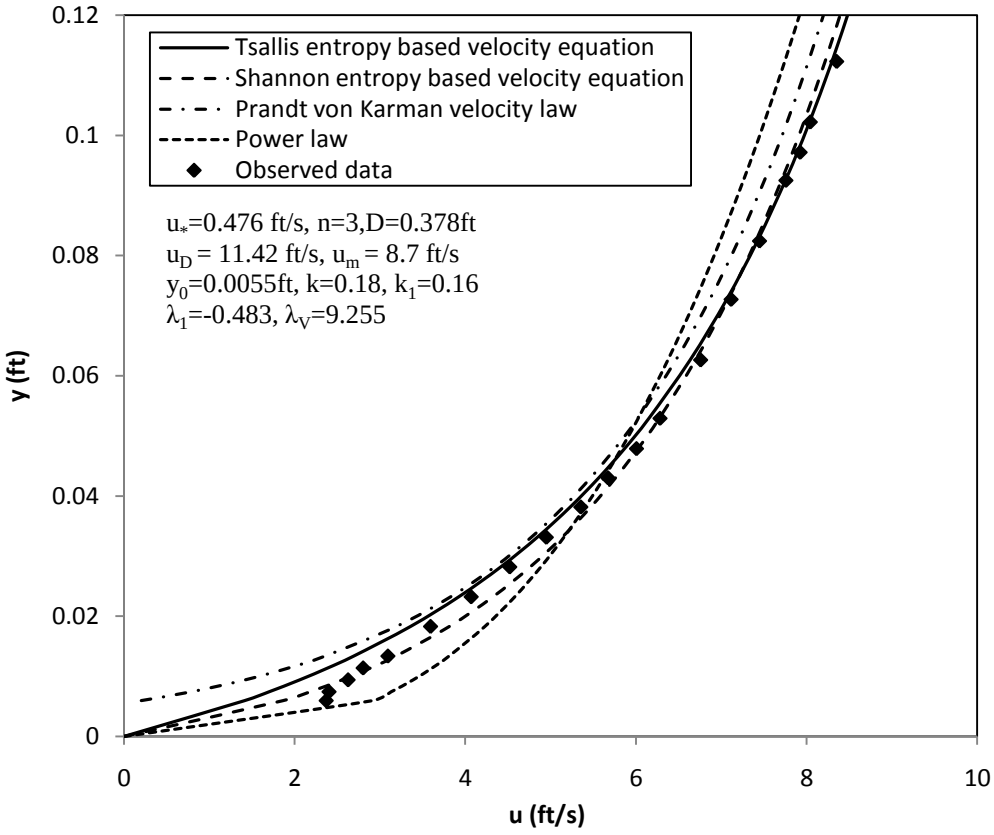

(a)

Fig. 49. Comparison of Tsallis entropy-based velocity distribution with observed velocity and velocity distributions based on Shannon entropy and Prandtl-von Karman universal velocity distribution and power law velocity distribution (Data from S5 series, Einstein and Chien 1955). (a) velocity distribution; (b) dimensionless velocity distribution.

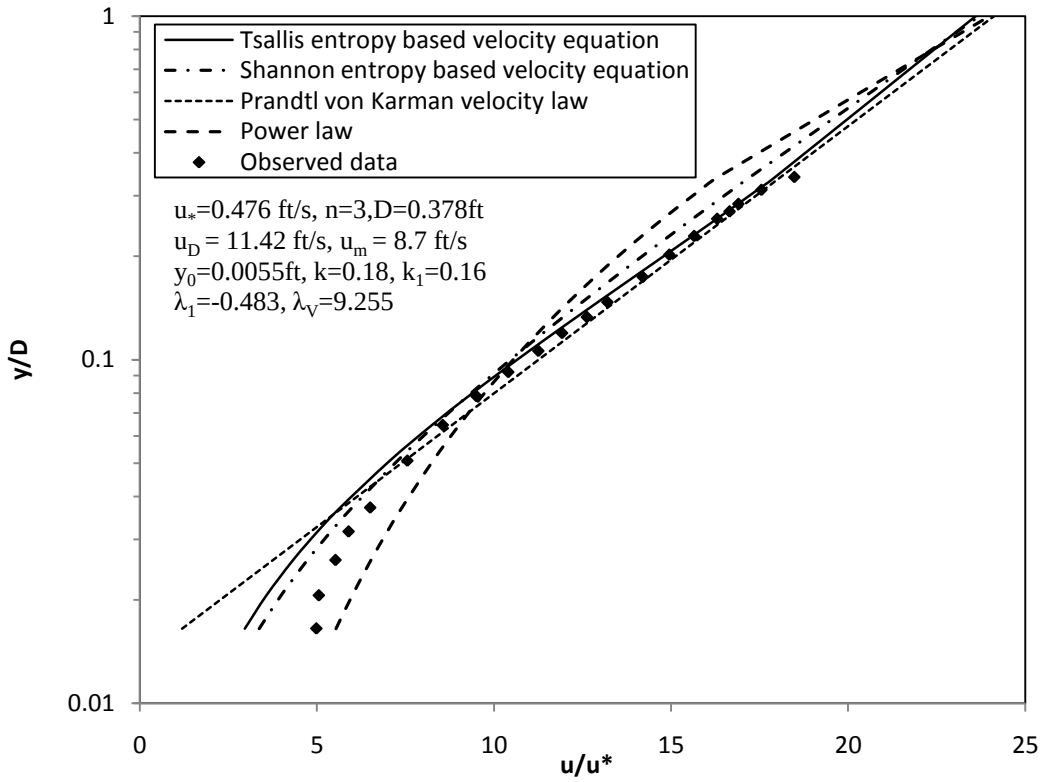

(b)

Fig. 49. continued

Table 18 Mean, μ(ε), and standard deviation, σ(ε), of error given by Eq. (27) considering Tsallis entropy-based velocity equation, Shannon entropy and Prandtl-von Karman universal velocity distribution and power law velocity distribution (Data from Run 12, Coleman 1986 and S5 series, Einstein and Chien 1955).

	Tsallis	Shannon	Prandtl-von Karman	Power law	Data
μ	-0.022	0.003	-0.035	0.046	Run 12
σ	0.091	0.090	0.090	0.106	
μ	-0.054	-0.006	-0.98	0.055	S5
σ	0.071	0.060	0.241	0.141	

The errors for experimental cases are tabulated in Table 18. Apparently, the four velocity distributions have more advantages in simulating under experimental conditions than in natural cases when comparing Fig. 48 and Fig. 49 using experimental data with Fig. 47 for field data. Especially for the average performance for the whole water depth as shown in Fig. 48, the mean error found did not exceed 0.046 and the maximum standard deviation was about 0.106. Some of the reasons are that the experimental conditions are ideal and simple for small scale flume, just under several major factors and requirements to simplify the experimental process, while for natural rivers and streams with a much larger scale, the flow velocity distributions are exposed to more factors, which cannot be taken or totally taken into account when doing simulation using velocity distribution equations. What is more, the measurement is more difficult to carry on in natural situations, and errors are more easily generated.

Based on the above Fig. 48 and Fig. 49, we can see the advantage of both entropy based velocity distributions was consistently found to increase with sediment concentration. Fig. 48 and Fig. 49 give an illustration in which the velocity data were collected from flow with relatively heavy sediment concentration over the channel bed of coarse sand (S5 series, Einstein and Chien 1955 and Run 12, Coleman 1986). In Fig. 48(b) and Fig. 49(b), as y/D decreases below 0.05 and 0.2, respectively, the data points begin to deviate considerably from the line given by Prandtl-von Karman equation, while they stay on or very close to the lines given by the Tsallis entropy based equation and Shannon entropy based equation. That's because the sediment laden flow is in itself very complicated and any simplified treatments like the conventional logarithmic

velocity formula can only apply as long as the effects of the particles on the flow and on each other remain negligible. On the other hand, in Fig. 49, as *y/D* increases beyond 0.1, the data points begin to deviate dramatically from the computed values based on the power law equation, while the Tsallis entropy based equation and Shannon entropy based equation still matched the observed data well. For natural rivers as shown in Fig. 47, Tsallis entropy based velocity equation led to a more accurate simulation while for Shannon entropy based velocity equation fitted the laboratory data better. Overall the entropy based velocity distributions can better predict the velocity distribution, no matter the depth very close to channel or for higher depths. For the two entropy methods, the accuracy of Shannon entropy based method relies on the good estimation of parameter *k* which is not always constant and shear velocity u_*. For Tsallis entropy based method, more accuracy and effectiveness can be expected which can be seen from Fig. 49 and Fig. 50, with the exact values of parameters λ_1 and λ_V.

4.3. Other 2-D velocity distributions

The popular velocity laws such as Prandtl von Karman velocity law and Power law presented in the previous section were used to roughly describe the 2-D velocity distribution. More recently, Chiu (1988) proposed a Shannon entropy based 2-D velocity equation to estimate the velocity distributions as:

$$u = \frac{u_{\max}}{M} \ln\left[1 + (e^{M} - 1)\frac{r - r_0}{r_{\max} - r_0}\right] \tag{70}$$

in which *M* is a dimensionless entropic parameter which can be determined from Eq. (56). The term $(r\text{-}r_0)/(r\text{-}r_{max})$ is the same as the one we used in Tsallis entropy based

velocity equation and so it can be replaced with Eq. (39) and (40) for different cases. The 2-D velocity distribution was introduced for the cases when the channel is non-wide and the maximum is not happening at the water surface. As we proved in the previous section, the entropy based methods have obvious advantages over Prandtl-von Karman and Power law velocity distribution in sediment laden flows in the region close to the channel bed. It may be interesting to see how these velocity distributions work for a non-wide channel with sediment laden flow. For this reason, Coleman's experiment data for Run 20 was used here for comparison.

4.4. Comparison between Tsallis entropy based 2-D velocity distribution and other velocity distributions using field data and laboratory data

The two dimensional model is proposed for channels that are not wide, where the maximum velocity does not always happen at the water surface. Therefore, a more universal distribution is described by Eq. (47) and Eq. (49) by transforming the Cartesian coordinate system (*y*-*z*) to curvilinear coordinate system (*r*-*s*). The Tsallis entropy based 2-D velocity distribution law can be treated as a generalized velocity law and its applicability and to sediment-laden flow and clear water control flow and the special characteristics it may have relative to other velocity distributions is presented in Fig. 50 using Coleman's experimental data (Coleman 1986) for a non-wide flume.

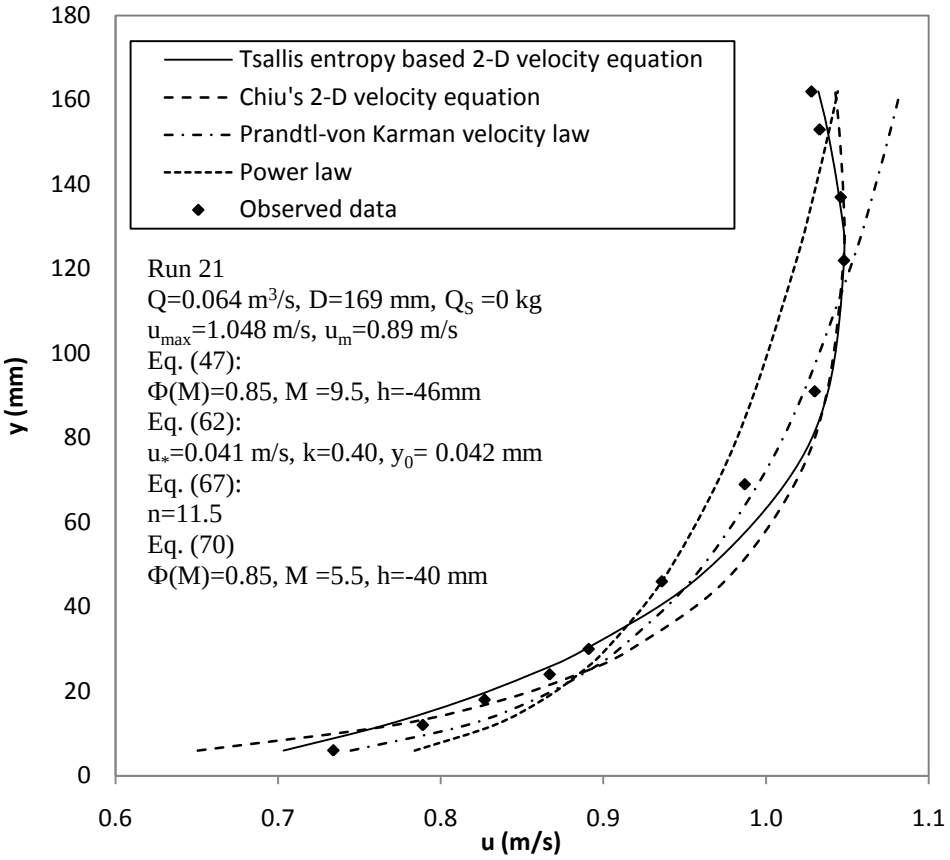

(a)

Fig. 50. Velocity profiles simulated in four ways compared with observations. (a) clear water flows and (b) sediment-laden flows in a non-wide flume.

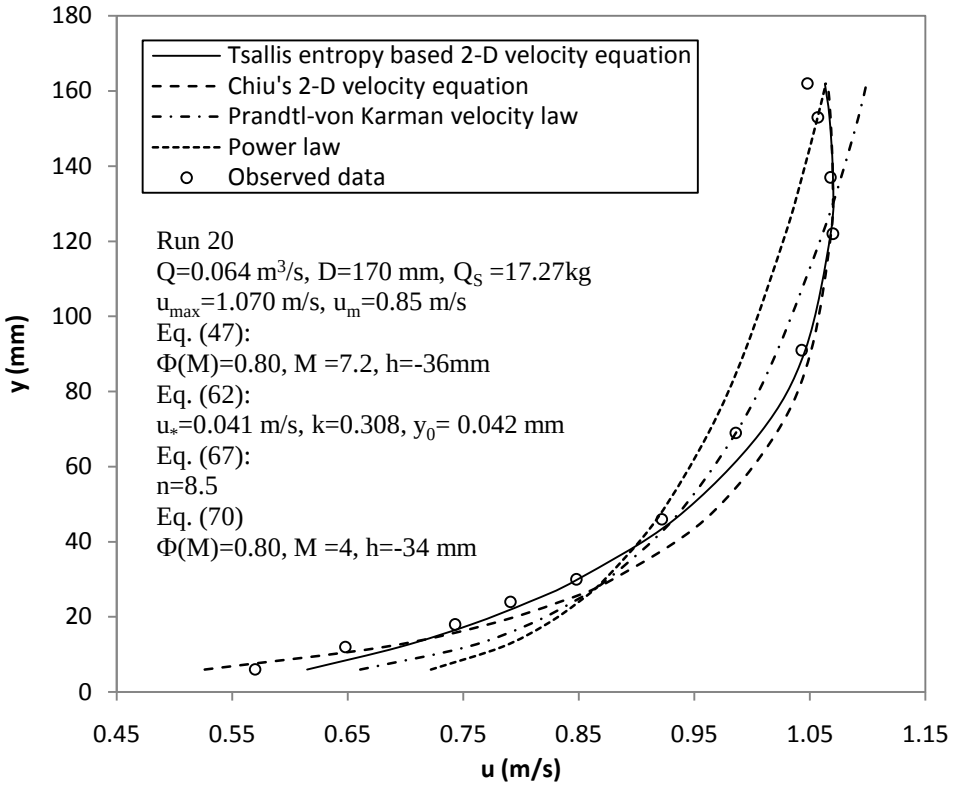

(b)

Fig. 50. continued

Table 19 Mean, μ(ε), and standard deviation, σ(ε), of error given by Eq. (27) considering Tsallis entropy-based 2-D velocity equation, Shannon entropy and Prandtl-von Karman universal velocity distribution and power law velocity distribution (Data from Run 20 and Run 21 (Coleman 1986)).

	Tsallis	Prandtl-von Karman	Chiu	Power law	Data
μ	0.021	0.048	0.018	0.047	Run 20
σ	0.027	0.061	0.035	0.100	
μ	-0.006	-0.016	0.009	0.010	Run 21
σ	0.021	0.044	0.034	0.033	

As in Fig. 50 the simulations using two entropy based velocity equations are proved to have obvious advantages over the Prandtl-von Karman and Power law velocity distributions in both the upper region close to water surface and the lower part of the flow which is under the influence of high sediment concentration and shear stress. The big gap found between the simulation using Prandtl-von Karman and Power law velocity distributions convinced us the classical velocity distributions based on 1-D assumptions are not sufficient to predict the velocity distributions that the velocity does not monotonically increase along water depth, especially for flows with suspended sediments where flows close to channel bed are under high sediment concentration effects. Error statistics concerning different velocity distributions are tabulated in Table 19. And the mean errors generated when using two entropy based methods did not exceed 0.021 and the maximum standard deviation was around 0.035, which statistically verified the applicability of the two entropy based in 2-D velocity distribution for both clear water and sediment laden flows. Though comparing the errors generated for two runs, higher errors were obtained for Run 20 with high sediment concentration, which means sediment concentration in the flow can influence the velocity distribution. So the further analysis is focus on the comparison between Tsallis entropy based 2-D velocity distribution and Chiu's 2-D velocity distribution.

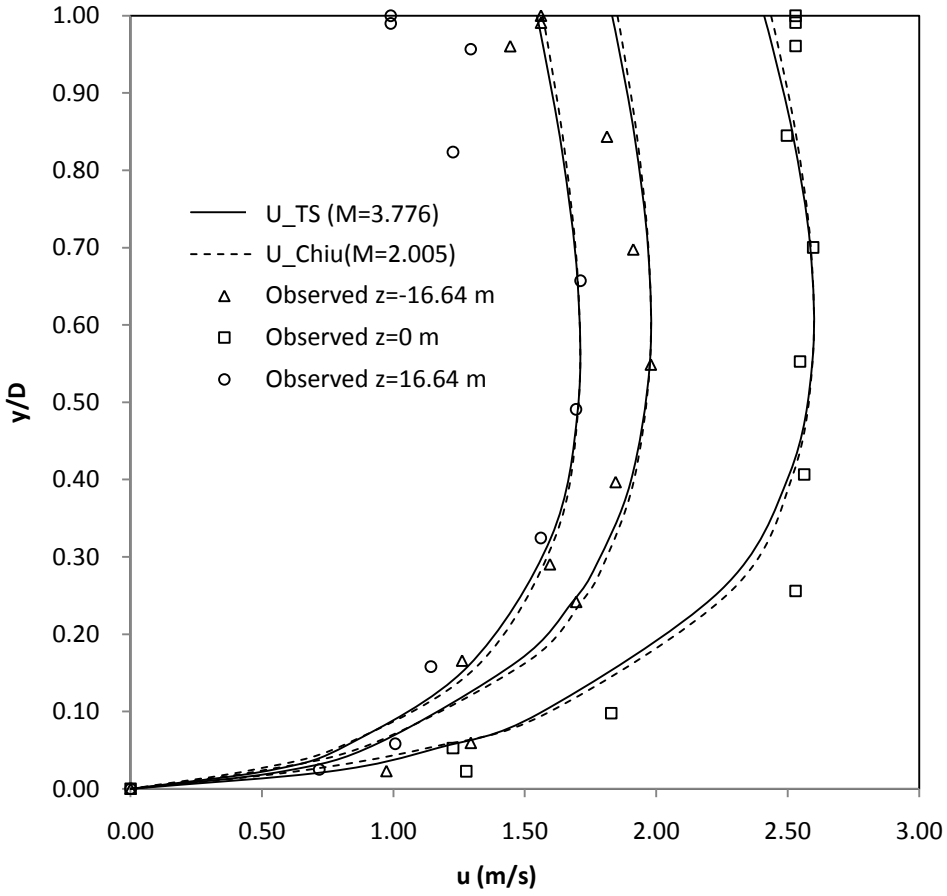

Fig. 51. Velocity distribution estimated using the Tsallis entropy based 2-D velocity distribution (U_TS) in comparison with Chiu's 2-D velocity distribution (U_Chiu) against velocity samples on selected verticals at P. Nuovo gauged station on Tiber River during flood event that occurred in November, 1996.

The two entropy based methods were applied to high flood events and unsteady flow cases as shown in Fig. 51 and Fig. 52.

Table 20 Mean, μ(ε), and standard deviation, σ(ε), of error given by Eq. (27) considering Tsallis entropy-based 2-D velocity equation and Chiu's 2-D velocity equation.

	z=-16.64m		z=0m		z=16.64m	
	μ	σ	μ	σ	μ	σ
Tsallis	0.030	0.193	-0.077	0.120	0.141	0.279
Chiu	0.030	0.223	-0.083	0.149	0.140	0.306

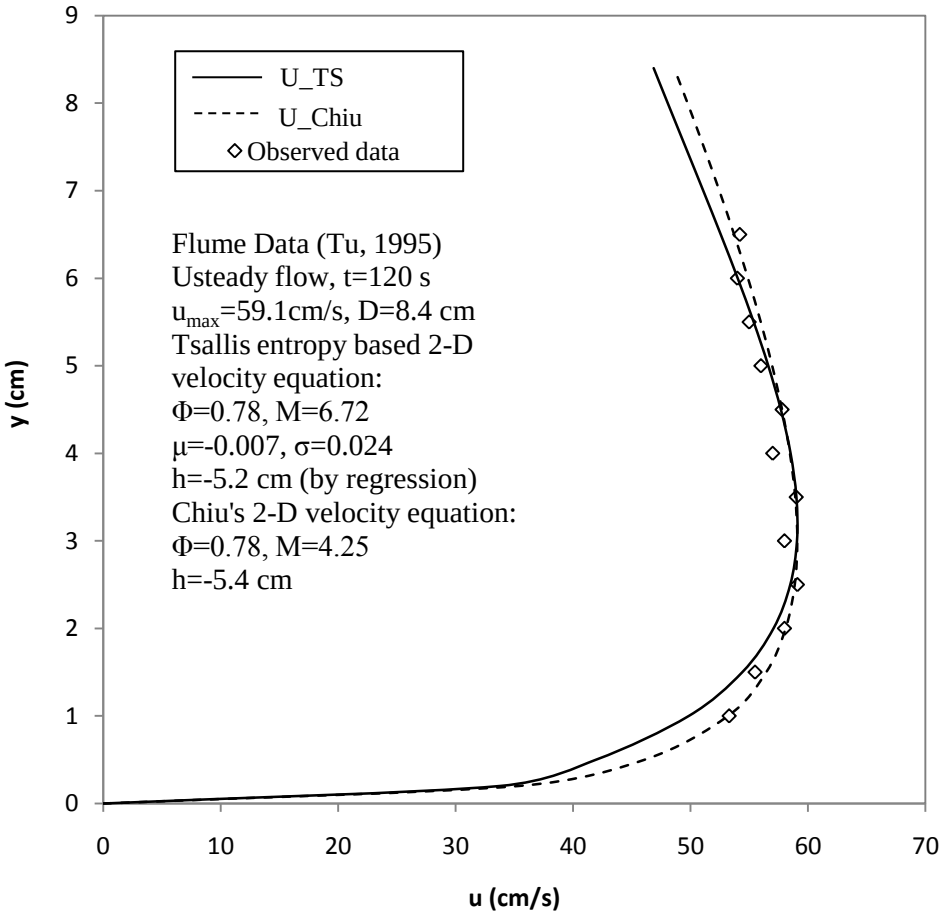

Fig. 52. Velocity distribution estimated using the Tsallis entropy based 2-D velocity distribution (U_TS) in comparison with Chiu's 2-D velocity distribution (U_Chiu) against laboratory vertical velocity samples. (Tu 1995).

As shown in Fig. 51 and Fig. 52, great similarities were found between the velocity curves simulated in two ways giving almost the same errors as shown in Table 20. First, Shannon entropy is one special case of Tsallis entropy when parameter *m* tends to be unity. Second, the two methods are in nature Tsallis entropy with *m* as 1 and 2 respectively; based on previous analysis on the sensitivity of parameter *m* of the 2-D velocity distribution, the velocity distribution is not sensitive to *m* within its possible range, the results displayed here in turn proved this argument again. Finally, these two methods were actually built up on the same curvilinear system; the initial probabilistic assumption and mathematical transformation were the same. Based on above, the regularities found using Chiu's 2-D velocity equation were also detected in Tsallis entropy based 2-D velocity distribution. For channels with a large scale, like the Tiber River shown in Fig. 51, where the effects of channel bed and the sediment concentration on velocity distribution is not so obvious, the results generated in two entropy based ways can be very subtle; for channels with a relatively small scale, like the flume shown in Fig. 52, the sediment concentration and the bed effects cannot be ignored, the higher the effects are, the more reduction of the velocity close to channel bed can be expected. Consistent with previous analysis, Tsallis entropy based 2-D velocity equation with m=2, led to more deceleration in lower regions so is more appropriate to use.

5. SUMMARY AND CONCLUSIONS

Based on the computations and investigations in the thesis, the following conclusions are drawn:

1. The velocity distribution varies with *m*, the proper *m* values for the 1-D case range from 0-1 and 3/4 is proved to be adequate.
2. Parameter λ_1 can be considered as a new hydraulic parameter which has a linear relationship with maximum entropy of the system. It can reflect the effect of roughness and sediment concentration and flow patterns.
3. *M* is an important new hydraulic parameter, it can be estimated using an analytical formula with the mean and maximum known, and somehow with a narrow range as -12-12 and easy to estimate.
4. The velocity distribution is not very sensitive to *M*, so the cross-sectional mean or the value derived from the historical records is acceptable for engineering.
5. For both 1-D and 2-D case the Tsallis entropy based velocity distribution as well as the Shannon entropy can predict the flow velocity well and has obvious advantages over other popular velocity distributions such as Prandtl von Karman and Power law velocity distributions. Since no assumption is involved in the parameter estimation, the derived Tsallis entropy based velocity distribution is highly unbiased, exact and effective.

In general, the velocity distribution equation used in the developed technique based on the Tsallis entropy is capable of accurately filling the missing data that is difficult to measure using acoustic device near the water surface and channel bed because of some

technical reasons. The *M* value of a channel section that can be determined from the u_{max}-u_m relationship contains information about the overall characteristics of the channel section. Therefore, the *M* value is an effective, diagnostic measure of changes in bed form and material, slope, shape, and alignment that may result from man's activities, such as construction of dams and bridges.

6. FUTURE WORK

The results of the foregoing analysis tend to project M as an important new parameter that characterizes the velocity distribution and related properties and processes in an open channel. Further investigations of M are required to determine factors affecting it and explore its physical meaning. Hence, it may be interesting to explore how it relates to open channel system and flow patterns and other factors that contribute to the velocity distribution.

On the other hand, though many sets of velocity distribution data are available, they seldom include accurate locations and values of maximum velocities. Available experimental data also fail to provide velocity distributions from channels of sufficiently wide ranges of shape (width–to-depth ratios), roughness, and slope. Therefore, another main task will be to estimate the value and location of the maximum velocity accurately. Using the *M* parameter and maximum velocity known or measured, the mean velocity can be obtained, so discharge can be also estimated based on these results. Application of this new method to the discharge estimation should be explored in the near future.

REFERENCES

Afzalmehr, L. (2008). “Iran open channel flow velocity data.” Personal communication.

Blaney, H. F. (1937). “Discussion of stable channels in erodible material.” *Trans*., *ASCE* 102: 152-153.

Chen, Y.C., and Chiu, C.L. (2004). “A fast method of flood discharge estimation.” *Hydrol. Process.*18, 1671-1684.

Chiu, C. L. (1987). “Entropy and probability concepts in hydraulics.” *J. Hydraul. Eng.*, 113(5):583-600.

Chiu, C. L. (1988). “Entropy and 2-D velocity distribution in open channels.” *J. Hydraul. Eng*., 114(7), 738-755.

Chiu, C. L. (1989). “Velocity distribution in open channel flows.” *J. Hydraul. Eng*., 115(5), 576-594.

Chiu, C. L. (1991). “Application of entropy concept in open channel flow study.” *J. Hydraul. Eng*., 117(5), 615-628.

Chiu, C. L., and Chiou, J.D. (1986). “Structure of 3-D flow and shear in open channels.” *J. Hydraul. Eng*., 109 (11), 1424-1440.

Chiu, C. L., and Lin, G.F. (1983). “Computation of 3-D flow and shear in open channels.” *J. Hydraul. Eng*., 113(5), 583-600.

Chiu, C. L., Lin, G. F., and Lu, J. M. (1993). “Application of probability and entropy concepts in pipe-flow study.” *J. Hydraul. Eng*., 119(6), 742-756.

Chiu, C. L., and Said, C.A.A. (1995). “Maximum and mean velocities in open channel flow.” *J. Hydraul. Eng.*, 121(1), 26-35.

Coleman, N. L. (1981). “Velocity profiles with suspended sediment.” *J. Hydraul. Res*., 19(3), 211-219.

Coleman, N. L. (1986). “Effects of suspended sediment on the open channel velocity distribution.” *J. Water Resources. Res*., 19(3), 211-219.

Coles, D. (1956). “The law of the wake in the turbulent boundary layer.” *J. Fluid Mech.*, 1(2), 191-226.

Crissman, R. D. (1993). “Uncertainties in flow modeling and forecasting for Niagara River. ” *J. Hydrologic Eng*., 119(11), 1231-1250.

Einstein, H. A., and Chien, N. (1955). “Effects of heavy sediment concentration near the bed on velocity and sediment distribution.” *Report No.8, M.R.D. Sediment series,* U.S. Army Corps of Engineers, Omaha, NE., August.

Gell-Mann, M., and Tsallis, C. (2004). “Nonextensive entropy interdisciplinary applications.” Oxford Universty Press, Inc., New York.

Gordon, L. (1992). *Mississippi River discharge*, RD Instruments, San Diego, CA.

Guo, Z. R. (1990). Personal communication. Southeast China Evironmental Science Institute, Yuancun, China.

Guy, H.P. (1966). “Summary of alluvial-channel data from Rio Grade experiments, 1956-61.” *Geological Survey Professional Paper 462-1*, U.S. Government Printing Office, Washington, D.C..

Herschy, R. W. (1985). *Streamflow measurement*, Elsevier, London.

Jaynes, E. T. (1957). “Information theory and statistical mechanics I.” *Physics Review*, 106(4), 620-630.

Karim, M. F., and Kennedy, J. F. (1987). “Velocity and sediment concentration profiles in river flows.” *J. Hydraul. Eng*., 113(2), 159-178.

Landweber, L. (1953). “The frictional resistance of flat plates in zero pressure gradient.” *Trans. So. Nav. Archit. Mar. Eng*., 61, 5-32

Leopold, L.B., Wolman, M. G., and Miller, J. P. (1995). *Fluvial processes in geomorphology*. Dover, NY.

Moramarco, T., and Singh, V.P. (2004). “Estimation of mean velocity in natural channels based on Chiu’s velocity distribution equation.” *J. Hydrologic Eng*., 9(1), 42-50.

Moramarco, T. (2008). “Italy open channel flow velocity data.”Personal communication.

Stearns, F.P. (1883). “On the currentmeter, together with a reason why the maximum velocity of water flowing in open channel is below the surface.” *Trans*., ASCE, August.

Singh, V.P. (1996). “Entropy-based parameter estimation in hydrology.” *Water Science and Technology Library*, Kluwer Academic Publishers, Dohrecht, Netherlands.

Tu, H. (1995). “Velocity measurements in unsteady compound open channel flows.” *Proceedings of the 26th IAHR Congress*, London, 1, 385-390.

Tu, H., and Graf, W.H. (1992). “Velocity distribution in unsteady open channel flow over gravel beds.” *J. Hydrosc. and Hydr. Eng*., 10(1), 11-25.

Tsallis, C. (1988). “Possible generalization of Boltzmann-Gibbs statistics.” *J. Statistical Physics,* 52,479-487.

Xia, R. (1997). “Relation between mean and maximum velocities in a natural river.” *J. Hydraul. Eng*., 123(8), 720-723.

Yen, B. C. (1965). “Characteristics of subcritical flow in a meandering channel.” *Tech. Rep.,* Institute of Hydraulic Research, University of Iowa, Iowa City, IA.

APPENDIX

Table A1 Velocity data for C3 series (Einstein and Chien 1955) and estimation using Tsallis entropy based 1-D velocity equation

y (ft)	u (Observed) (ft/s)	u (TS) (ft/s)	ε
0.00	0.000	0.000	0.000
0.01	3.182	2.810	-0.117
0.01	3.234	3.020	-0.066
0.01	3.530	3.282	-0.070
0.01	3.767	3.570	-0.052
0.01	3.960	3.800	-0.041
0.02	4.150	4.080	-0.017
0.02	4.283	4.307	0.006
0.02	4.558	4.545	-0.003
0.03	4.730	4.740	0.002
0.03	4.954	4.825	-0.026
0.03	4.859	4.940	0.017
0.04	5.083	5.102	0.004
0.04	5.194	5.263	0.013
0.05	5.375	5.400	0.005
0.06	5.504	5.532	0.005
0.06	5.676	5.647	-0.005
0.07	5.771	5.757	-0.002
0.08	5.835	5.855	0.003
0.09	5.964	5.960	-0.001
0.10	6.106	6.049	-0.009
0.12	6.287	6.198	-0.014

Note: u (Observed) denotes velocity observations; u (TS) denotes velocity estimation based on Tsallis entropy based velocity model.

ε= relative error = (u (TS) - u (Observed))/ u (Observed).

Table A2 Velocity data for S4 series (Einstein and Chien 1955) and estimation using Tsallis entropy based 1-D velocity equation

y (ft)	u(Observed) (ft/s)	u (TS) (ft/s)	ε
0.00	0.000	0.000	0.000
0.01	2.221	1.314	-0.408
0.01	2.497	1.736	-0.305
0.01	2.720	2.038	-0.251
0.01	2.858	2.176	-0.239
0.01	2.964	2.565	-0.135
0.02	3.329	2.797	-0.160
0.02	3.573	3.107	-0.130
0.02	3.898	3.558	-0.087
0.03	4.519	4.296	-0.049
0.04	4.831	4.597	-0.049
0.04	5.075	4.868	-0.041
0.05	5.298	5.102	-0.037
0.05	5.522	5.315	-0.037
0.06	5.806	5.695	-0.019
0.07	6.090	6.017	-0.012
0.08	6.293	6.291	0.000
0.09	6.516	6.541	0.004
0.10	6.699	6.754	0.008
0.12	7.113	7.125	0.002

Table A3 Velocity data for S5 series (Einstein and Chien 1955) and estimation using Tsallis entropy based 1-D velocity equation

y (ft)	u(Observed) (ft/s)	u (TS) (ft/s)	ε
0.00	0.000	0.000	0.000
0.01	2.370	1.297	-0.453
0.01	2.404	1.569	-0.347
0.01	2.628	1.909	-0.273
0.01	2.804	2.225	-0.206
0.01	3.094	2.518	-0.186
0.02	3.594	3.170	-0.118
0.02	4.070	3.730	-0.083
0.03	4.522	4.223	-0.066
0.03	4.950	4.655	-0.060
0.04	5.355	5.049	-0.057
0.04	5.674	5.391	-0.050
0.05	6.007	5.702	-0.051
0.05	6.283	5.997	-0.045
0.06	6.759	6.501	-0.038
0.07	7.116	6.950	-0.023
0.08	7.449	7.328	-0.016
0.09	7.759	7.675	-0.011
0.10	7.925	7.823	-0.013
0.10	8.044	7.975	-0.009
0.11	8.354	8.254	-0.012
0.12	8.796	8.508	-0.033

Table A4 Iran velocity data 1 (Afzalmeh, 2008) and estimation using Tsallis entropy based 1D velocity equation

y (m)	u(Observed) (m/s)	u (TS) (m/s)	ε
0.05	0.200	0.210	0.052
0.06	0.229	0.234	0.019
0.07	0.277	0.254	-0.083
0.08	0.288	0.272	-0.055
0.09	0.299	0.289	-0.035
0.11	0.314	0.317	0.009
0.13	0.347	0.340	-0.020
0.16	0.366	0.369	0.010
0.20	0.369	0.400	0.083
0.24	0.424	0.424	0.000
0.29	0.410	0.449	0.097
0.34	0.447	0.470	0.052
0.40	0.458	0.490	0.070
0.47	0.483	0.509	0.053
0.55	0.506	0.527	0.043
0.59	0.535	0.535	0.000

Table A5 Iran velocity data 2 (Afzalmehr 2008) and estimation using Tsallis entropy based 1D velocity equation

y (m)	u(Observed) (m/s)	u (TS) (m/s)	ε
0.01	0.512	0.390	-0.238
0.03	0.540	0.632	0.170
0.05	0.642	0.739	0.150
0.06	0.721	0.775	0.075
0.07	0.735	0.804	0.094
0.08	0.692	0.829	0.197
0.09	0.746	0.850	0.139
0.10	0.792	0.868	0.096
0.11	0.807	0.884	0.096
0.13	0.882	0.912	0.034
0.15	0.885	0.934	0.055
0.17	0.946	0.953	0.008
0.20	0.960	0.977	0.017
0.23	0.989	0.996	0.007
0.26	1.003	1.012	0.009
0.29	1.017	1.026	0.009
0.32	1.039	1.039	0.000
0.34	1.046	1.046	0.000

Table A6 Velocity observations for Run 01 (Coleman 1986) and estimation using Tsallis entropy based 1-D velocity equation

y (mm)	u (Observed) (m/s)	u (TS) (m/s)	ε
6	0.709	0.613	-0.135
12	0.773	0.742	-0.040
18	0.823	0.810	-0.016
24	0.849	0.853	0.005
30	0.884	0.885	0.001
46	0.927	0.940	0.014
69	0.981	0.986	0.005
91	1.026	1.014	-0.012
122	1.054	1.041	-0.012
137	1.053	1.051	-0.002
153	1.048	1.061	0.012
162	1.039	1.065	0.025

Table A7 Velocity observations for Run 09 (Coleman 1986) and estimation using Tsallis entropy based 1-D velocity equation

y (mm)	u (Observed) (m/s)	u (TS) (m/s)	ε
6	0.621	0.537	-0.136
12	0.683	0.676	-0.010
18	0.751	0.751	0.000
24	0.804	0.800	-0.004
30	0.842	0.836	-0.007
46	0.897	0.899	0.003
69	0.945	0.952	0.008
91	1.028	0.985	-0.042
122	1.048	1.016	-0.030
137	1.05	1.028	-0.021
153	1.04	1.039	-0.001
162	1.032	1.044	0.012

Table A8 Velocity observations for Run 20 (Coleman 1986) and estimation using Tsallis entropy based 1-D velocity equation

y (mm)	u (Observed) (m/s)	u (TS) (m/s)	ε
6	0.57	0.438	-0.232
12	0.648	0.595	-0.082
18	0.743	0.685	-0.078
24	0.791	0.746	-0.056
30	0.848	0.792	-0.066
46	0.922	0.873	-0.054
69	0.986	0.942	-0.045
91	1.043	0.985	-0.056
122	1.07	1.027	-0.040
137	1.068	1.042	-0.024
153	1.057	1.057	0.000
162	1.048	1.064	0.015

Table A9 Velocity observations for Run 29 (Coleman 1986) and estimation using Tsallis entropy based 1-D velocity equation

y (mm)	u (Observed) (m/s)	u (TS) (m/s)	ε
6	0.648	0.563	-0.131
12	0.701	0.706	0.007
18	0.776	0.783	0.008
24	0.823	0.833	0.012
30	0.853	0.869	0.019
46	0.930	0.933	0.003
69	0.991	0.987	-0.004
91	1.055	1.020	-0.033
122	1.084	1.052	-0.029
137	1.082	1.064	-0.017
153	1.066	1.075	0.008
162	1.064	1.081	0.016

Table A10 Velocity observations for unsteady flows t=21s (Tu and Graf 1992) and estimation using Tsallis entropy based 1-D velocity equation

y (cm)	u (Observed) (m/s)	u (TS) (m/s)	ε
1.22	0.339	0.326	-0.039
1.34	0.408	0.345	-0.155
1.71	0.421	0.394	-0.064
2.04	0.443	0.431	-0.026
2.44	0.471	0.470	-0.002
2.98	0.500	0.513	0.027
3.66	0.529	0.558	0.055
4.06	0.543	0.581	0.069
4.48	0.579	0.601	0.039
6.23	0.671	0.671	0.000
7.59	0.700	0.710	0.015
8.41	0.730	0.730	0.001
9.36	0.779	0.751	-0.036
10.49	0.781	0.772	-0.011
10.98	0.800	0.781	-0.024
12.20	0.580	0.800	0.380

Table A11 Velocity observations for unsteady flows t=41s (Tu and Graf 1992) and estimation using Tsallis entropy based 1-D velocity equation

y (cm)	u (Observed) (m/s)	u (TS) (m/s)	ε
1.57	0.536	0.529	-0.013
1.21	0.557	0.463	-0.169
2.01	0.614	0.593	-0.033
2.67	0.650	0.667	0.027
3.14	0.657	0.709	0.078
3.62	0.720	0.745	0.035
4.02	0.700	0.771	0.102
4.68	0.800	0.809	0.011
5.81	0.800	0.860	0.076
6.69	0.864	0.893	0.034
7.60	0.914	0.922	0.008
8.48	0.910	0.946	0.039
9.83	1.000	0.977	-0.023
10.71	0.980	0.995	0.015
11.62	1.020	1.012	-0.008
12.50	1.050	1.026	-0.023
13.41	1.056	1.040	-0.015
14.29	1.100	1.052	-0.044
15.42	1.079	1.066	-0.012
16.52	1.114	1.079	-0.031
16.96	1.071	1.084	0.012
20.10	0.866	1.114	0.286

Table A12 Velocity observations for unsteady flows t=61s (Tu and Graf 1992) and estimation using Tsallis entropy based 1-D velocity equation

y (cm)	u (Observed) (m/s)	u (TS) (m/s)	ε
1.39	0.486	0.535	0.100
1.84	0.520	0.601	0.156
2.30	0.629	0.652	0.037
2.75	0.671	0.694	0.034
3.23	0.700	0.729	0.041
4.14	0.710	0.783	0.102
5.53	0.815	0.842	0.033
6.44	0.840	0.871	0.037
7.37	0.864	0.897	0.038
8.74	0.943	0.928	-0.016
9.67	0.950	0.946	-0.005
10.58	1.010	0.961	-0.049
11.51	1.036	0.975	-0.059
12.42	1.014	0.987	-0.026
13.33	1.046	0.999	-0.045
15.17	1.064	1.019	-0.042
16.08	1.050	1.028	-0.021
17.60	1.048	1.041	-0.007
20.70	0.855	1.064	0.244

Table A13 Velocity observations for unsteady flows t=81s (Tu and Graf 1992) and estimation using Tsallis entropy based 1-D velocity equation

y (cm)	u (Observed) (m/s)	u (TS) (m/s)	ε
1.25	0.457	0.445	-0.026
1.66	0.493	0.506	0.027
2.08	0.557	0.554	-0.006
2.49	0.600	0.592	-0.013
2.92	0.614	0.626	0.020
3.33	0.650	0.653	0.005
4.11	0.671	0.696	0.037
5.61	0.736	0.756	0.027
7.48	0.814	0.808	-0.008
8.30	0.845	0.826	-0.023
9.56	0.900	0.849	-0.056
10.40	0.857	0.863	0.007
11.59	0.886	0.880	-0.007
12.47	0.929	0.891	-0.040
13.30	0.943	0.901	-0.044
14.14	0.950	0.910	-0.042
15.33	0.943	0.922	-0.022
16.21	0.950	0.930	-0.021
16.83	0.940	0.935	-0.005
18.70	0.776	0.950	0.225

Table A14 Velocity observations for unsteady flows t=101s (Tu and Graf 1992) and estimation using Tsallis entropy based 1-D velocity equation

y (cm)	u (Observed) (m/s)	u (TS) (m/s)	ε
0.00	0.378	0.308	-0.185
0.03	0.400	0.377	-0.058
0.04	0.429	0.420	-0.022
0.06	0.514	0.483	-0.060
0.08	0.500	0.528	0.057
0.09	0.543	0.556	0.024
0.11	0.550	0.587	0.067
0.09	0.579	0.561	-0.031
0.13	0.600	0.623	0.039
0.16	0.657	0.656	-0.002
0.18	0.648	0.673	0.038
0.20	0.714	0.693	-0.030
0.23	0.715	0.711	-0.006
0.25	0.750	0.726	-0.032
0.27	0.764	0.735	-0.038
0.30	0.779	0.751	-0.035
0.32	0.781	0.761	-0.026
0.34	0.748	0.767	0.026
0.38	0.614	0.781	0.272

Table A15 Velocity observations for P.Nuovo Vertical No.1 (Moramarco 2008) and estimation using Tsallis entropy based 2-D velocity equation

y (m)	u (Observed) (m/s)	u (TS) (m/s)	ε
0	0	0.000	0.000
0.15	1.365	0.834	-0.389
0.39	1.777	1.332	-0.251
1.09	1.967	2.023	0.028
2.09	2.323	2.395	0.031
3.09	2.481	2.480	0.000
4.06	2.344	2.428	0.036
5.03	2.323	2.307	-0.007
5.73	2.148	2.195	0.022
6.03	1.982	2.143	0.081
6.09	1.982	2.133	0.076

Table A16 Velocity observations for P.Nuovo Vertical No.2 (Moramarco 2008) and estimation using Tsallis entropy based 2-D velocity equation

y (m)	u (Observed) (m/s)	u (TS) (m/s)	ε
0	0.000	0.000	0.000
0.15	1.473	0.912	-0.381
0.37	1.923	1.418	-0.262
1.1	2.323	2.215	-0.046
2.13	2.607	2.629	0.008
3.13	2.719	2.720	0.000
4.07	2.662	2.669	0.003
5.04	2.607	2.542	-0.025
5.71	2.581	2.429	-0.059
6.01	2.662	2.374	-0.108
6.07	2.662	2.363	-0.112

Table A17 Velocity observations for Run 16 (Coleman 1986) and estimation using Tsallis entropy based 2-D velocity equation

y (mm)	u (Observed) (m/s)	u (TS) (m/s)	ε
6	0.583	0.646	0.107
12	0.661	0.718	0.087
18	0.744	0.776	0.042
24	0.804	0.822	0.023
36	0.854	0.895	0.048
46	0.922	0.941	0.020
69	0.978	1.011	0.034
91	1.051	1.049	-0.002
122	1.074	1.072	-0.002
137	1.070	1.074	0.004
152	1.057	1.072	0.014
162	1.046	1.068	0.021

Table A18 Velocity observations for vertical located at z=16.64 m at P. Nuovo gauged section during flood event that occurred in November, 1996 and estimation using Tsallis entropy based 2-D velocity equation

y (m)	u (Observed) (m/s)	u (TS with M=5.041) (m/s)	u (TS with M=5.697) (m/s)
6.58	1.561	1.853	1.862
6.52	1.561	1.858	1.866
6.32	1.444	1.873	1.881
5.55	1.812	1.927	1.930
4.59	1.912	1.971	1.971
3.61	1.979	1.976	1.976
2.61	1.845	1.913	1.918
1.91	1.595	1.802	1.814
1.59	1.695	1.723	1.741
1.09	1.261	1.547	1.578
0.39	1.294	1.095	1.162
0.15	0.973	0.795	0.894

Table A19 Velocity observations for y axis at P. Nuovo gauged section during flood event that occurred in November, 1996 and estimation using Tsallis entropy based 2-D velocity equation

y (m)	u (Observed) (m/s)	u (TS with M=5.041) (m/s)	u (TS with M=6.923) (m/s)
6.64	2.530	2.437	2.466
6.58	2.530	2.444	2.471
6.38	2.530	2.464	2.487
5.61	2.497	2.532	2.543
4.65	2.597	2.588	2.590
3.67	2.547	2.595	2.596
2.70	2.563	2.519	2.533
1.70	2.530	2.293	2.347
0.65	1.829	1.707	1.874
0.35	1.227	1.378	1.619
0.15	1.277	1.039	1.374

Table A20 Velocity observations for vertical located at z=-20.8 m at P. Nuovo gauged section during flood event that occurred in November, 1996 and estimation using Tsallis entropy based 2-D velocity equation

y (m)	u (Observed) (m/s)	u (TS with M=5.041) (m/s)	u (TS with M=6.923) (m/s)
6.01	0.990	1.569	1.545
5.95	0.990	1.574	1.551
5.75	1.294	1.591	1.571
4.95	1.227	1.651	1.641
3.95	1.712	1.701	1.700
2.95	1.695	1.702	1.701
1.95	1.561	1.614	1.598
0.95	1.143	1.343	1.280
0.35	1.007	0.961	0.828
0.15	0.718	0.721	0.539

Table A21 Pairs of mean and maximum velocities collected at S. Lucia gauged section during 20 years

u_m (m/s)	u_{max} (m/s)	u_m (m/s)	u_{max} (m/s)
0.047	0.088	0.154	0.268
0.182	0.269	0.697	1.227
0.948	1.208	1.604	2.555
1.072	1.467	0.870	1.403
1.135	1.773	1.543	2.436
1.179	1.631	1.945	3.094
1.478	2.760	2.109	3.062
1.648	2.243	0.305	0.496
0.067	0.129	0.147	0.234
0.324	0.495	0.996	1.603
0.401	0.644	1.062	1.678
0.736	1.155	1.816	2.816
1.497	2.194	1.882	2.781
1.873	2.437	1.803	2.781
0.052	0.107	0.570	0.888
0.315	0.482	0.153	0.270
0.497	0.735	1.040	1.511
0.672	1.022	0.262	0.453
1.151	1.678	1.984	2.948
0.123	0.209	2.020	2.989
1.736	2.625	1.819	2.781
1.910	2.778	1.707	2.580
0.541	0.781	0.152	0.228
0.926	1.462	1.836	2.739
1.397	2.182	1.750	2.581
0.052	0.095	0.979	1.453

Table A22 Pairs of mean and maximum velocities collected at P.Felcino gauged section during 20 years

u_m (m/s)	u_{max} (m/s)	u_m (m/s)	u_{max} (m/s)
0.186	0.274	1.190	1.810
0.492	0.771	1.373	2.079
0.471	0.794	1.874	2.680
1.110	1.678	0.957	1.461
0.409	0.594	1.687	2.637
0.820	1.130	1.858	2.906
0.041	0.082	1.900	2.580
0.111	0.146	0.885	1.340
1.292	1.902	1.060	1.394
1.802	2.608	1.594	2.405
2.296	3.362	2.163	3.320
0.604	0.868	2.074	3.181
0.777	1.122	1.815	2.660
1.734	2.547	2.120	3.365
2.025	2.924	0.123	0.206
2.154	3.118	2.097	3.410
1.026	1.421	0.726	1.102
0.023	0.061	1.449	2.164

Table A23 Pairs of mean and maximum velocities collected at P.Nuovo gauged section during 20 years

u_m (m/s)	u_{max} (m/s)	u_m (m/s)	u_{max} (m/s)
0.620	0.978	1.255	2.029
1.373	2.243	0.710	1.050
1.593	2.384	1.640	2.280
1.085	2.023	1.634	2.387
0.262	0.420	1.847	2.699
1.186	1.803	1.825	2.778
1.464	2.097	1.463	2.097
0.471	0.694	1.669	2.405
1.833	2.972	0.566	0.884
1.487	2.194	1.257	1.954
0.448	0.690	1.276	1.904
0.923	1.288	0.825	1.202
1.406	2.048	0.828	1.221
0.442	0.673	0.207	0.387
1.136	1.578	0.854	1.261
0.117	0.209	0.232	0.349
1.324	2.024	1.339	2.054
1.331	2.048	0.249	0.357
1.946	2.972	1.736	2.597
1.966	2.924	1.798	2.480
1.712	2.521	1.330	1.925
0.615	0.965	1.820	2.719
1.791	2.827	1.151	1.779
0.201	0.346	1.211	1.777
1.627	2.480	0.507	0.736
1.623	2.730	0.146	0.221
1.157	1.954	1.173	1.777
1.106	1.850	1.391	2.169
1.148	2.060		

Table A24 Velocity observations for vertical located at z=-14.66 m at P.Felcino gauged section during flood event that occurred in November, 1996 and estimation using Tsallis entropy based 2-D velocity equation

y (m)	u (Observed) (m/s)	U _Mm (m/s)	U_Mh (m/s)	U_Mi (m/s)
4.15	1.210	1.483	1.471	1.464
4.09	1.210	1.488	1.477	1.470
3.95	1.210	1.500	1.491	1.485
3.15	1.450	1.549	1.548	1.547
2.15	1.560	1.546	1.544	1.543
1.15	1.290	1.390	1.365	1.348
0.35	0.830	0.970	0.878	0.820
0.15	0.710	0.735	0.599	0.520

Table A25 Velocity observations for y axis at P.Felcino gauged section during flood event that occurred in November, 1996 and estimation using Tsallis entropy based 2-D velocity equation

y (m)	u (Observed) (m/s)	U _Mm (m/s)	U_Mh (m/s)	U_Mi (m/s)
6.15	3.360	3.298	3.289	3.305
6.09	3.360	3.302	3.294	3.309
5.95	3.160	3.312	3.305	3.317
5.15	3.200	3.352	3.351	3.353
4.15	3.280	3.351	3.350	3.352
3.15	3.100	3.264	3.250	3.275
2.15	2.780	3.039	2.991	3.075
1.15	2.320	2.561	2.439	2.652
0.35	2.030	1.735	1.472	1.941
0.15	1.860	1.338	0.990	1.618

Table A26 Velocity observations for vertical located at z=7.34 m at P.Felcino gauged section during flood event that occurred in November, 1996 and estimation using Tsallis entropy based 2-D velocity equation

y (m)	u (Observed) (m/s)	U _Mm (m/s)	U_Mh (m/s)	U_Mi (m/s)
5.85	2.360	2.683	2.675	2.687
5.79	2.360	2.687	2.679	2.691
5.65	2.610	2.696	2.690	2.699
4.85	2.700	2.733	2.732	2.733
3.85	2.740	2.732	2.730	2.732
2.92	2.610	2.659	2.646	2.664
1.97	2.530	2.466	2.426	2.484
0.97	2.000	2.022	1.912	2.071
0.47	1.300	1.594	1.413	1.677
0.15	1.190	1.112	0.833	1.245

Table A27 Velocity observations for vertical located at z=25 m at Pontelagoscuro gauged section on Po River during the flood event that occurred in March, 1991 and estimation using Tsallis entropy based 2-D velocity equation

y (m)	u (Observed) (m/s)	u (TS) (m/s)	ε
8.00	1.803	1.800	-0.002
7.70	1.790	1.802	0.007
7.20	1.756	1.803	0.027
6.20	1.685	1.794	0.064
5.20	1.697	1.765	0.040
4.20	1.693	1.711	0.010
3.20	1.689	1.620	-0.041
2.20	1.533	1.475	-0.038
1.20	1.335	1.236	-0.074
0.20	0.513	0.755	0.471

Table A28 Velocity observations for vertical located at z=-27 m at Pontelagoscuro gauged section on Po River during the flood event that occurred in March, 1991 and estimation using Tsallis entropy based 2-D velocity equation

y (m)	u (Observed) (m/s)	u (TS) (m/s)	ε
8.10	1.486	1.483	-0.002
7.80	1.432	1.485	0.037
7.30	1.411	1.486	0.053
6.30	1.347	1.478	0.098
5.30	1.486	1.456	-0.020
4.30	1.423	1.412	-0.007
3.30	1.364	1.340	-0.017
2.30	1.402	1.226	-0.126
1.30	1.090	1.040	-0.046
0.30	0.433	0.682	0.575
0.00	0.000	0.000	0.000

Table A29 Uniform rectangular flume data (Guy 1966) and estimation using Tsallis entropy based 2-D velocity equation and Chiu's 2-D velocity equation

y (ft)	u (Observed) (ft/s)	u (TS) (ft/s)	u (Chiu) (ft/s)	ε
0.03	2.130	2.171	2.170	0.019
0.06	2.940	2.879	2.725	-0.021
0.08	2.960	3.213	3.037	0.085
0.10	3.280	3.448	3.279	0.051
0.16	3.700	3.809	3.694	0.030
0.26	3.990	4.082	4.051	0.023
0.36	4.060	4.140	4.140	0.020
0.46	4.140	4.090	4.083	-0.012
0.56	3.960	3.983	3.952	0.006

Table A30 Nonuniform rectangular flume data (Guo 1990) and estimation using Tsallis entropy based 2-D velocity equation and Chiu's 2-D velocity equation

y (cm)	u (Observed) (cm/s)	u (TS) (cm/s)	u (Chiu) (cm/s)	ε
0.13	14.150	22.300	22.272	0.576
0.16	22.330	24.108	23.579	0.080
0.25	26.600	27.864	26.736	0.048
0.34	29.940	30.300	29.131	0.012
0.44	32.460	32.039	31.021	-0.013
0.66	35.020	34.655	34.134	-0.010
0.84	35.900	36.002	35.832	0.003
1.06	36.760	36.983	37.058	0.006
1.34	37.510	37.661	37.804	0.004
1.66	37.640	37.923	37.887	0.008
1.97	37.550	37.840	37.442	0.008
2.25	37.510	37.556	36.736	0.001

Table A31 Velocity observations for Run 21 (Coleman 1986) and estimation using Tsallis entropy based 2-D velocity equation and Prandtl-von Karman velocity law

y (mm)	u (Observed) (m/s)	u (TS) (m/s)	u (Prandtl) (m/s)	ε
6	0.709	0.699	0.644	-0.014
12	0.773	0.757	0.736	-0.021
18	0.823	0.804	0.790	-0.023
24	0.849	0.843	0.828	-0.007
30	0.884	0.876	0.857	-0.009
46	0.927	0.942	0.914	0.017
69	0.981	1.002	0.967	0.022
91	1.026	1.034	1.004	0.008
122	1.054	1.053	1.043	-0.001
137	1.053	1.054	1.058	0.001
153	1.048	1.051	1.073	0.003
162	1.039	1.048	1.080	0.009

Table A32 Velocity observations for Run 20 (Coleman 1986) and estimation using Tsallis entropy based 2-D velocity equation and Prandtl-von Karman velocity law

y (mm)	u (Observed) (m/s)	u (TS) (m/s)	u (Prandtl) (m/s)	ε
6	0.57	0.615	0.661	0.079
12	0.648	0.695	0.753	0.072
18	0.743	0.757	0.807	0.019
24	0.791	0.807	0.845	0.021
30	0.848	0.849	0.875	0.001
46	0.922	0.933	0.932	0.012
69	0.986	1.007	0.986	0.021
91	1.043	1.046	1.022	0.003
122	1.07	1.068	1.061	-0.001
137	1.068	1.070	1.077	0.002
153	1.057	1.067	1.092	0.009
162	1.048	1.063	1.099	0.014

Table A33 Velocity observations for vertical z=-16.64 m at P. Nuovo gauged station and estimation using Tsallis entropy based 2-D velocity equation and Chiu's 2-D velocity equation

y	u (Observed)	u (TS)	u(Chiu)	ε
(m)	(m/s)	(m/s)	(m/s)	
6.58	1.56	1.832	1.853	0.174
6.52	1.56	1.838	1.858	0.177
6.32	1.44	1.856	1.874	0.285
5.55	1.81	1.918	1.927	0.058
4.59	1.91	1.969	1.971	0.030
3.61	1.98	1.975	1.976	-0.002
2.61	1.85	1.902	1.914	0.031
1.91	1.60	1.773	1.800	0.112
1.59	1.70	1.681	1.715	-0.008
1.09	1.26	1.476	1.515	0.170
0.39	1.29	0.944	0.925	-0.270
0.15	0.97	0.584	0.485	-0.400
0	0.00	0.000	0.000	0.000

Table A34 Velocity observations for vertical z=0 m at P. Nuovo gauged station and estimation using Tsallis entropy based 2-D velocity equation and Chiu's 2-D velocity equation

y	u (Observed)	u (TS)	u(Chiu)	ε
m	(m/s)	(m/s)	(m/s)	
6.64	2.53	2.411	2.437	-0.047
6.58	2.53	2.418	2.443	-0.044
6.38	2.53	2.441	2.464	-0.035
5.61	2.50	2.521	2.533	0.009
4.65	2.60	2.586	2.588	-0.004
3.67	2.55	2.594	2.595	0.018
2.7	2.56	2.506	2.520	-0.022
1.7	2.53	2.243	2.285	-0.113
0.65	1.83	1.558	1.584	-0.148
0.35	1.23	1.169	1.129	-0.047
0.15	1.28	0.761	0.630	-0.404
0	0.00	0.000	0.000	0.000

Table A35 Velocity observations for vertical z=0 m at P. Nuovo gauged station and estimation using Tsallis entropy based 2-D velocity equation and Chiu's 2-D velocity equation

y	u (Observed)	u (TS)	u(Chiu)	ε
(m)	(m/s)	(m/s)	(m/s)	
6.01	0.99	1.546	1.568	0.562
5.95	0.99	1.552	1.573	0.568
5.75	1.29	1.572	1.591	0.215
4.95	1.23	1.642	1.652	0.338
3.95	1.71	1.700	1.702	-0.007
2.95	1.70	1.701	1.703	0.004
1.95	1.56	1.599	1.614	0.024
0.95	1.14	1.283	1.317	0.122
0.35	1.01	0.834	0.821	-0.172
0.15	0.72	0.547	0.470	-0.238
0	0.00	0.000	0.000	0.000

Table A36 Velocity observations for unsteady flows at t=120s (Tu 1995) and estimation using Tsallis entropy based 2-D velocity equation and Chiu's 2-D velocity equation

y	u (Observed)	u (TS)	u (Chiu)	
(cm)	(cm/s)	(cm/s)	(cm/s)	ε
1.00	53.300	49.844	53.200	-0.065
1.50	55.500	54.397	56.456	-0.020
2.00	58.000	57.057	58.112	-0.016
2.50	59.100	58.485	58.885	-0.010
3.00	58.000	59.055	59.100	0.018
3.50	59.000	59.009	58.928	0.000
4.00	57.000	58.512	58.474	0.027
4.50	57.800	57.684	57.805	-0.002
5.00	56.000	56.615	56.966	0.011
5.50	55.000	55.372	55.991	0.007
6.00	54.000	54.009	54.904	0.000
6.50	54.200	52.567	53.724	-0.030

Table A37 D estimated by Eq. (68) in comparison with actual values

D(computed)	D(Actual)	ε
0.285	0.392	-0.273
0.274	0.381	-0.281
0.231	0.378	-0.389
0.241	0.364	-0.338
0.356	0.470	-0.242
0.343	0.470	-0.270
0.298	0.455	-0.345
0.397	0.447	-0.113
0.343	0.432	-0.205
0.263	0.397	-0.337
0.496	0.582	-0.148
0.382	0.399	-0.043

Note:ε=(D(computed)-D(Actual))/(D(Actual))

VITA

Hao Luo received her Bachelor of Engineering degree in Aerospace Engineering and Bachelor of Arts degree in English from Beijing University of Aeronautics and Astronautics in 2006. She entered the Biological and Agricultural program at Texas A&M University in August 2007 and received her Master of Science degree in 2009. Her research interests include Environmental Fluid Mechanics, Hydraulics and Hydrology.

Ms. Luo may be reached at 236 Scoates Hall, Texas A&M University, College Station, TX 77843-2117. Her email is luohao@tamu.edu.